ESTIMATION OF MACRO VELOCITY MODELS BY WAVE FIELD EXTRAPOLATION

PROEFSCHRIFT

ter verkrijging van de graad van doctor
aan de Technische Universiteit Delft,
op gezag van de Rector Magnificus,
prof.drs. P.A. Schenck,
in het openbaar te verdedigen
ten overstaan van een commissie
aangewezen door het College van Dekanen
op dinsdag 15 januari 1991 te 16.00 uur door

HENDRICUS LAMBERTUS HUBERTUS COX

geboren te Utrecht
natuurkundig ingenieur

Dit proefschrift is goedgekeurd door de promotor

prof.dr.ir. A.J. Berkhout

CIP-DATA KONINKLIJKE BIBLIOTHEEK, DEN HAAG
Cox, Hendricus Lambertus Hubertus
Estimation of macro velocity models by wave field exploration / Hendricus Lambertus Hubertus Cox
[S.l. : s.n.] (Zoetermeer : Gebotekst). – Ill.
Thesis Delft. – With ref. – With summary in Dutch
ISBN 90–9003926–0
SISO 567.2 UDC 531.76:550.34(043.3)
Subject headings: exploration seismology / velocity analysis / wave field extrapolation

printed in The Netherlands by: N.K.B. Offset bv, Bleiswijk

Opgedragen aan Cora
en mijn ouders

ACKNOWLEDGMENT

The research presented in this thesis was started in 1986 as part of the TRITON consortium project on 3-D target-oriented processing at the Delft University of Technology, and was continued in the succeeding DELPHI project (Delft philosophy on inversion) in 1989. As a member of the research team I am very grateful to all the colleagues I was able to work with. I am especially grateful to Gerrit Blacquière and Niels Kinneging, my "colleagues of the first hour". Not only the discussions I had with them but also their computer programs were invaluable tools in my research topic.

I would like to acknowledge all participating companies of the aforementioned projects for their support. Especially I would like to thank Dr. Postma of Marathon Oil Company[1] to provide us with the watertank data and Dr. K.K. Sekharan of the Seismics Acoustics Laboratories in Houston, who built the scale model and performed the measurements.

I thank Placid Oil for their permission to use and publish the field data example.

I am obliged to Joke Ligterink for her suggestions on improving my English writing and to Gerda Boone for helping me with preparing the final version.

---

[1]Marathon does not necessarily endorse the processing procedures described in this thesis.

I want to express my gratitude to Kees Wapenaar for his guidance during the research and during the stage of the thesis. His patience and persistence will always be an example to me.

I am grateful that I had the possibility to study in one of the leading research groups in the seismic industry. For that I thank my promotor prof. A.J. Berkhout who I admire for being the stimulating force behind this group.

There are a few people I would especially like to thank: my parents for their support I had from them during my studies, and Cora, my wife, who plays an invaluable role in my life. Therefore I dedicate this thesis to both my parents and my wife.

Delft, 1991

TABLE OF CONTENTS

CHAPTER 1

INTRODUCTION

1.1 INTRODUCTION

Geophysical exploration

Geophysics is the study of the earth by means of quantitative physical methods. It plays an important role in the ever increasing demand for energy resources in our modern society. Different techniques have been developed in the search for oil, gas and minerals. Several principal methods are being used in geophysical exploration, such as the gravimetry method, the magnetic method and the seismic method. The strength of the gravitational field of a body is proportional to its density. Similarly, the strength of the magnetic field of a body is in proportion to its magnetization. These potential fields can be observed at a distance from the object. Thus it is possible, at least in principle, to study the distribution of density or magnetization in the subsurface from the gravitational or magnetic fields at the surface, provided that the appropriate physical measurements can be made. An extensive discussion on these and other geophysical methods is given by Grant and West (1965) and Parasnis (1986). It is worthwile mentioning that there is a growing interest in geo-radar techniques, by which low frequency magnetic pulses (MHz range) are transmitted into the subsurface.

Seismic exploration

Today, the most widely used exploration technique is based on seismology. Seismology is the science that deals with the propagation and reflection of

elastic waves in the earth's interior. It can be divided into two main fields of applications. In earthquake seismology the waves excited by an earthquake are recorded and investigated to get a better understanding of the generation of earthquakes and of the propagation of the resulting waves. In exploration seismology the response of the earth is measured by recording the waves that are generated by man-made sources. A seismic survey can be carried out both on land and at sea. Surface acquisition is the most commonly used data acquisition method in the seismic industry. In surface acquisition sources and receivers are located at (or just below) the surface (Figure 1.1). A discussion of other acquisition geometries is beyond the scope of this introduction.

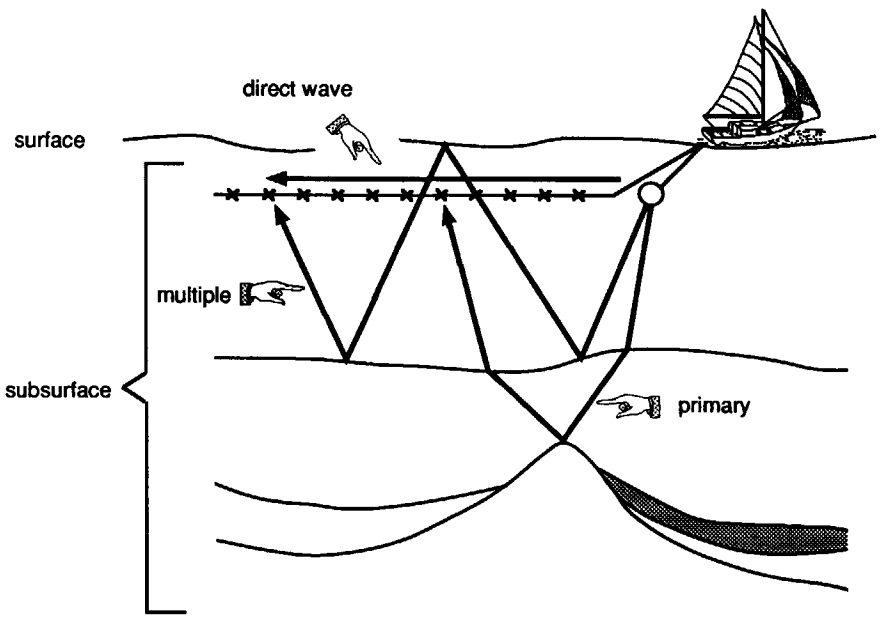

Figure 1.1
Seismic data acquisition at sea.

Seismic experiment, P and S waves

A seismic experiment is carried out by initiating a source that emits elastic waves into the subsurface. Elastic waves can be subdivided into two basic types, longitudinal or pressure waves, also called P waves and transverse or shear waves, also called S waves. In solids both P and S waves can occur. So in land acquisition the source emits a combination of

P and S waves. In (ideal) fluids no shear stresses can be generated. So at sea the source only emits P waves. The response is recorded by detectors at the surface. A wave that travels directly from the source to the detector is called a direct wave. If the wave includes one reflection it is called a primary. If more than one reflection has occurred the recorded wave is called a multiple. Although the direct wave and the multiple reflections contain information about the (sub)surface, they are generally considered as noise in seismic processing.

1.1.1 Forward models

Two-way

The response of the subsurface on elastic waves can be described by the so-called *two-way* elastic forward model (Figure 1.2a). Upward traveling and downward traveling wave fields are handled simultaneously in this formulation. Multiple reflections and wave conversions (from P to S and vice versa) are also included. The two-way method is a rigorous way to describe *forward modeling* of seismic data and can be readily implemented in a computer (Alterman and Karal (1968), Kelly et al., (1976)).

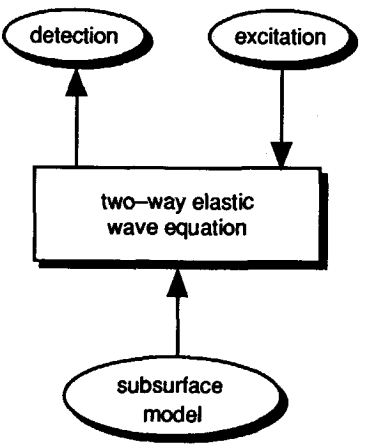

Figure 1.2a
Two-way elastic forward model for the simulation of seismic data.

One-way

Another possible description of the response of the subsurface is by means of the *one-way* forward model as introduced by Berkhout (1982) and further refined by Wapenaar and Berkhout (1989). This can be elegantly illustrated by the picture shown in Figure 1.2b:

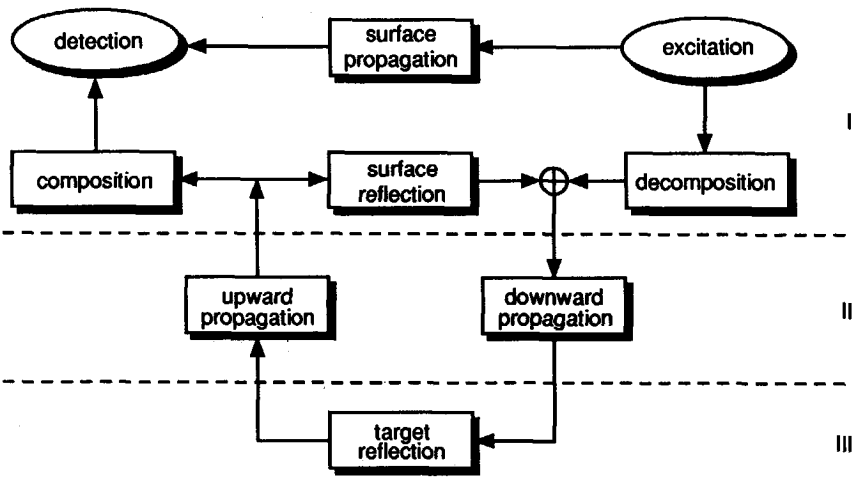

Figure 1.2b
One-way forward model of seismic data.

The *decomposition* operator transforms the total two-way source wave field into downward traveling P and S wave fields at the source position. Note that in case of marine acquisition the expression for the operator will simplify since then we are only dealing with emitted P waves.
The waves emitted by the source propagate down into the subsurface, the propagation being described by the *downward propagation* operator.
Whenever the waves encounter changes in the elastic parameters of the subsurface *reflection* occurs (described by a reflection operator), which generally depends on the angle of the incident wave. For reasons of clarity only the reflections of a target zone are shown. The reflected waves propagate up to the surface (*upward propagation*) where they will be detected. The *composition* operator transforms the one-way upward traveling P and S wave fields into the recorded two-way seismic data at the detector positions. Again, in marine acquisition the composition operator will simplify as we are dealing with received P waves only. The surface acts as a perfect reflector and therefore all waves traveling upwards are

reflected at the surface and propagate down into the subsurface where they will again be reflected and so on. These multiple reflections will arrive at the detectors at a later time and often mask the (primary) reflections of deeper layers. Waves that travel along the surface ("surface propagation") are incorporated by a separate operator. In the on-shore situation this operator describes the so-called "ground roll". In the off-shore situation the operator describes the direct P wave.

Wapenaar and Berkhout have shown that at the surface the two-way wave theory can be coupled to the one-way wave theory through the composition and decomposition operators. In their theory it is assumed that horizontally traveling waves have already been removed from the data. Internal multiple reflections that occur in the subsurface are, in principle, taken into account by this forward model. However, internal multiples are generally treated statistically and taken into account in the deconvolution problem. As will be shown in the next section, the one-way method is an elegant description when the goal is to obtain the geologic parameters from the seismic measurements, the so-called *inverse problem.*

1.1.2 The inverse problem

Two-way, the traditional approach

The aim in seismic inversion is to obtain the medium parameters from the seismic measurements. The traditional approach to this problem is the inversion of all propagation and reflection effects by one iterative process, as described by e.g. Tarantola (1987), and shown in Figure 1.3a. With the two-way wave equation shot records are simulated using an initial description of the subsurface parameters (subsurface model). The simulated data are then compared with the observed measurements. From the data mismatch the necessary perturbations of the parameters are calculated and the subsurface model is updated accordingly. Then the whole procedure is repeated until an acceptable data mismatch is obtained.

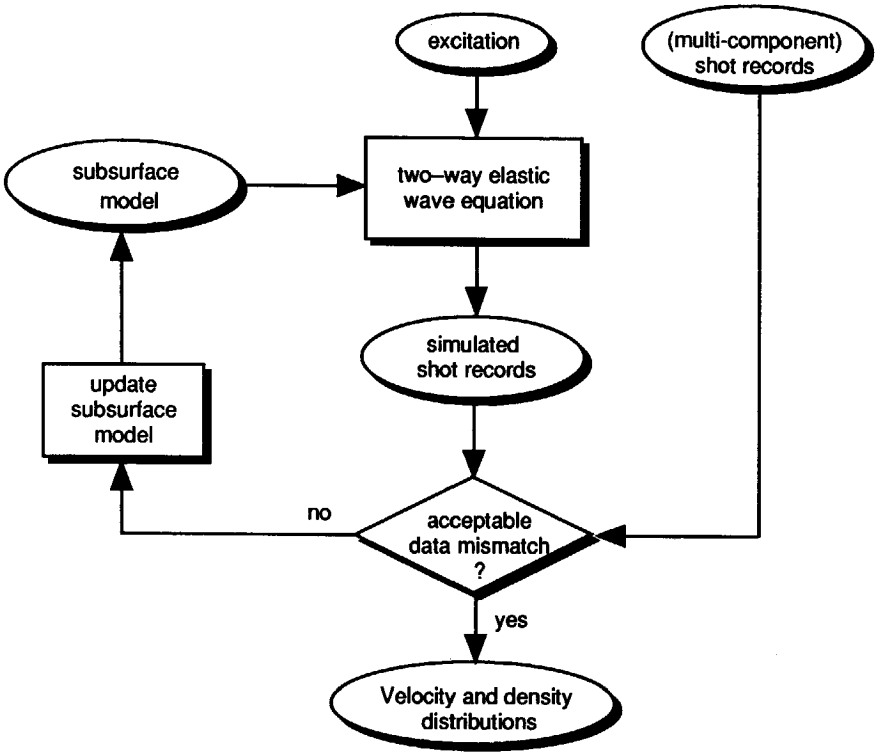

Figure 1.3a
In the traditional seismic inversion scheme the earth is described as a *gridded* medium. The elastic parameters at each subsurface grid point are obtained from the data by iterative forward modeling.

One-way, the Delphi approach

Our considerations to propose an alternative for inversion involve the fact that the subsurface response is determined by different types of parameters, i.e. *surface* parameters, *overburden* parameters and *target* parameters. This can be easily seen from Figure 1.2b.

The operators in level I are determined by the (near) surface parameters, the propagation operators in level II depend on the macro parameters of the overburden, and the reflection operator in level III is determined by the target parameters. These parameters can be determined

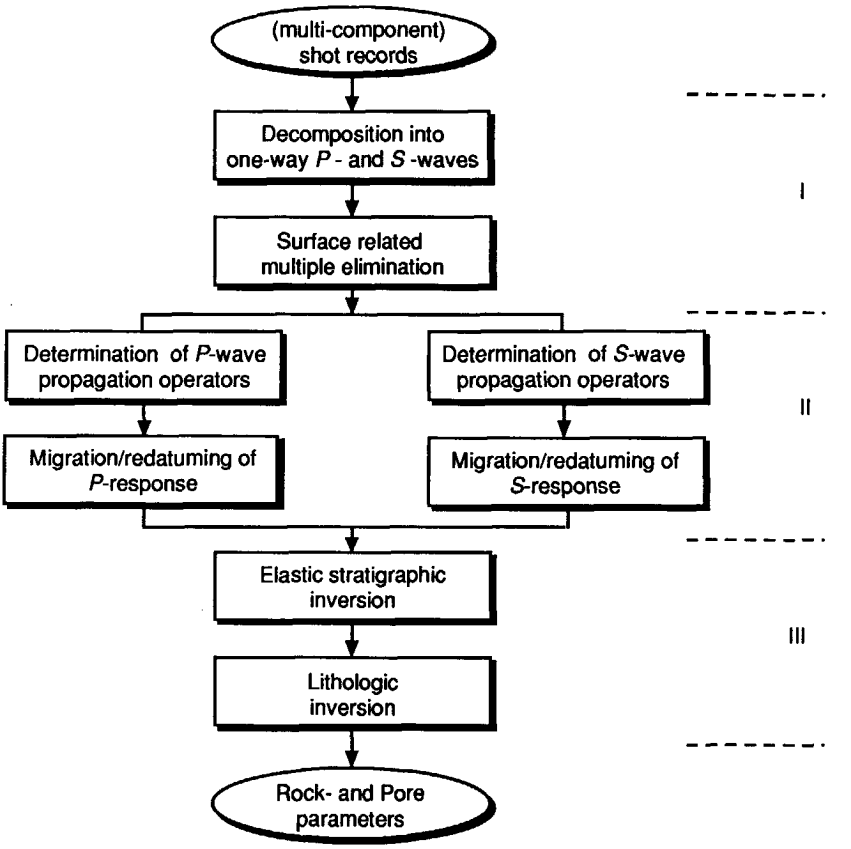

Figure 1.3b
In the Delphi inversion scheme the earth is described as an irregularly *layered* medium. The inverse problem is divided into separate consecutive steps related to the surface (I), the overburden (II) and the target (III) respectively.

independently. Therefore, I will follow the *stepwise* inversion approach that is being developed in the DELPHI[1] consortium project (Figure 1.3b).

In the ideal situation the assumption is made that *multi-component* data are recorded at the surface, the nine measured components being the three Cartesian projections of the particle velocity due to horizontally (x and y) and vertically (z) vibrating sources. Note that the multi-component

[1]DELPHI stands for DELft PHilosophy on Inversion.

data represent *vector* quantities. As mentioned before, in fluids only one (*scalar*) quantity remains.

Similar to the situation in the one-way forward model (Figure 1.2b), in the inversion approach three steps may be distinguished related to the surface (step I), the overburden (step II) and the target (step III):

I. In the *decomposition* module the elastic data at the surface are decomposed into separate upward traveling P and S waves at the receiver locations due to downward traveling P and S waves at the source locations. In this process knowledge about the elastic parameters is only required at the surface! In the acoustic situation (marine data) the decomposition simplifies to a decomposition of the total P wave field into an upward traveling and a downward traveling part (i.e. wave theory based deghosting).
The removal of the (strong) surface reflection and wave conversion effects from the upward traveling subsurface response is called *elimination* of the surface-related multiples. After the surface-related preprocessing (decomposition and multiple elimination) the obtained wave fields can be subdivided into different types. The PP data represent recorded upward traveling P waves due to a downward traveling P source wave field. The PS_x data represent recorded upward traveling P waves due to a downward traveling S_x source wave field (an S_x wave is a shear wave polarized in the (y,z) plane); wave conversion occurs *during primary reflection*. Similar representations can be given for the other wave types. Note that the preprocessing is performed at the surface. In the PP data waves converted *during propagation* from P via S to P are still present, as well as internal multiples. Both effects are generally considered to be second order effects in the DELPHI approach, since reflection coefficients in the subsurface are of lower magnitude than the reflection coefficients of the free surface. For strong reflectors, such as the seabottom, conversion *during propagation* may be included. For an extensive discussion on elastic decomposition and multiple elimination the reader is referred to the article of Wapenaar et al. (1990). After surface-related preprocessing the data represent scalar quantities

(potentials) and further processing steps can be performed by algorithms working on scalar data.

II. After the surface-related preprocessing the target reflections are still distorted by propagation effects caused by the overburden (cf. Figure 1.2b). The processing dealing with the removal of the propagation effects is applied in the second step of the DELPHI scheme. Without going into detail now, the estimation of the macro parameters of the subsurface (the subject of this thesis) is done in the *macro model estimation* module; next, the inverse propagation operators are computed and finally the computed operators are applied in the *migration/redatuming* module. Note that these modules operate on the P and S data separately. It may be stated that migration techniques as discussed amongst others by Schultz and Sherwood (1980), and Berkhout (1982) are actually the second step of the DELPHI inversion scheme.

III. After migration or redatuming the reflections of the target are properly revealed. From these reflections, which depend on the incidence angles, the elastic medium parameters (detailed velocities and densities) can be estimated through *elastic stratigraphic inversion* (de Haas and Berkhout, 1989) and subsequently the lithologic properties (rock and pore parameters) are estimated by *lithologic inversion* (Lörtzer, 1989).

After each step the quality of the resulting data can be checked before going on to the next step of the scheme.

1.2 WHAT IS A MACRO MODEL?

If a well has been drilled and measurements have been taken in the well, then Figure 1.4a shows a typical result in terms of velocity. An interesting and important analysis of the measurement curve (velocity log) is given by a subdivision into *trend* and *detail*. The trend (Figure 1.4b) gives information on the depth dependent compaction properties of the subsurface. The detail (Figure 1.4c) gives information on the different rock and pore properties of the individual geologic layers (within the resolution of the velocity log). The subsurface may be subdivided in so-called macro layers, where each macro layer can be seen as a package of geologically related layers with the same compaction property. A macro boundary may

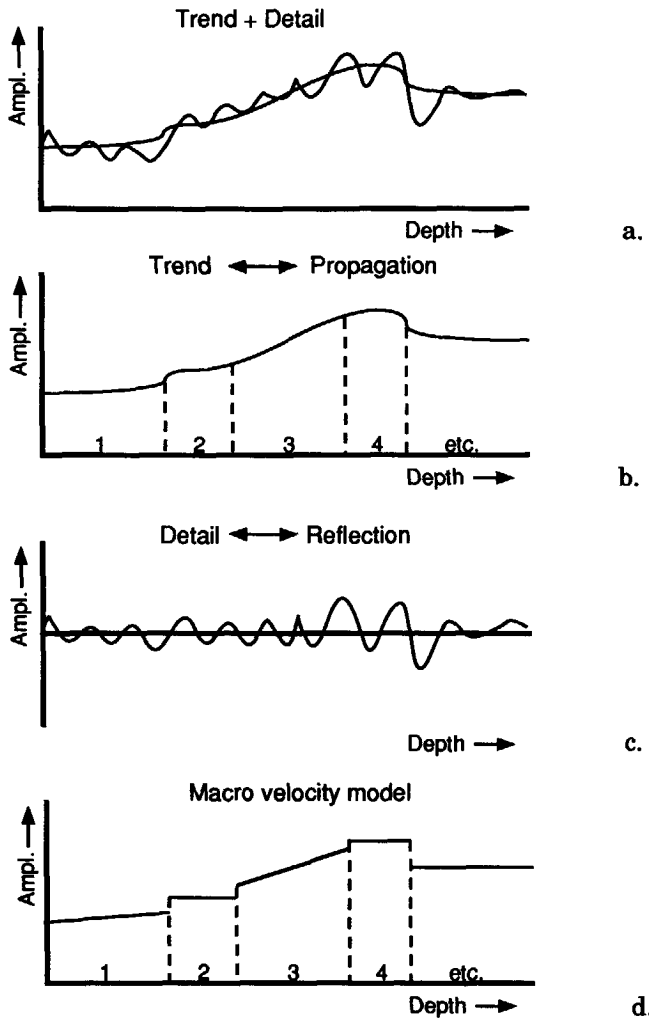

Figure 1.4
Description of the subsurface in terms of trend and detail.

generate a significant reflection. The distinction between macro layering and fine layering plays an important role in seismic inversion.

The physical essence of the seismic method is given by propagation and reflection (Figure 1.5). The source wave field propagates down into the subsurface, reflects at the layer boundaries and the reflected wave fields propagate back to the surface. Hence, the seismic response we measure at the surface represents a mixture of propagation and reflection information. The major part of seismic processing is dedicated to

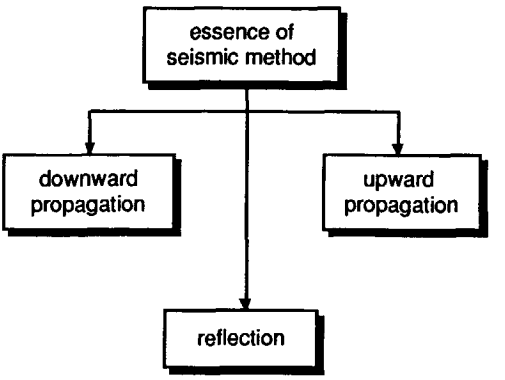

Figure 1.5
Seismic responses are defined by the *propagation* and *reflection* properties of the subsurface.

eliminate propagation effects from the seismic response, aiming at correctly positioned true amplitude reflectivity (second step in DELPHI).

Going back to the afore-mentioned description of the subsurface, we may make the following important statements (Figure 1.6). Propagation is primarily determined by the macro layering of the subsurface. Reflection is mainly determined by the fine layering of the subsurface. The macro parameters are mainly expressed in the traveltimes of the recorded signals, whereas the detail parameters are mainly expressed in the amplitudes of the reflected events. For the elimination of the propagation effects a *macro model* of the subsurface should be available. A macro model is defined as a description of the propagation parameters in terms of macro velocities and densities as a function of lateral position and depth. Figure 1.4d shows a typical macro velocity model (1-D). The macro layers have sharp boundaries. Transition zones may also be parameterized by a sharp discontinuity, thus reducing the number of parameters needed to describe the macro model. It has been shown (Peels, 1988; Kinneging, 1989) that this way of parameterization is fully legitimate as far as propagation effects are concerned. Seismic processing should be based on macro subsurface models. This means that estimation of macro models should be a key issue in the seismic industry.

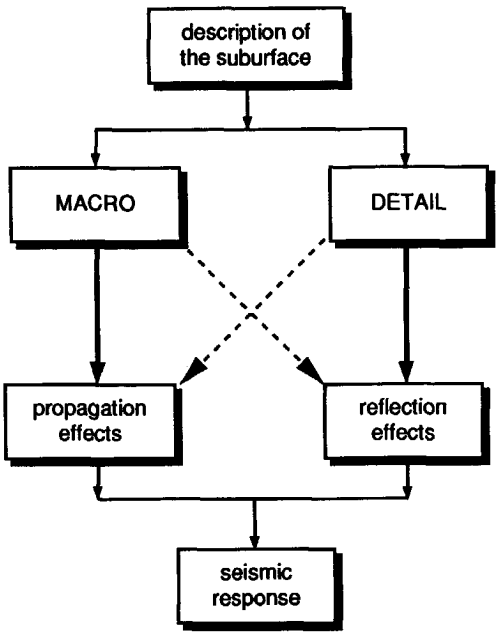

Figure 1.6
The macro layering and the fine layering in the subsurface determine the propagation and reflection effects in the seismic response.

Simultaneous or separate estimation of macro and detail

In principle, macro properties and detail properties can be estimated *simultaneously* from the data by nonlinear iterative inversion as is claimed by Mora (1989). However, his technique suffers severely from the fact that seismic inversion is highly nonlinear in the estimation of the macro properties, which yields bad convergence. Furthermore, the algorithms based on nonlinear iterative inversion may easily get trapped in local minima. Opposed to this technique the Delphi approach allows for inversion in steps. The macro parameters and the detail parameters are estimated *separately*. In order to estimate the reflection properties of the medium the propagation effects have to be removed from the data first. Estimation of the propagation effects, (i.e. macro model estimation) is the subject of this thesis. Once the macro model is known the propagation effects that are present in the recorded data can be computed. The application of the inverse propagation operators can be done by redatuming or by migration. Redatuming is the computational process that extrapolates seismic surface data to a new data acquisition plane

("datum plane") in the subsurface. This process is based on the elimination of wave propagation effects between the surface and the new datum in the subsurface. Hence, the redatumed data represent measurements as if they were recorded on the new datum level. Migration involves redatuming to all depth levels and "imaging". This yields the (angle-dependent) reflection properties of the subsurface. In the Delphi approach the data may be redatumed to the upper boundary of a target zone (for economic reasons), followed by migration in the target zone. Redatuming to the target and migration in the target zone require a macro model, of the overburden and the target zone respectively, as input. Redatuming and migration will be explained in more detail in Chapter 2.

So instead of inverting for macro and detail simultaneously, in the Delphi approach the macro properties are estimated through macro model estimation and the detail is then revealed by the migration process.

Gridded or layered parameterization of the macro model

In principle the macro model can be defined as gridded. This means that the medium should be divided into grid cells. At each grid cell the velocity has to be determined. However, since the subsurface is layered preference goes towards a definition of a macro model through a layered parameterization. The layer interfaces are defined by the major changes of the medium parameters (macro boundaries). Note that when a layered parameterization is chosen this implicitly means that geologic information is included in the description of the macro model.

1.3 ON THE WAVENUMBER CONTENT OF REFLECTION DATA

Resolution in terms of wavenumbers

The resolution of the seismic method can be defined in terms of wavenumbers, or equivalently wavelengths, of the recorded waves. The low wavenumbers (large wavelengths) are related to the trend and the high wavenumbers (small wavelengths) are related to the detail. In practice the very low wavenumbers are not present in the seismic data. This means that the trend information cannot be completely retrieved from the seismic data alone. Also the very high wavenumbers are not present in the seismic data and therefore the detailed variations

(reflection properties) can only be obtained with a limited resolution. By including a priori information, such as geological knowledge of the area under investigation, the bandwidth of the final solution can be extended. Considerations on seismic resolution are elaborately discussed by Berkhout (1984).

What wavenumbers are needed?

To illustrate the effect of high and low band limitation, consider the following one-dimensional depth model, consisting of two homogeneous layers with densities ρ_1 and ρ_2 respectively, yielding a step function along the z-coordinate (Figure 1.7a):

$$\rho(z) = \rho_1 + (\rho_2 - \rho_1)U(z - z_r) \ , \tag{1.1}$$

where U denotes a unit step function. The velocity is constant across the interface. Let k_z and z be Fourier pairs (k_z is called the vertical wavenumber). The Fourier transform of the step function contains non-zero information for all values of k_z from zero to infinity. The reflectivity function is given by

$$r(z) = \frac{\rho_2 - \rho_1}{\rho_2 + \rho_1} \delta(z - z_r) \ , \tag{1.2}$$

where δ denotes a delta pulse. Since r(z) is a real-valued function of z, it is sufficient to consider positive wavenumbers only. If we were able to perform a seismic experiment that measures waves for all k_z-values, a proper inversion scheme would exactly reconstruct the step function. In practice, however, there are limits to the k_z-values. If the measurements are restricted to some maximum value, say $k_{z,max}$, then only a low-pass version of the step function can be obtained (Figure 1.7b and c). The influence is relatively small and affects the steepness of the slope of the step function. However, the step function is dramatically affected if also small k_z-values are missing (Figure 1.7d and e)! So, as can be seen from the above example, high wavenumber information determines the obtainable detail, whereas low wavenumber information determines the obtainable trend (macro model).

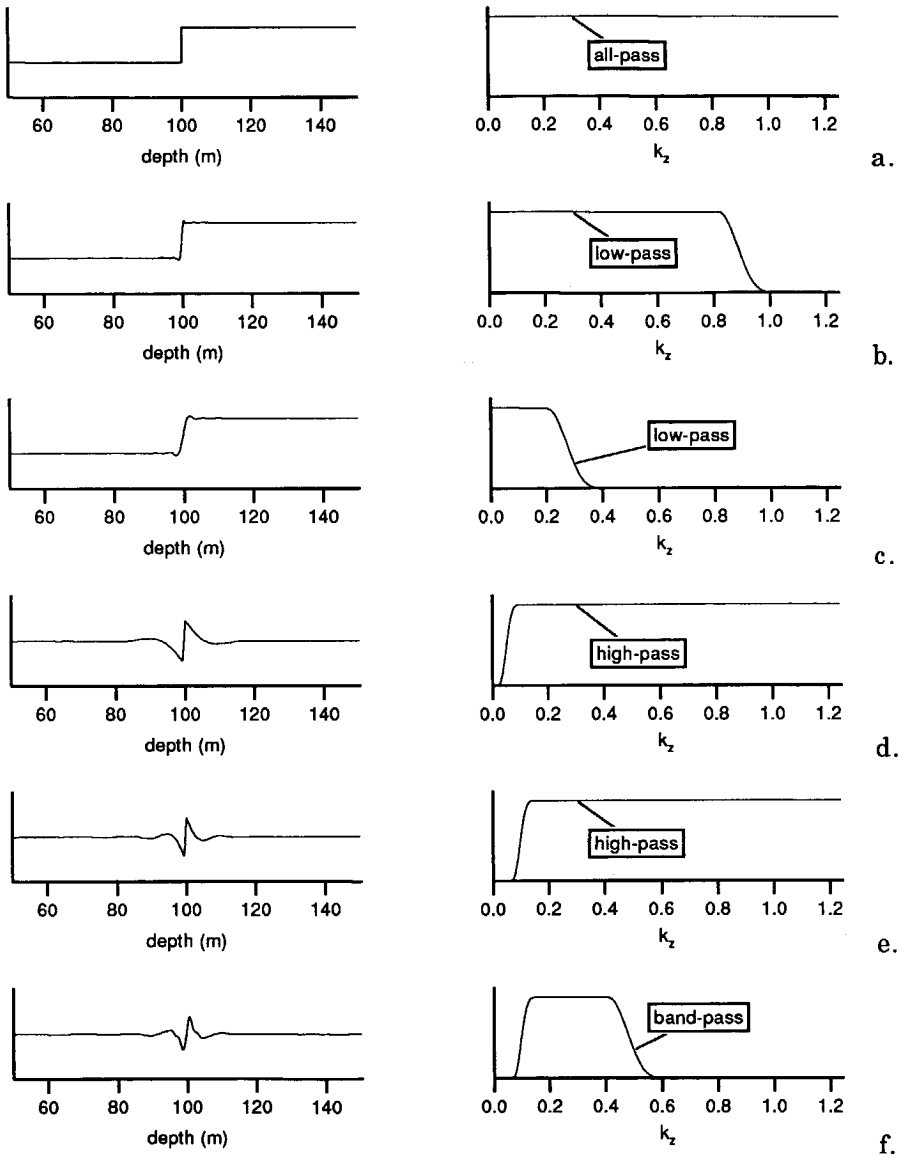

Figure 1.7

a. One-dimensional depth model containing a density contrast at depth z_r = 100 m.
b. Low-pass filtered version of figure a ($k_{z,max}$ = 1).
c. Low-pass filtered version of figure a ($k_{z,max}$ = 0.4).
d. High-pass filtered version of figure a ($k_{z,min}$ = 0.025).
e. High-pass filtered version of figure a ($k_{z,min}$ = 0.07).
f. Band-pass filtered version of figure a ($k_{z,min}$ = 0.07, $k_{z,max}$ = 0.6).

The displays on the right show the applied filters.

Which wavenumbers are present in reflection data?

To see which wavenumbers are actually present in the recorded data, consider the convolutional model. The response, p(t), of a *normal* incident plane wave, s(t), in a 1-D medium may be described by

$$p(t) = r(t) * s(t)\,, \tag{1.3a}$$

where r(t) represents the reflectivity of the medium as a function of time and $*$ denotes convolution along the t-axis. The variable t may be considered as a scaled "depth" variable according to (Figure 1.8a):

$$t = \int_0^z \frac{2dz'}{c(z')}\,, \tag{1.3b}$$

where c(z) represents the velocity function of the 1-D medium.

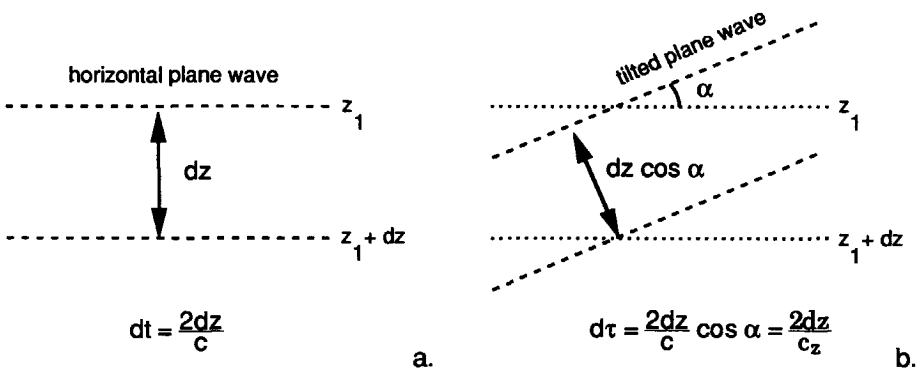

Figure 1.8
a. t may be seen as a scaled "depth" variable according to equation (1.3b).
b. τ may be seen as a scaled "depth" variable according to equation (1.4b).

Similarly, the response $\tilde{P}(p,\tau)$ of an *oblique* incident plane wave $\tilde{S}(p,\tau)$ in a 1-D medium may be described by a convolution , according to

$$\tilde{P}(p,\tau) = \tilde{R}(p,\tau) * \tilde{S}(p,\tau)\,, \tag{1.4a}$$

where $\tilde{R}(p,\tau)$ represents the reflectivity function of the medium and $*$ denotes convolution along the τ-axis. The variable τ represents a scaled "depth" variable according to (Figure 1.8b):

$$\tau = \int_0^z \frac{2dz'}{c_z(p,z')} \quad , \text{ with } \quad \frac{1}{c_z} = \left(\frac{1}{c^2} - p^2\right)^{1/2} \tag{1.4b}$$

where p denotes the ray parameter:

$$p = \sin\alpha/c \tag{1.4c}$$

and where α denotes the propagation angle of the source wave field. Note that the vertical wavenumber depends on the ray parameter and on the frequency according to $k_z = \omega/c_z = \omega\left(\frac{1}{c^2} - p^2\right)^{1/2}$.

A thorough derivation of this convolutional model is beyond the scope of this introduction. The interested reader is referred to Appendix A. Note that for a normal incident plane wave (p=0), "τ" reduces to "t", and consequently (1.4a) reduces to (1.3a).

The reflectivity function can be obtained by deconvolution for the source wave field, according to

$$\tilde{R}(p,\tau) = \tilde{P}(p,\tau) * \tilde{S}^{-1}(p,\tau) \ . \tag{1.5}$$

The inverse $\tilde{S}^{-1}(p,\tau)$ is only stable within the frequency band of the source wave field. Hence, if $\tilde{S}(p,\tau)$ does not contain low wavenumbers, the low wavenumber information of the reflectivity function can not be recovered. This will be illustrated for the special case of a constant velocity medium. Then we may also write

$$\tilde{R}(p,z) = \tilde{P}(p,z) * \tilde{S}^{-1}(p,z) \ , \tag{1.6a}$$

where the deconvolution takes place along the z-axis and where z and τ are related by

$$\tau = \frac{2z}{c_z} \ . \tag{1.6b}$$

Note that, due to equations (1.4b) and (1.6b), the "spatial wavelet" $s(p,z)$ is stretched for increasing p-values. This is illustrated by Figure 1.9, which shows the resolved reflectivity of the 1-D medium of Figure 1.7, obtained for different values of the ray parameter p, i.e. for different angles of propagation.

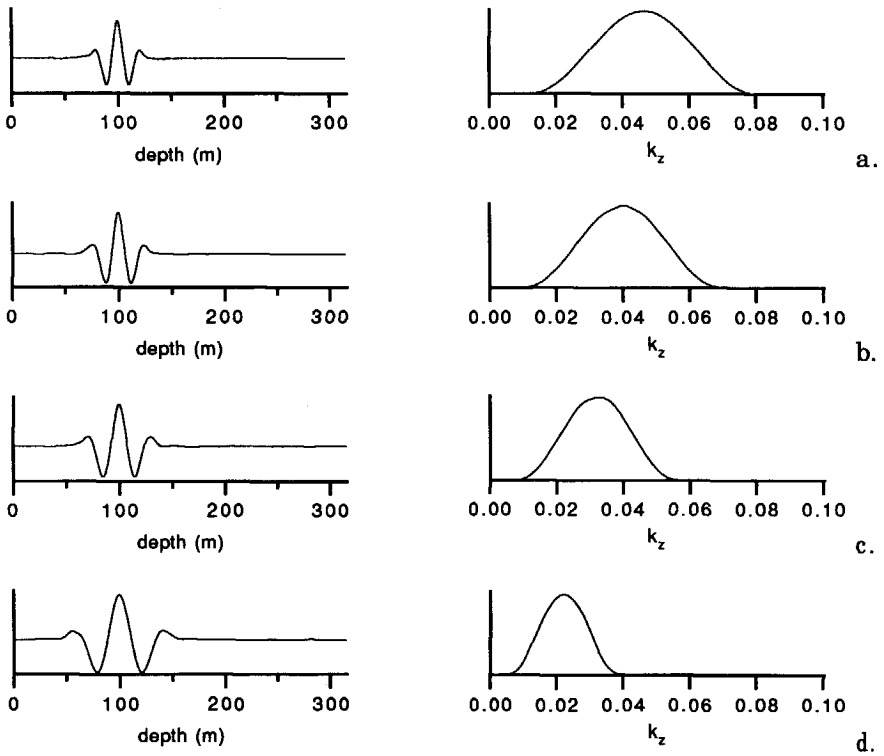

Figure 1.9
Reflectivity of the 1-D model of Figure 1.7, obtained for different p-values, i.e. different angles of the incident wave field. Note that the "spatial wavelet" is stretched for increasing p-values.

a. propagation angle $\alpha=0^0$ (p= 0 s/m).
b. propagation angle $\alpha=30^0$ (p= 0.33 e^{-3} s/m).
c. propagation angle $\alpha=45^0$ (p=0.47 e^{-3} s/m).
d. propagation angle $\alpha=60^0$ (p=0.577 e^{-3} s/m).

The displays on the right show the corresponding spectra.

In conclusion, increasing propagation angles (and decreasing frequencies) introduce low wavenumber information, as can be seen from the corresponding spectra. In seismics multi-frequency, multi-angle experiments are carried out, but in practice neither the zero frequency component nor the 90 degree angle is present. Consequently the data only contains (vertical) wavenumbers above a certain *non-zero* minimum value (Table 1.1) and therefore trend info cannot be obtained from seismic data alone.

Table 1.1
Different values of the minimum vertical wavenumber $k_{z,min}$, and the corresponding maximum vertical wavelength $\lambda_{z,max}$ ($=2\pi/k_{z,min}$), for different propagation angles. The propagation velocity was c=1500 m/s. The frequency was f=5Hz.

	$k_{z,min}$ [m^{-1}]	$\lambda_{z,max}$ [m]
$\alpha_{max} = 0^0$	0.021	300
$\alpha_{max} = 45^0$	0.015	424
$\alpha_{max} = 60^0$	0.010	600
$\alpha_{max} = 75^0$	0.005	1159

As stated before, the low wavenumber information that is missing in the seismic data has to be introduced using a priori information.

1.4 OUTLINE OF THIS THESIS

In conventional seismic processing techniques the measured seismic wave fields at the surface are processed in the time-domain (deconvolution, CMP stacking, time migration). Therefore, conventional seismic processing may be referred to as time-oriented. In the modern view of seismic processing it is realized that accurate information (structural, stratigraphic, lithologic) on the subsurface can only be obtained if the wave fields, measured at the surface, are downward extrapolated to the subsurface grid points (depth points) of interest. Therefore, modern seismic processing may be referred to as depth-oriented. It may be stated that the conventional time-domain approach provides an economic preview of the subsurface. However, if at selected areas a more accurate image is required then a depth point-oriented approach is a prerequisite. Unfortunately, the data related to a depth point

is not readily obtainable from the surface measurements. Hence, wave field extrapolation is required in depth point-oriented processing. Three-dimensional, depth point-oriented, elastic seismic processing is the subject of the Delphi research consortium.

Wave field extrapolation in general and shot record redatuming in particular play an important role in the depth point-oriented macro model estimation procedure that has been developed. Therefore Chapter 2 is dedicated to the explanation of shot record redatuming. In Chapter 3 an overview is given on existing macro model estimation techniques. The heart of the thesis is Chapter 4, where the theory on the investigated macro model estimation scheme is presented. Finally, the method is illustrated in Chapter 5, where it is applied to numerically simulated (finite difference) data, to data that have been recorded in a controlled environment (water tank) and to real data.

CHAPTER 2

THE PRINCIPLE OF SHOT RECORD REDATUMING

2.1 INTRODUCTION

Prestack redatuming and prestack migration are methods that are becoming more and more important in current processing of seismic data. This is mainly due to the progress made in computer technology; both techniques are computationally intensive processes as compared to conventional poststack data treatment. On the other hand they offer the accuracy needed for the exploration of (small) reservoirs in complex subsurfaces. In this chapter I will discuss prestack redatuming and prestack migration. In the DELPHI scheme the redatuming and/or migration is carried out after decomposition of the (single- or multi-component) data and after elimination of the surface-related multiples. As a result of surface-related preprocessing, the one-way forward model reduces to the one shown in Figure 2.1.

2.2 MATHEMATICAL DESCRIPTION OF THE ONE-WAY FORWARD MODEL

2.2.1 Single-source experiment

Various Delft-related authors (Berkhout, 1982; Wapenaar, 1985) have shown that the one-way forward model can be elegantly represented using a matrix notation according to

$$\mathbf{P}^{-}(z_0) = \underset{\sim}{\mathbf{W}}^{-}(z_0,z_m)\underset{\sim}{\mathbf{R}}(z_m)\underset{\sim}{\mathbf{W}}^{+}(z_m,z_0)\mathbf{S}^{+}(z_0) \ , \tag{2.1}$$

where the vector $\mathbf{S}^{+}(z_0)$ represents the downward travelling scalar source wave field at the surface (excitation). Matrix $\underset{\sim}{\mathbf{W}}^{+}(z_m,z_0)$ describes the downward propagation operator from the surface z_0 to the reflector depth z_m (for reasons of clarity it is assumed that the medium contains one reflector at z_m only (cf. Figure 2.1)). Matrix $\underset{\sim}{\mathbf{R}}(z_m)$ describes the reflection operator at z_m, matrix $\underset{\sim}{\mathbf{W}}^{-}(z_0,z_m)$ describes upward propagation from z_m to z_0 and the vector $\mathbf{P}^{-}(z_0)$ represents the upward travelling scalar wave field at the surface.

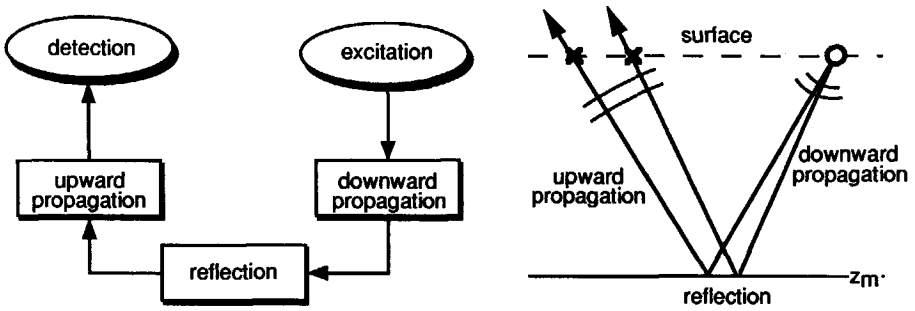

Figure 2.1
One-way forward model after surface-related preprocessing (for reasons of clarity the response of only one reflector is shown).

Equation (2.1) is a frequency-domain representation of the one-way forward model, although the frequency parameter ω is omitted for notational convenience. The equation can be divided into three parts: downward propagation, reflection and upward propagation.

Downward propagation (cf. Figure 2.2a)

Downward propagation from the surface z_0 to level z_m is described by

$$\mathbf{S}^{+}(z_m) = \underset{\sim}{\mathbf{W}}^{+}(z_m,z_0)\mathbf{S}^{+}(z_0) \ . \tag{2.2a}$$

Each element of the source vector $\mathbf{S}^{+}(z_0)$ corresponds to a different surface position; if there would be a point source (dipole) at the surface only one

element of the source vector would be non-zero. When the source is distributed over some distance, like e.g. an array of vibrators, the source vector contains more non-zero elements. The wave generated at the surface propagates down to level z_m. One row in matrix $\underset{\sim}{\mathbf{W}}^{+}(z_m,z_o)$ contains the weighting factors that describe the amplitude and phase distortion of the wave field when propagating from the surface, as described by (2.2a), to one particular depth point at z_m. The weighted summation of the source wave field at the surface is simply the discrete representation of the well-known Rayleigh-II integral. So, a row in the propagation matrix represents the z-derivative of the discrete Green's function, where the Green's function is the wave field at the surface due to a monopole at depth level z_m. It accounts for the phase and amplitude distortion of the propagating wave. The phase in the monochromatic representation contributes to a corresponding traveltime in the time-domain representation. The Rayleigh integral is a special version of the Kirchhoff integral and is applicable if the surface on which the wave field is known is flat. A derivation of the matrix notation from the Rayleigh integral is beyond the scope of this chapter, but the interested reader is referred to Appendix B.

Reflection (cf. Figure 2.2b)

The downward traveling incident wave at z_m is reflected and transformed into an upward travelling wave according to

$$\mathbf{P}^{-}(z_m) = \underset{\sim}{\mathbf{R}}(z_m)\mathbf{S}^{+}(z_m) \quad . \tag{2.2b}$$

The matrix $\underset{\sim}{\mathbf{R}}(z_m)$ describes angle-dependent reflection at level z_m. Each row contains the inverse Fourier transformed angle-dependent reflection function for one depth point (Berkhout,1982). Note that when there is no angle-dependence, as is the case with a density contrast across z_m, the reflection function is constant in the horizontal wavenumber (k_x)-domain. Consequently, the inverse Fourier transform from k_x to x yields a delta pulse at one location in each row, the amplitude of which equals the corresponding reflection coefficient. This results in a diagonal reflection matrix. In this case the incident wave field at a specific point on z_m does not contribute to the reflected wave field at other points and therefore such a reflector may be called 'locally reacting'. In general, reflection is angle-dependent and the reflection matrix will have a band structure.

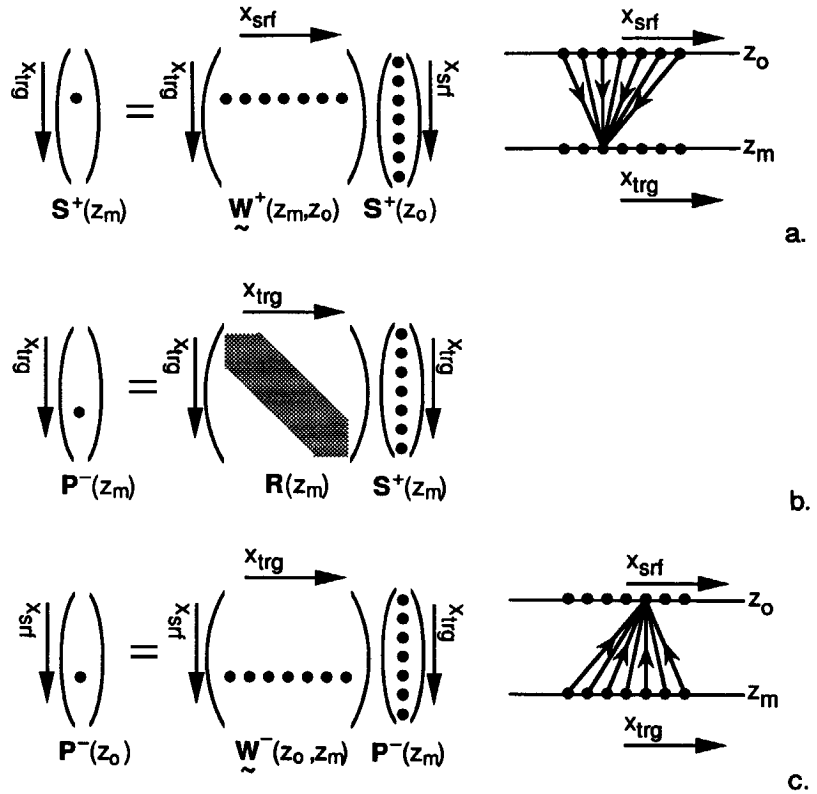

Figure 2.2

a. Downward propagation from the surface (z_o) to a target level (z_m). x_{srf} denotes the lateral position along z_o and x_{trg} denotes the lateral position along z_m.

b. Generally, the reflection matrix has a band structure. It transforms the incident wave field at z_m into a reflected wave field at z_m.

c. Upward propagation from a target level (z_m) to the surface (z_o).

Upward propagation (cf. Figure 2.2c)

The reflected wave field at z_m propagates upward where it is detected by the receivers on the surface. The upward propagation is described by

$$\bar{\mathbf{P}}(z_o) = \underset{\sim}{\bar{\mathbf{W}}}(z_o,z_m)\bar{\mathbf{P}}(z_m) \quad . \tag{2.2c}$$

In analogy with equation (2.2a), one row of matrix $\underset{\sim}{\bar{\mathbf{W}}}(z_o,z_m)$ represents the z-derivative of the discrete Green's function, which is the wave field at the target level due to a monopole at the surface. As mentioned before, the

propagation operators mainly depend on the macro layering and the reflection operator mainly depends on the fine layering.

In practice, inhomogeneities are present at all depth levels and equation (2.1) should be extended to a summation over all depth levels. Therefore, the extension of equation (2.1) reads

$$\mathbf{P}^{-}(z_0) = \sum_{m=1}^{M} \underset{\sim}{\mathbf{W}}^{-}(z_0,z_m)\underset{\sim}{\mathbf{R}}(z_m)\underset{\sim}{\mathbf{W}}^{+}(z_m,z_0)\,\mathbf{S}^{+}(z_0)\,, \tag{2.3}$$

where $\sum$ denotes summation over all relevant depth levels $(z_1,\ldots,z_m,\ldots,z_M)$. The operators $\underset{\sim}{\mathbf{R}}(z_m)$ in equation (2.3) suggest that reflection should occur at any depth point. However, if at depth point (x_i,z_m) no inhomogeneity is present the i^{th} row of matrix $\underset{\sim}{\mathbf{R}}(z_m)$ will contain zero values. Hence, this depth point does not contribute to the upward travelling wave field.

2.2.2 Multi-source experiment

So far, I discussed the one-way forward model for one seismic experiment (single shot record). The matrix notation can be extended to incorporate multi-source experiments by placing the vectors $\mathbf{P}^{-}(z_0)$ and $\mathbf{S}^{+}(z_0)$ of the single-source experiments in the columns of matrices $\underset{\sim}{\mathbf{P}}^{-}(z_0)$ and $\underset{\sim}{\mathbf{S}}^{+}(z_0)$ according to

$$\underset{\sim}{\mathbf{P}}^{-}(z_0) = \sum_{m=1}^{M} \underset{\sim}{\mathbf{W}}^{-}(z_0,z_m)\underset{\sim}{\mathbf{R}}(z_m)\underset{\sim}{\mathbf{W}}^{+}(z_m,z_0)\,\underset{\sim}{\mathbf{S}}^{+}(z_0)\,. \tag{2.4}$$

The reason why more than one shot record is recorded in acquisition is because the medium varies laterally. If it would be laterally invariant, all shot records would be the same (apart from noise) and only one single shot record experiment would suffice. In principle the matrix formulation also holds for 3-D as was shown by Kinneging (1989).

Cross sections of the prestack data volume

In seismic data processing different cross sections of the prestack data volume play an important role. As $\underset{\sim}{\mathbf{P}}^{-}(z_0)$ represents the *monochromatic*

prestack data matrix each element represents a complex number for the current frequency (one monochromatic trace). By taking into account all frequencies within the band of interest, and by applying an inverse Fourier transform from frequency to time, a *broadband* prestack data matrix can be constructed (Figure 2.3).

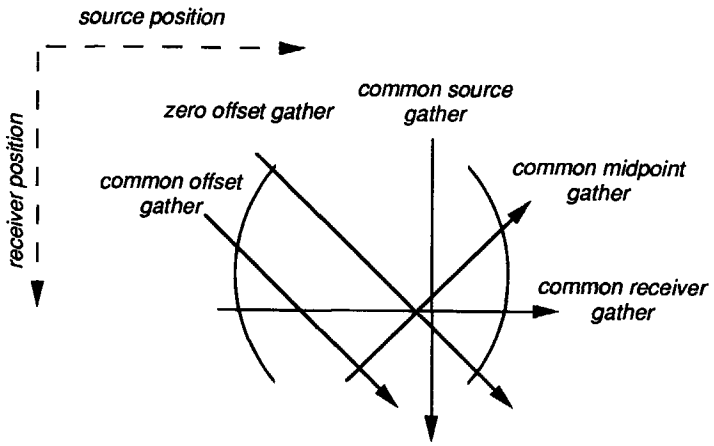

Figure 2.3
Different cross sections from the (broadband) prestack data matrix.

Each element represents a broadband trace of many time samples now. The columns of the prestack data matrix contain *common source gathers,* also referred to as *shot records*. These are the fundamental seismic experiments. A row represents data with a fixed receiver coordinate, and is called a *common receiver gather*. In a *common midpoint gather* the sources and receivers are positioned symmetrically around a surface location (the Common MidPoint). CMP-gathers can be extracted from the anti-diagonals of the data matrix. A *common offset gather* is obtained by extracting data along a diagonal. In a common offset gather the source/detector distance is constant. A special common offset gather is obtained when the sources coincide with the receivers, the so-called zero offset gather. Although zero offset data are generally not recorded in seismic practice, they play an important role in seismic processing. Therefore, a zero offset trace is often simulated by summation of the time samples in a CMP-gather along hyperbolas, a process which is called CMP-stacking.

2.3 INVERSE EXTRAPOLATION

In the previous section the mathematical formulation of the one-way forward model is discussed, i.e. incident and reflected waves are adressed separately. In this section inverse extrapolation (the key process in redatuming and migration) is treated. Redatuming aims to bring the surface data down to a virtual acquisition level in the subsurface by removing the propagation effects, between the surface and the new level from the recorded data. The new acquisition level is also called the new 'datum', hence the term 'redatuming'.

2.3.1 Full prestack redatuming

After correction of the data for the source properties equation (2.4) is reduced to

$$\underset{\sim}{\mathbf{Q}}(z_0,z_0) = \underset{\sim}{\mathbf{P}}^{-}(z_0)\left[\underset{\sim}{\mathbf{S}}^{+}(z_0)\right]^{-1} ,$$

where

$$\underset{\sim}{\mathbf{Q}}(z_0,z_0) = \sum_{m=1}^{M} \underset{\sim}{\mathbf{W}}^{-}(z_0,z_m)\underset{\sim}{\mathbf{R}}(z_m)\underset{\sim}{\mathbf{W}}^{+}(z_m,z_0) . \tag{2.5}$$

Suppose the data need to be redatumed to level z_t, the target level. In that case equation (2.5) can also be written as

$$\underset{\sim}{\mathbf{Q}}(z_0,z_0) = \sum_{m=1}^{t-1} \underset{\sim}{\mathbf{W}}^{-}(z_0,z_m)\underset{\sim}{\mathbf{R}}(z_m)\underset{\sim}{\mathbf{W}}^{+}(z_m,z_0)$$

$$+\underset{\sim}{\mathbf{W}}^{-}(z_0,z_t)\underset{\sim}{\mathbf{R}}(z_t)\underset{\sim}{\mathbf{W}}^{+}(z_t,z_0)$$

$$+ \sum_{m=t+1}^{M} \underset{\sim}{\mathbf{W}}^{-}(z_0,z_m)\underset{\sim}{\mathbf{R}}(z_m)\underset{\sim}{\mathbf{W}}^{+}(z_m,z_0) , \tag{2.6}$$

with z_t being the depth of the new datum (target depth). The first term in equation (2.6) represents the response from all depth levels above z_t. The second term represents the response from z_t and the response from below z_t is defined by the third term. Redatuming to the new datum involves correction for the operators $\underset{\sim}{W}^{+}(z_t,z_0)$ and $\underset{\sim}{W}^{-}(z_0,z_t)$ through inverse operators $\underset{\sim}{F}^{+}(z_0,z_t)$ and $\underset{\sim}{F}^{-}(z_t,z_0)$ respectively. The ideal inverse operators are related to the forward operators according to

$$\underset{\sim}{W}^{+}(z_t,z_0)\underset{\sim}{F}^{+}(z_0,z_t) = \underset{\sim}{I} \tag{2.7a}$$

and

$$\underset{\sim}{F}^{-}(z_t,z_0)\underset{\sim}{W}^{-}(z_0,z_t) = \underset{\sim}{I} \ , \tag{2.7b}$$

where $\underset{\sim}{I}$ represents the identity matrix. Application of the inverse matrices to the surface data yields the redatumed data set at z_t

$$\underset{\sim}{Q}(z_t,z_t) = \underset{\sim}{F}^{-}(z_t,z_0)\,\underset{\sim}{Q}(z_0,z_0)\,\underset{\sim}{F}^{+}(z_0,z_t) \ . \tag{2.8a}$$

Substitution of (2.6) in (2.8a) yields

$$\begin{aligned}\underset{\sim}{Q}(z_t,z_t) = {} & \underset{\sim}{F}^{-}(z_t,z_0)\left[\sum_{m=1}^{t-1}\underset{\sim}{W}^{-}(z_0,z_m)\underset{\sim}{R}(z_m)\underset{\sim}{W}^{+}(z_m,z_0)\right]\underset{\sim}{F}^{+}(z_0,z_t) \\ & + \underset{\sim}{F}^{-}(z_t,z_0)\left[\underset{\sim}{W}^{-}(z_0,z_t)\underset{\sim}{R}(z_t)\underset{\sim}{W}^{+}(z_t,z_0)\right]\underset{\sim}{F}^{+}(z_0,z_t) \\ & + \underset{\sim}{F}^{-}(z_t,z_0)\left[\sum_{m=t+1}^{\infty}\underset{\sim}{W}^{-}(z_0,z_m)\underset{\sim}{R}(z_m)\underset{\sim}{W}^{+}(z_m,z_0)\right]\underset{\sim}{F}^{+}(z_0,z_t) \ .\end{aligned} \tag{2.8b}$$

If the macro model is correct, i.e. if relations (2.7) hold, the inverse operators properly correct for the phase and amplitude distortion introduced by propagation of the waves to and from the datum level. So,

after redatuming to z_t there is no residual traveltime from the reflections at z_t. Hence, after redatuming these reflections occur at t=0 (the second term in (2.8b) reduces to $\underset{\sim}{\mathbf{R}}(z_t)$). This very important observation will play a key role in the remainder of this thesis. It should be noted that the macro *densities* only affect the *amplitude* correction, whereas the macro *velocities* affect both the amplitude correction and, more importantly, the *traveltime* correction. Therefore, the macro densities cannot be obtained from traveltime analysis.

Reflections from above the new datum are overcorrected and will after redatuming occur at negative time (first term in (2.8b)). Similarly, reflections from below the new datum will occur at positive times (third term in (2.8b)), but the residual traveltimes are less than the traveltimes observed in the recorded data set. In fact, by leaving out the first term the complete prestack dataset is obtained that would have been recorded if both sources and receivers were located at the new datum z_t. The process described above is called full prestack redatuming or wave equation datuming. It was also described by Berryhill (1984).

The reflection coefficients at z_t can be retrieved through extraction of the zero-time components from the redatumed data set, the so-called *imaging* step. In migration the aim is to extract the reflection coefficients not only at z_t but at all depth points. This can be achieved by redatuming to all depth levels (of interest) followed by imaging. Redatuming, and consequently migration, rely on the accuracy of the inverse extrapolation operators. Only if these are correct the result will be optimum.

Direct inversion of relations (2.7) involves matrix inversions of the forward propagation operators according to

$$\underset{\sim}{\mathbf{F}}^{+}(z_0,z_t) = \left[\underset{\sim}{\mathbf{W}}^{+}(z_t,z_0)\right]^{-1} \tag{2.9a}$$

and

$$\underset{\sim}{\mathbf{F}}^{-}(z_t,z_0) = \left[\underset{\sim}{\mathbf{W}}^{-}(z_0,z_t)\right]^{-1} . \tag{2.9b}$$

However, the inverse operators as defined by (2.9) are unstable for the evanescent wavenumber area. A stable solution is obtained by least-squares inversion according to

$$<\underset{\sim}{\mathbf{F}}^{+}(z_0,z_t)> = \left[\underset{\sim}{\mathbf{W}}^{+}(z_t,z_0)^{*T} \underset{\sim}{\mathbf{W}}^{+}(z_t,z_0) + \varepsilon \underset{\sim}{\mathbf{I}} \right]^{-1} \underset{\sim}{\mathbf{W}}^{+}(z_t,z_0)^{*T} \tag{2.10a}$$

and

$$<\underset{\sim}{\mathbf{F}}^{-}(z_t,z_0)> = \left[\underset{\sim}{\mathbf{W}}^{-}(z_0,z_t)^{*T} \underset{\sim}{\mathbf{W}}^{-}(z_0,z_t) + \varepsilon \underset{\sim}{\mathbf{I}} \right]^{-1} \underset{\sim}{\mathbf{W}}^{-}(z_0,z_t)^{*T} , \tag{2.10b}$$

where * denotes complex conjugation and T denotes matrix transposition. The stabilization is ensured by the term $\varepsilon\underset{\sim}{\mathbf{I}}$, where $|\varepsilon|<<1$. The brackets < > indicate that an approximation is made.

By neglecting the denominator relations (2.10a) and (2.10b) simplify to

$$<\underset{\sim}{\mathbf{F}}^{+}(z_0,z_t)> = \left[\underset{\sim}{\mathbf{W}}^{+}(z_t,z_0) \right]^{*T} \tag{2.11a}$$

and

$$<\underset{\sim}{\mathbf{F}}^{-}(z_t,z_0)> = \left[\underset{\sim}{\mathbf{W}}^{-}(z_0,z_t) \right]^{*T} \tag{2.11b}$$

respectively. This is called the *matched filter* approach (Berkhout, 1982). The matched filter approach states that the inverse propagation operators can be approximated by taking the complex conjugate of the forward propagation operators. Operators (2.11) represent spatially band-limited versions of the exact inverse operators and therefore impose restrictions on the maximum obtainable spatial resolution (Berkhout, 1984). The matched inverse operators are correct for a homogeneous medium within the propagating wavenumber area. For the evanescent wavenumber area the inverse operators are exponentionally decaying.

For an arbitrarily inhomogeneous medium the least squares inversion (2.10) can not be reduced to the matched inverse operators (2.11). Therefore, to obtain simple expressions for the inverse operators in an arbitrarily inhomogeneous medium a different approach must be followed. Before I discuss the inverse operators for an arbitrarily inhomogeneous medium let us first take a closer look at the forward operators. The forward propagation operators are related to the Green's matrices according to

$$\underset{\sim}{W}^{+}(z_t,z_0) = 2\frac{\partial \underset{\sim}{G}^{+}(z_t,z=z_0)}{\partial z}\underset{\sim}{M}^{-1}(z_0) \tag{2.12a}$$

and

$$\underset{\sim}{W}^{-}(z_0,z_t) = -2\frac{\partial \underset{\sim}{G}^{-}(z_0,z=z_t)}{\partial z}\underset{\sim}{M}^{-1}(z_t)\ . \tag{2.12b}$$

Each column of $\underset{\sim}{G}^{+}(z_t,z_0)$ contains the discretized version of a monochromatic downward traveling Green's wave field at z_t, due to a monopole source at z_0. Similarly, each column of $\underset{\sim}{G}^{-}(z_0,z_t)$ contains the discretized version of a monochromatic upward traveling Green's wave field at z_0, due to a monopole source at z_t. The z-derivatives transform the Green's wave fields from monopole responses to dipole responses. Matrices $\underset{\sim}{M}(z_0)$ and $\underset{\sim}{M}(z_t)$ are diagonal matrices, the diagonal elements representing the discretized versions of the densities $\rho(x,y,z_0)$ and $\rho(x,y,z_t)$ respectively. For the Green's matrices the following reciprocity principle is applicable:

$$\underset{\sim}{G}^{+}(z_t,z_0) = \left[\underset{\sim}{G}^{-}(z_0,z_t)\right]^{T}\ . \tag{2.13}$$

This principle holds for an arbitrarily inhomogeneous medium. It can be shown that stable inverse propagation operators are obtained by introducing *backward propagating*[1] Green's wave fields in the Kirchhoff-Helmoltz integral. A derivation of these operators is beyond the scope of this thesis, but the reader is referred to Peels (1988) or to the excellent textbook by Wapenaar and Berkhout (1989). The stabilized (spatially band-limited) inverse propagation operators for an arbitrarily inhomogeneous medium read

$$\langle \underset{\sim}{F}^{+}(z_0,z_t) \rangle = -2 \frac{\partial \underset{\sim}{G}^{-}(z_0,z=z_t)^{*}}{\partial z} \underset{\sim}{M}^{-1}(z_t) \tag{2.14a}$$

and

$$\langle \underset{\sim}{F}^{-}(z_t,z_0) \rangle = 2 \frac{\partial \underset{\sim}{G}^{+}(z_t,z=z_0)^{*}}{\partial z} \underset{\sim}{M}^{-1}(z_0) \ , \tag{2.14b}$$

respectively. The combination of (2.12) and (2.14) yields

$$\langle \underset{\sim}{F}^{+}(z_0,z_t) \rangle = \left[\underset{\sim}{W}^{-}(z_0,z_t) \right]^{*} \tag{2.15a}$$

and

$$\langle \underset{\sim}{F}^{-}(z_t,z_0) \rangle = \left[\underset{\sim}{W}^{+}(z_t,z_0) \right]^{*} \ , \tag{2.15b}$$

---

[1] A backward propagating Green's wave field G^{*} is defined as the complex conjugate of the forward propagating Green's wave field G.

respectively. Note that again the inverse operators are obtained by complex conjugation of forward operators. Wapenaar and Berkhout show that, for the propagating wavenumber area, the operators contain amplitude errors that are proportional to the squared reflectivity of the interfaces between z_0 and z_t. For the phase behavior these operators are exact. Hence, the use of these operators involves amplitude errors that are of the same order as the errors that occur when internal multiple reflections are ignored. For weak to moderate contrasts between z_0 and z_t this approach is justified. For strong contrasts operators (2.15a) and (2.15b) can be modified iteratively. A further discussion is beyond the scope of this thesis.

Equations (2.12) and (2.15) seem to contradict. However, for a homogeneous medium the reciprocity principle (2.13) implies that

$$\underset{\sim}{\mathbf{W}}^{+}(z_t,z_0) = \left[\underset{\sim}{\mathbf{W}}^{-}(z_0,z_t)\right]^{T}, \tag{2.16}$$

and upon substitution in (2.15a) and (2.15b) respectively, the matched inverse operators (2.11a and 2.11b respectively) are obtained.

2.3.2 Shot record redatuming

Equation (2.8) can be split in two parts. The first part is the downward extrapolation of the detectors,

$$\underset{\sim}{\mathbf{Q}}(z_t,z_0) = \underset{\sim}{\mathbf{F}}^{-}(z_t,z_0)\,\underset{\sim}{\mathbf{Q}}(z_0,z_0) \ . \tag{2.17a}$$

After this process the data represent experiments with the virtual detectors located at the new datum z_t, but with the sources still located at the surface z_0. The second part describes the downward extrapolation of the sources from the surface to the new datum,

$$\underset{\sim}{\mathbf{Q}}(z_t,z_t) = \underset{\sim}{\mathbf{Q}}(z_t,z_0)\,\underset{\sim}{\mathbf{F}}^{+}(z_0,z_t) \ . \tag{2.17b}$$

Downward extrapolation of the detectors involves dot products of rows of $\underset{\sim}{\mathbf{F}}^{-}(z_t,z_0)$ and columns of $\underset{\sim}{\mathbf{Q}}(z_0,z_0)$. Since the columns of $\underset{\sim}{\mathbf{Q}}(z_0,z_0)$ represent

shot records, downward extrapolation of detectors can be calculated per shot record. The second step involves dot products of rows of $\underset{\sim}{Q}(z_t,z_0)$ and columns of $\underset{\sim}{F}^{+}(z_0,z_t)$. The rows of $\underset{\sim}{Q}(z_t,z_0)$ represent common receiver gathers and therefore in a straightforward application of equation (2.17b) a reordering into common receiver gathers is required. Especially in 3-D applications this is not even feasible on large computer systems. The reordering is avoided in shot record redatuming, which consists of the following three steps.

If $\mathbf{Q}_j(z_0,z_0)$ represents a column vector containing the j^{th} column of $\underset{\sim}{Q}(z_0,z_0)$, then

$$\mathbf{Q}_j(z_t,z_0) = \underset{\sim}{F}^{-}(z_t,z_0)\,\mathbf{Q}_j(z_0,z_0) \tag{2.18a}$$

defines downward extrapolation of the detectors per shot record $\mathbf{Q}_j(z_0,z_0)$, $j=1,2,\cdots,n$. This first step is essentially the same as in full prestack redatuming (cf. equation 2.17a). The second step involves correction (deconvolution) for the incident source wave field. If $\mathbf{H}_j(z_0,z_t)$ represents a column vector containing the j^{th} *row* of matrix $\underset{\sim}{F}^{+}(z_0,z_t)$ (see also Figure 2.4), then this deconvolution process can be written as

$$<\underset{\sim}{Q}(z_t,z_t)>_j = \mathbf{Q}_j(z_t,z_0)\left[\mathbf{H}_j(z_0,z_t)\right]^T, \tag{2.18b}$$

where T denotes transposition of the column vector into a row vector. Note that $<\underset{\sim}{Q}(z_t,z_t)>_j$ represents a matrix.

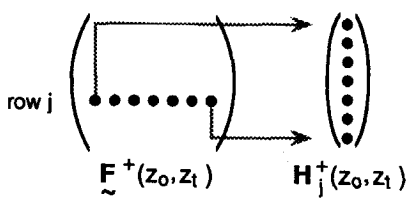

Figure 2.4
$\mathbf{H}_j(z_0,z_t)$ represents a column vector containing the j^{th} *row* of matrix $\underset{\sim}{F}^{+}(z_0,z_t)$.

Equations (2.18a) and (2.18b) yield a single shot redatumed result for shot j. Note that the depth point is illuminated from one direction which depends on the shot location at the surface. In Figure 2.5a this is schematically shown for one depth point.

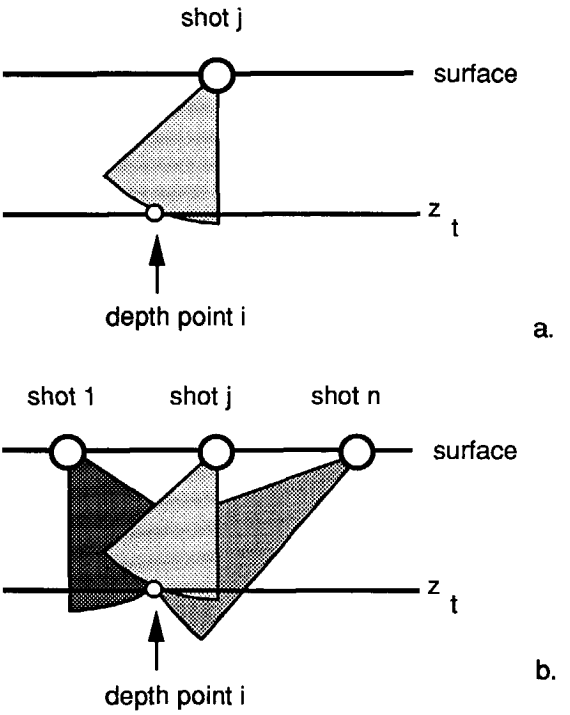

Figure 2.5

a. Depth point i is illuminated by shot j from one direction.

b. More shot records are needed to build an omnidirectional source at depth point i.

By superposition of all single shot redatumed results (third step),

$$\underset{\sim}{Q}(z_t,z_t) = \sum_{j=1}^{n} \langle \underset{\sim}{Q}(z_t,z_t) \rangle_j \ , \qquad (2.18c)$$

the complete redatumed data set at the new datum is obtained, which is exactly the same as would have been obtained through full prestack redatuming. The summation process (2.18c) is called Common Depth Point (CDP-)stacking and should not be confused with Common Mid Point stacking. Here all information that is related to one depth point in the subsurface is summed, whereas in CMP-stacking the information related to one midpoint location at the surface is summed.

In imaging applications, like migration, the redatumed data are obtained at zero offset only. In that case only the elements on the main diagonal of the matrices $<\underset{\sim}{Q}(z_t,z_t)>_j$ need to be calculated according to

$$<Q_{ii}(z_t,z_t)>_j = Q_{ij}(z_t,z_0)\, F^{+}_{ji}(z_0,z_t) \quad , \tag{2.19}$$

where $F^{+}_{ji}(z_0,z_t)$ is element i of row j of matrix $\underset{\sim}{F}^{+}(z_0,z_t)$, $Q_{ij}(z_t,z_0)$ is element i of vector $Q_j(z_t,z_0)$, and i denotes depth point i.

CDP-gathers

Consider a depth point located on a reflector (Figure 2.6). Redatuming of one shot record to the depth point in the subsurface results in one CDP-trace. If the macro model used in redatuming is correct, then an event will occur at t=0, since the upward and downward propagation between the surface and the depth point have been properly corrected for. Before CDP-stacking the CDP-traces related to the depth point can be gathered in a so-called Common Depth Point gather (Figure 2.7). The dimensions of a CDP-gather are shot number versus time. In each CDP-trace an event

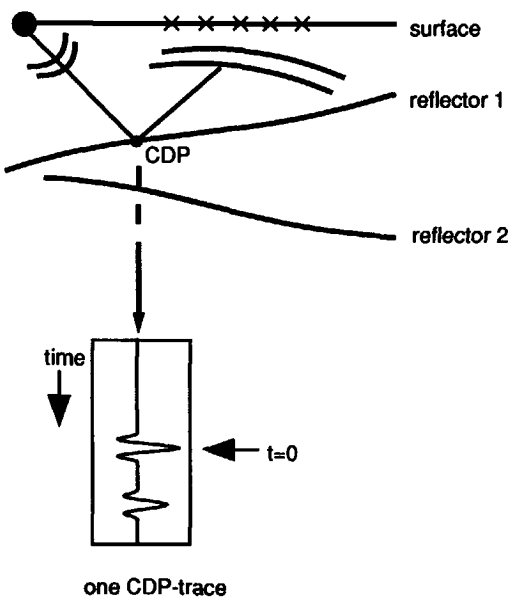

Figure 2.6
Redatuming of one shot record to one depth point in the subsurface yields one CDP-trace.

occurs at t=0, i.e. provided that the macro model is correct. This yields horizontal alignment in the CDP-gather. Note that the alignment is irrespective of the dip and curvature of the interface and of the complexity of the overburden.

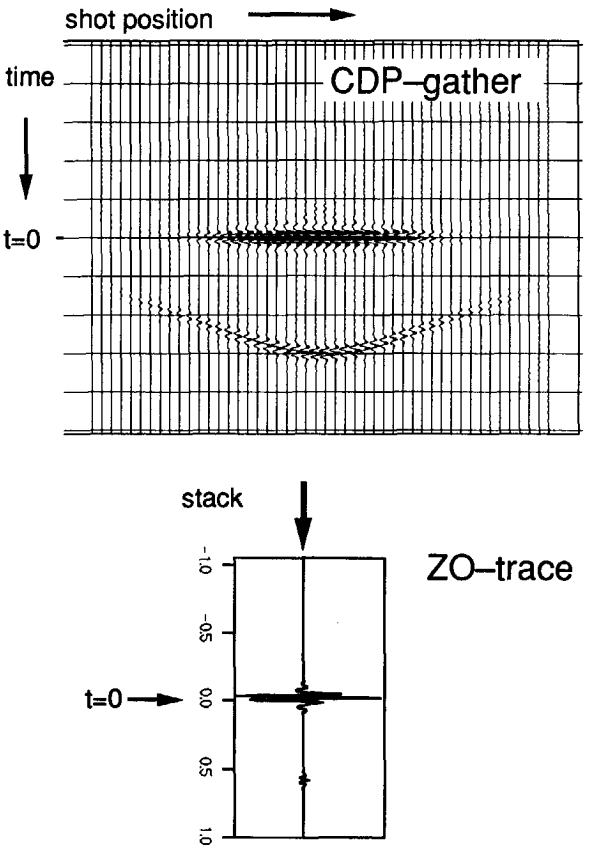

Figure 2.7
A CDP-gather consists of the CDP-traces at one depth point due to many redatumed shot records. Summation of the traces (CDP-stacking) yields a true zero offset trace at the considered depth point.

CDP-gathers have no physical meaning, but nevertheless they play an important role in estimating the macro model. As will be shown in Chapter 4 alignment analysis of CDP-gathers is used in the macro model estimation procedure. One-way of measuring the alignment is by means of CDP-stacking, i.e. by a simple summation of all traces in a CDP-gather (Figure 2.7b). In each CDP-trace the virtual detector is already located at

the depth point. Besides that, there has been corrected for the incident wave field as well. By the summation process a virtual omnidirectional source is constructed at the depth point by the contributions from all sources at the surface. This is visualized by Figure 2.5b. So, by CDP-stacking a true zero offset trace is obtained (Berkhout, 1984; Kinneging et al., 1989). If the depth point is located at a macro boundary and if the macro model is correct, the amplitude in the zero offset trace will be maximum due to the alignment in the CDP-gather. This is in accordance with the physical interpretation of the ZO-trace: on top of an interface the highest amplitude is obtained since no geometrical spreading has yet occurred. Note also that the two-way traveltime of such a ZO-trace equals zero.

2.3.3 Recursive versus non-recursive extrapolation

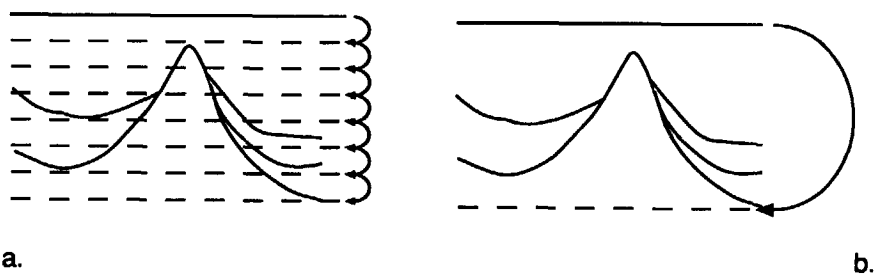

Figure 2.8
a. Recursive extrapolation.
b. Non-recursive extrapolation.

The redatuming process can be performed by extrapolation from one depth level to the next, as is shown in Figure 2.8a. This is called recursive extrapolation. For homogeneous media large extrapolation steps can be taken. The operators can be calculated analytically which is done very fast. By taking small extrapolation steps an inhomogeneous medium can be considered as locally homogeneous within the operator range. However, with decreasing extrapolation steps the spatial bandwidth of the operator increases and operator aliasing becomes a serious problem to cope with. Blacquière (1989) developed a method to design alias-free operators which are filtered versions of the analytic operators.

Recursive extrapolation involves repeated matrix multiplications which is computationally intensive. Inverse extrapolation operator $\underset{\sim}{\mathbf{F}}^{-}(z_t,z_0)$ is calculated using the (recursive) expression

$$\underset{\sim}{\mathbf{F}}^{-}(z_t,z_0) = \underset{\sim}{\mathbf{F}}^{-}(z_t,z_{t-1})\underset{\sim}{\mathbf{F}}^{-}(z_{t-1},z_0) \ , \tag{2.20}$$

where $\underset{\sim}{\mathbf{F}}^{-}(z_t,z_{t-1})$ is the inverse extrapolation operator from $z_{t-1}$to z_t.

All intermediate levels (computional levels) have to be flat in order to be able to use the Rayleigh integral rather than the Kirchhoff integral. Furthermore, the depth points should be properly sampled at each intermediate level to avoid spatial aliasing.

Non-recursive extrapolation transforms the wave field at the surface into a wave field at the new depth points in the subsurface in one pass (Figure 2.8b). For inhomogeneous media it is not possible to calculate the extrapolation operators analytically, since now the medium can no longer be considered homogeneous within the operator range. Therefore, the inverse operators (backward propagating Green's functions) need to be modeled. If accurate amplitudes for the Green's functions are required, the modeling can be done by finite difference or finite element modeling, which are relatively slow algorithms. If the main interest is to obtain correct traveltimes the efficient raytracing method would be more suitable (Kinneging, 1989). In non-recursive extrapolation the wave field can be calculated at any depth point in the subsurface. The depth points do not have to be related. So, there is no need for the depth point to be located on a flat datum, nor is it required that the depth points satisfy the anti-aliasing conditions imposed by recursive redatuming. Of course, the surface data do have to obey the anti-aliasing conditions. If further processing is needed the data at the new datum must suffice the demands for further processing and be alias-free too.

Which would be the best suited type of extrapolation depends on the objective. In migration a reflectivity image of the subsurface is calculated at many depth points in the subsurface. So recursive extrapolation is appropriate in this case. In redatuming the surface data are extrapolated to one new datum and non-recursive extrapolation is more appropriate.

CHAPTER 3

AN OVERVIEW OF EXISTING MACRO MODEL ESTIMATION TECHNIQUES

3.1 INTRODUCTION

In this chapter I will give an overview of a number of existing macro model estimation techniques. Without claiming completeness this chapter covers most of the estimation techniques that are in use in current seismic processing. Two classes of techniques may be distinguished, depending on the type of data that is used in the estimation procedure:

1. *Midpoint-oriented macro model estimation*
   Conventional velocity analysis techniques use the traveltimes (versus offset) in *surface* data for the estimation of velocities. Generally, these techniques require a reordering of the surface data into CMP-gathers. I will refer to these methods as midpoint-oriented, the midpoint being located at the surface.
2. *Depth point-oriented macro model estimation*
   In recent years a new class of estimation procedures has been developed, that utilize wave field extrapolation techniques. By wave field extrapolation it is possible to obtain data related to a *depth* point in the subsurface (CDP-gathers). I will refer to these methods as depth point-oriented, the depth point (also referred to as subsurface grid point) being located in the subsurface.

This chapter is divided into two sections according to the subdivision made above. Section 3.2 deals with the conventional midpoint-oriented techniques and in section 3.3 the depth point-oriented techniques are discussed.

3.2 MIDPOINT-ORIENTED MACRO MODEL ESTIMATION

The conventional velocity analysis methods are based on the moveout observed in CMP-gathers. Before discussing these methods, I will first describe some basic concepts that need to be used.

3.2.1 Introduction

1. One horizontal interface

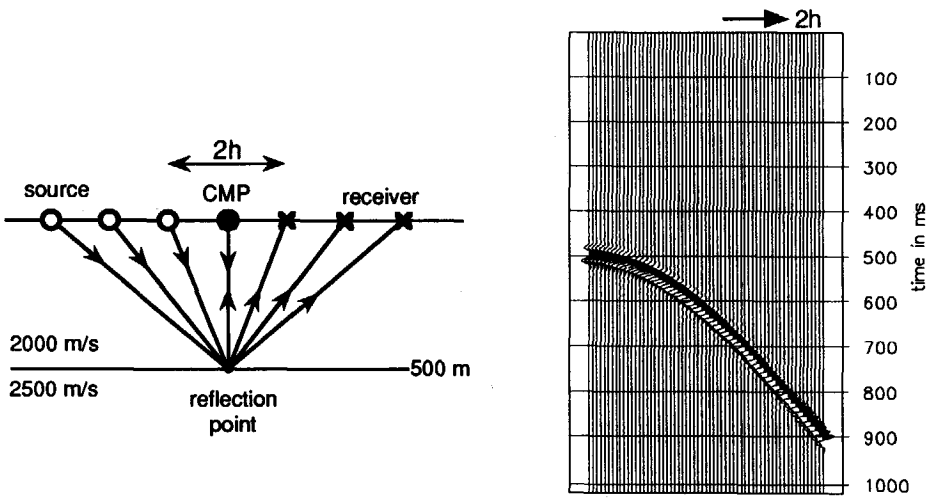

Figure 3.1

a. Model containing one plane horizontal interface, which separates two layers with different velocities.

b. CMP-gather simulated for the model shown in Figure 3.1a.

Consider the model shown in Figure 3.1a. It contains one plane horizontal interface, which separates two layers that have different velocities. A CMP-gather simulated for this model is shown in Figure 3.1b. Note that all CMP-gathers at different midpoint locations will be exactly the same as the one shown (apart from different noise realizations), because the

medium is laterally invariant. Each CMP-trace contains an event due to reflection of the incident source wave field. It follows from simple geometric considerations (Pythagorean theorem) that the two-way traveltime at offset 2h, is related to the velocity of the first layer according to

$$T^2(h) = T^2(o) + \frac{(2h)^2}{c^2}, \tag{3.1a}$$

where c is the interval velocity in the first layer, where the symbol h is used for *half* the source-receiver distance and where T(h) represents the two-way traveltime of the reflection event at offset 2h. In addition,

$$T(o) = \frac{2z}{c}, \tag{3.1b}$$

with z being the reflector depth, is called the zero offset (ZO-)traveltime. Note that for this simple subsurface model relations (3.1) are exact. All data in the CMP-gather are related to a single reflection point that is located vertically below the midpoint. The traveltime versus offset relation as defined by (3.1) represents a hyperbola, its asymptote being determined by the velocity in the first layer: $T(h) = 2h/c$ for $h \rightarrow \infty$.

Normal moveout correction and stacking

The deviation between the ZO-traveltime and the offset traveltimes is called normal moveout (NMO). After correction for this moveout the reflections in the offset traces are horizontally aligned at the *zero* offset traveltime T(o). The NMO correction is given by the difference between T(h) and T(o):

$$T_{nmo}(h) = T(h) - T(o)$$

$$= T(o)\left\{\sqrt{1 + \left(\frac{2h}{cT(o)}\right)^2} - 1\right\}. \tag{3.2}$$

After NMO correction the (moveout corrected) CMP-traces are generally stacked. The stacked trace simulates the zero offset trace with enhanced signal-to-noise ratio.

The NMO correction depends on the zero offset traveltime T(o) and on the velocity c. In practice, both T(o) and c are unknown. Therefore the NMO correction is made time dependent by replacing traveltime T(o) by variable t(o). In addition, the NMO correction is applied for a range of velocities v:

$$T_{nmo}(h,v,t(o)) = t(o)\left\{\sqrt{1+\left(\frac{2h}{vt(o)}\right)^2}-1\right\}, \tag{3.3}$$

yielding a 3-D data volume as a function of h, v and t(o).

When the correct velocity is used in the NMO correction, the hyperbola is completely flattened (Figure 3.2a). When too high a velocity is used, the hyperbola is not completely flattened resulting in undercorrection of the traveltimes (Figure 3.2b). Overcorrection occurs if too low a velocity is used in the NMO correction (Figure 3.2c). Since T_{nmo} is a function of t(o), a time dependent stretch of the wavelet occurs, as can be observed in the moveout corrected CMP-gathers.

Semblance, stacking velocity

By inspection or by measuring the alignment, the correct velocity can be obtained for a given t(o). The best known coherence measure used in this respect is the *semblance coefficient* (Taner and Koehler, 1969), which is defined as

$$S(k) = \frac{1}{M}\frac{\sum_{j=k-N}^{k+N}\left(\sum_{i=1}^{M} p_{ij}\right)^2}{\sum_{j=k-N}^{k+N}\sum_{i=1}^{M}(p_{ij})^2}, \tag{3.4}$$

where p_{ij} is the j^{th} sample of the i^{th} trace in the moveout corrected CMP-gather and M represents the number of traces.

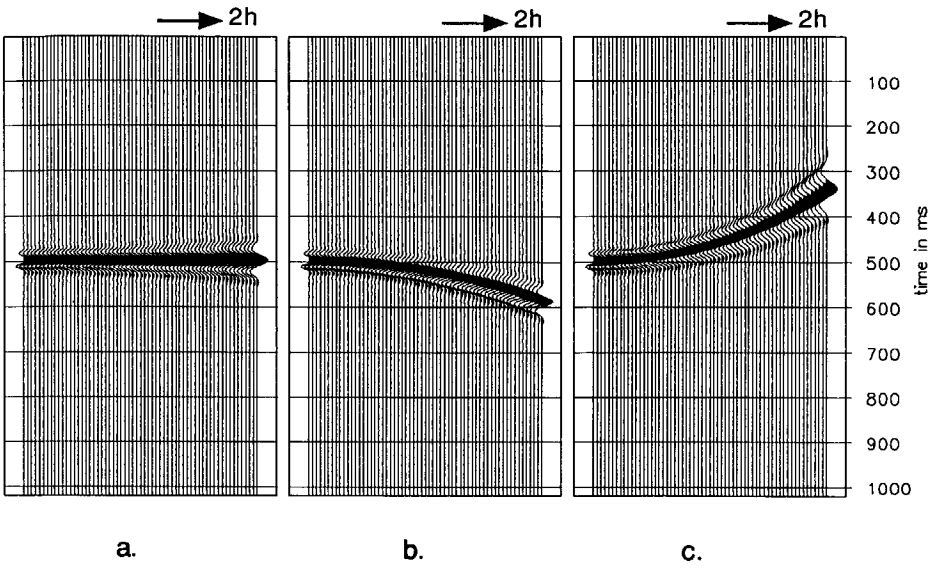

Figure 3.2

a. CMP-gather which is NMO corrected with the correct velocity (v = 2000 m/s).
b. CMP-gather which is NMO corrected with too high a velocity (v = 2200 m/s).
c. CMP-gather which is NMO corrected with too low a velocity (v = 1800 m/s).

The semblance coefficient is evaluated for a time window of length $2N\Delta t$ centered at traveltime $t(o)=k\Delta t$, where Δt is the time sampling interval. It represents the energy of the stacked trace in a window, normalized by the total energy in the individual traces. The denominator can be related to the correlation sum; for a derivation of this relation the reader is referred to Yilmaz (1987).

For each velocity one semblance *trace* can be produced as a function of time t(o). A semblance *panel* is obtained as a function of v (horizontal axis) and t(o) (vertical axis) by gathering all semblance traces. Figure 3.3 shows the semblance panel, for the example of Figure 3.1, after contouring. When the correct velocity/time pair is used, the lateral coherence is optimum and the semblance will have a high value. By picking the 'focus' from the semblance panel the parameter combination of velocity and time that best aligns the event in the CMP-gather is extracted. These parameters are called *stacking time* (T_{st}) and *stacking velocity* (V_{st}), respectively. Note that in this simple situation the stacking velocity equals the interval velocity of the first layer ($V_{st}=c$) and the stacking time equals the zero offset time ($T_{st}=T(o)$).

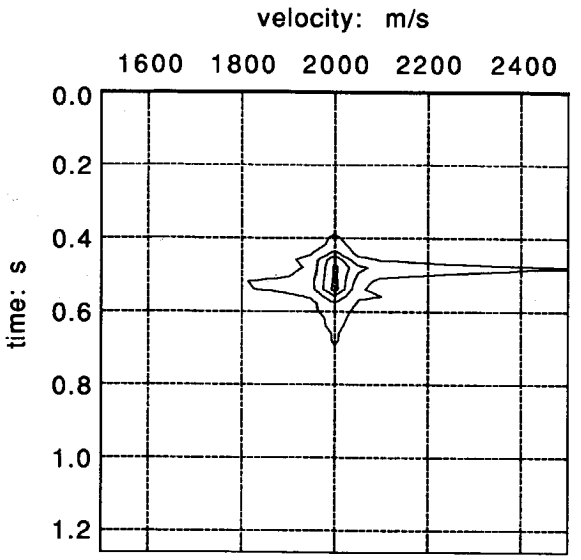

Figure 3.3
CMP-oriented velocity spectrum (semblance panel) from the model of Figure 3.1a. The length of the moving time window was 40 ms.

Residual normal moveout correction

Suppose an initial moveout correction has been applied with a slightly erroneous stacking velocity $\hat{V}_{st} \neq c$. Then the NMO corrected CMP data still exhibits some residual moveout, which (for small errors) may be approximated by a first order Taylor series expansion according to

$$\Delta T_{nmo} = T(h) - T_{nmo}\left(h, \hat{V}_{st}, T(o)\right) \approx T(o) + \frac{2h^2}{T(o)} \left(\frac{1}{c^2} - \frac{1}{\hat{V}_{st}^2}\right) . \qquad (3.5)$$

Note that the remaining moveout is approximated by a *parabolic* relation. The removal of this residual moveout is called *residual NMO correction.*

2. One dipping interface

For one plane dipping interface (Figure 3.4a) the moveout curve can be described by

$$T^2(h) = T^2(o) + \frac{(2h)^2}{(c/\cos\beta)^2} \quad , \tag{3.6a}$$

where β is the angle between the zero offset ray emerging at the surface and the normal to the surface. Note that, for this simple situation, the angle β is equal to the dip angle α of the reflector. Figure (3.4a) shows that the reflections in the CMP-gather occur at different reflection points; this is called reflection point smear. As can be seen from equation (3.6a) and from Figure 3.4b, the traveltime curve is still hyperbolic. For this situation the (dip dependent) stacking velocity amounts to

$$V_{st} = c/\cos\beta \quad . \tag{3.6b}$$

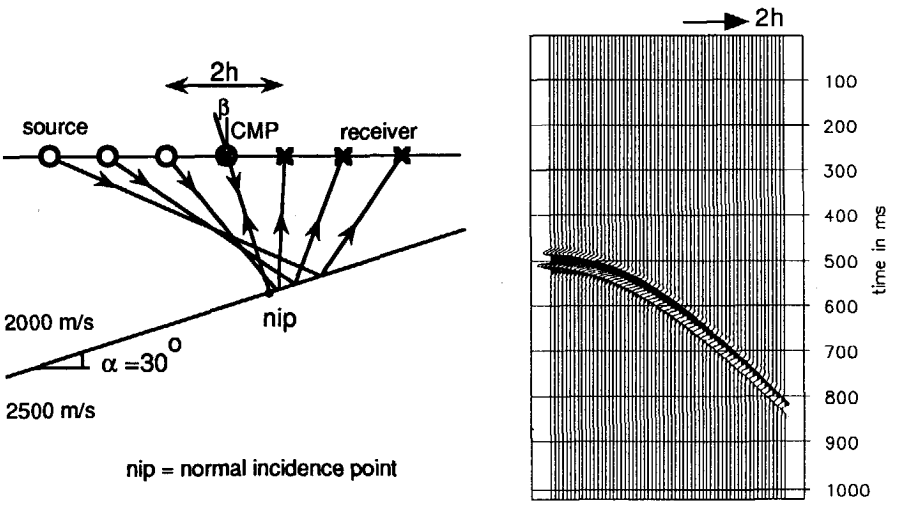

a. b.

Figure 3.4

a. Model containing one plane dipping interface, which separates two layers with different velocities.

b. CMP-gather simulated for the model shown in Figure 3.4a.

Equation 3.6 can be obtained by replacing h in (3.1a) by hcosβ. The validity of this substitution can be proven by inspection of Figure 3.5.

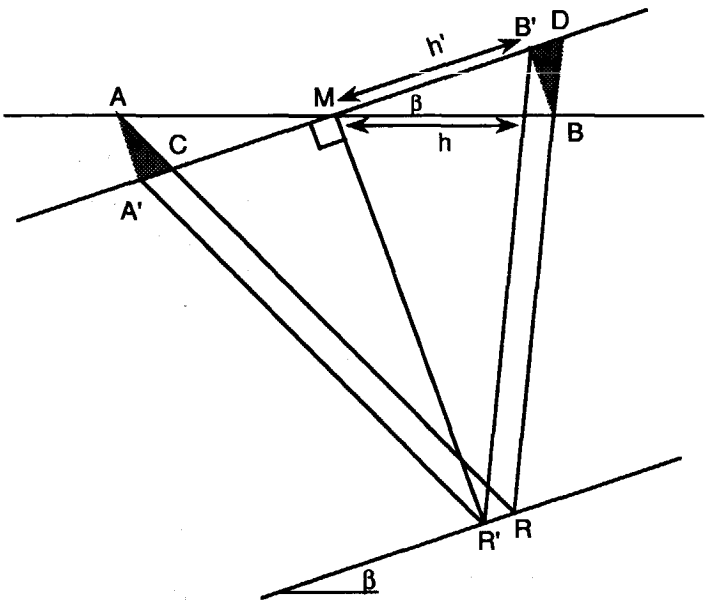

Figure 3.5
CMP configuration for a dipping acquisition level (angle β) and for a horizontal aquisition level.

Suppose the CMP data would be measured at a dipping acquisition level perpendicular to the zero offset ray. Then the traveltime of the reflection event measured by a detector at B' due to a source at A' is described by (cf. equation (3.1a))

$$T^2(h') = T^2(o) + \frac{(2h')^2}{c^2} , \tag{3.7}$$

where 2h' is the distance from A' to B'. Let A be the projection of A' on the horizontal acquisition surface. Similarly, let B be the projection of B'. Then it can be derived from Figure (3.5) that

$$AM = MB = h'/\cos\beta \hat{=} h . \tag{3.8}$$

where 2h is the distance from A to B. A and B define the source position and receiver position, respectively, of the actual CMP-trace. The traveltime of the reflection event measured by the receiver at B due to the source at A may be obtained by shifting the triangle A'R'B' along the

h'-axis towards CRD such that A lies on the line through R and C, and B lies on the line through R and D. Then,

$$CR + RD = A'R' + R'B' \quad , \tag{3.9}$$

or in terms of traveltimes:

$$T_{CR} + T_{RD} = T_{A'R'} + T_{R'B'} \quad , \tag{3.10}$$

where the subscripts denote the path along which the traveltime is measured. Since $T_{AC} = T_{BD}$ relation (3.10) may be rewritten as:

$$T(h) \hat{=} T_{AR} + T_{RB} = T_{A'R'} + T_{R'B'} \hat{=} T(h') \quad , \tag{3.11}$$

Because of (3.8) and (3.11) equation (3.7) may be replaced by

$$T^2(h) = T^2(o) + \frac{(2h \cos \beta)^2}{c^2} \quad , \tag{3.12}$$

yielding equation (3.6a). Hence, the velocity parameter that describes the moveout in a CMP-gather depends on the angle of the normal ray with respect to the acquisition surface.

Note that the reflection recorded by B is related to the reflection point R, which is shifted with respect to R' (reflection point smear). Again from the figure we may derive

$$\frac{A'C}{A'A} = \frac{MA'}{MR'} \tag{3.13}$$

Furthermore,

$$\begin{aligned} A'C &= R'R \\ A'A &= h \sin \beta \\ MA' &= h \cos \beta \\ MR' &= cT(o)/2 \quad . \end{aligned} \tag{3.14}$$

Upon substitution of relations (3.14) into (3.13) we obtain

$$\frac{RR'}{h\sin\beta} = \frac{h\cos\beta}{cT(o)/2} \tag{3.15}$$

Hence, the reflection point smear amounts to

$$RR' = \frac{2h^2 \sin\beta\cos\beta}{cT(o)} = \frac{h^2 \sin 2\beta}{cT(o)} \tag{3.16}$$

3. Arbitrarily layered system

For an arbitrarily layered system (Figure 3.6), the traveltime function in the CMP-data may be written as an infinite MacLaurin series (Durbaum,1954):

$$T_N^2(h) = \sum_{k=0}^{\infty} A_{N,k}(2h)^k \,, \tag{3.17}$$

where 2h is the source-receiver distance (offset) and $T_N(h)$ is the traveltime of a seismic pulse reflected by the N^{th} interface in the system. The coefficients $A_{N,k}$ are related to layer thicknesses, interval velocities and reflector shapes. By interchanging sources and receivers in a CMP-gather the observed traveltimes remain the same. Consequently, the traveltime function is symmetric around the midpoint location.

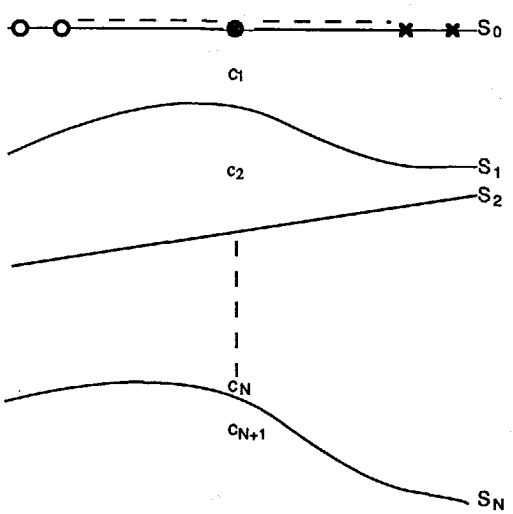

Figure 3.6
Arbitrarily layered system containing curved interfaces.

Hence, it should be an even function of the offset parameter h. Therefore, for CMP configurations the coefficients $A_{N,k}$ are zero for odd values of k. In general, the moveout curve no longer represents a hyperbola, because of the higher order terms present in equation (3.17).

NMO velocity

For one horizontal reflector only the coefficients $A_{1,0}$ and $A_{1,2}$ are non-zero and relation (3.17) reduces to relation (3.1). For a horizontally layered system Dix (1955) approximated the MacLaurin series by a hyperbolic relation (neglecting terms of $O(h^4)$ and higher):

$$T_N^2(h) \approx T_N^2(o) + \frac{4h^2}{V_{nmo,N}^2} \quad , \tag{3.18}$$

where $V_{nmo,N}$ is called the NMO velocity for reflector N and $T_N(o)$ is the zero offset two-way traveltime to this reflector. Equation (3.18) is a *small offset approximation*. It states that, for small offsets, the N^{th} traveltime curve in a CMP-gather may be approximated by a hyperbola, its moveout being defined by $V_{nmo,N}$.

The NMO velocity between the surface and the N^{th} reflector is related to the interval velocities of all overlying layers by (Dix, 1955):

$$V_{nmo,N}^2 = \sum_{n=1}^{N} c_n^2 \, \Delta T_n \Big/ \sum_{n=1}^{N} \Delta T_n \quad , \tag{3.19}$$

where c_n is the interval velocity in layer n, and

$$\Delta T_n = 2\frac{z_n - z_{n-1}}{c_n} \tag{3.20}$$

is the two-way vertical traveltime in layer n; z_{n-1} and z_n are the upper and lower boundary of layer n, respectively.

The NMO velocity, which determines the second coefficient of the MacLaurin series, does not always account best for the observed moveout, i.e. in the general case of an arbitrarily layered medium the NMO velocity

and the stacking velocity, which is related to the best-fit hyperbola, are not exactly equal. The equality only holds when the moveout is hyperbolic. Note that the right-hand side of (3.19) defines an rms velocity ($V_{rms,N}$). Hence, for horizontally layered systems, the NMO velocity equals the rms velocity.

Wavefront curvature

It is interesting to see that the NMO velocity observed in CMP data is related to the radius of curvature of a (hypothetical) spherical wavefront originating from the normal incidence reflection point and emerging at the surface. Suppose the acquisition surface is perpendicular to the normal incidence ray (Figure 3.7a).

The NMO velocity (denoted by $V_{\perp\,nmo,N}$) observed in a CMP-gather recorded perpendicular to the normal ray may be expressed in terms of the wavefront curvature by (Hubral,1976)

$$R_N = \frac{V_{\perp\,nmo,N}^2 \, \frac{T_N(o)}{2}}{c_1}, \tag{3.21}$$

where R_N is the radius of the curvature of the wave at the midpoint location, c_1 is the velocity in the top layer, $T_N(o)/2$ denotes the one-way zero offset traveltime to reflector N and $V_{\perp\,nmo,N}$ represents the NMO velocity of the N^{th} reflection. Note that the recorded traveltimes of a spherical wave are defined by a hyperbola.

In general the acquisition level is not perpendicular to the normal ray (Figure 3.7b). Similar to the situation of a single plane dipping layer, the NMO velocity observed in a CMP-gather recorded along the horizontal surface differs from the NMO velocity mentioned above by a factor $\cos\beta_0$,

$$V_{nmo,N} = \frac{V_{\perp\,nmo,N}}{\cos\beta_0}, \tag{3.22}$$

where β_0 is the angle at which the normal ray approaches the surface. The wavefront curvature, however, does not change by tilting the acquisition level. Therefore, relation (3.21) becomes

$$R_N = \frac{\cos^2\beta_0 V^2_{nmo,N}\,(T_N(o)/2)}{c_1}\ , \tag{3.23}$$

where $V_{nmo,N}$ is the NMO velocity observed in the actual CMP-gather recorded along the surface.

For a single plane dipping reflector relation (3.21) reduces to

$$R_1 = c_1 T_1(0)/2\ . \tag{3.24}$$

For a two-dimensional model consisting of plane dipping layers the wavefront curvature is related to the medium parameters by (Shah, 1973):

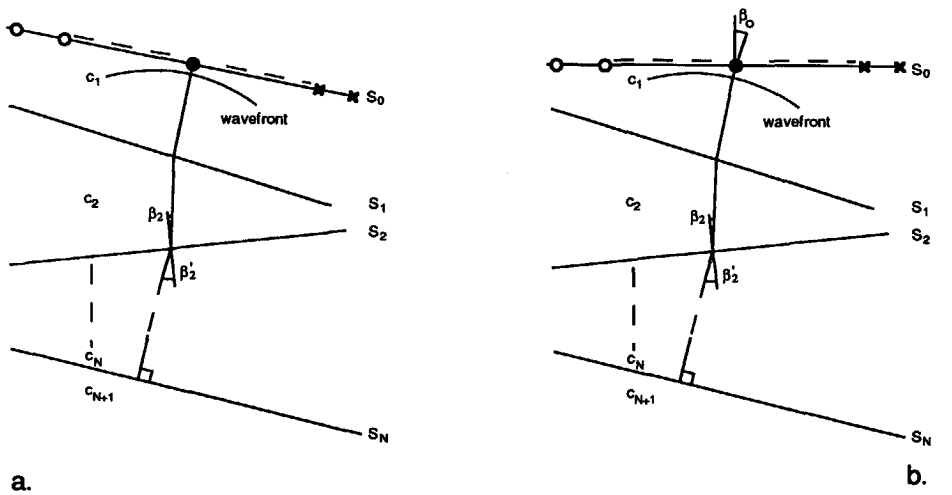

Figure 3.7
The NMO velocity is related to the curvature of the wavefront emerging at the midpoint due to a source located at the normal incidence reflection point .

a. When the acquisition level is perpendicular to the normal ray, the wavefront curvature is defined by (3.21).

b. When the acquisition level is not perpendicular to the normal ray, the wavefront curvature is defined by (3.23).

$$R_N = \frac{1}{c_1} \sum_{n=1}^{N} \gamma_n c_n^2 \Delta T_n/2 \ , \tag{3.25}$$

where γ_n is defined by

$$\gamma_n = \prod_{k=0}^{n-1} \frac{\cos^2\beta_k}{\cos^2\beta_k'} \ , \text{ with } \beta_o \triangleq \beta_o' \ .$$

β_k denotes the incidence angle of the zero offset ray on interface k, β_k' denotes the transmission angle at interface k and $\Delta T_n/2$ denote the one-way traveltime of the zero offset ray in layer n. So, by combining equations (3.23) and (3.25), the observed quantities $V_{nmo,N}$ and $T_N(o)$ can be related to the medium parameters, yielding

$$V_{nmo,N}^2 = \frac{1}{\cos^2\beta_o} \sum_{n=1}^{N} \gamma_n c_n^2 \Delta T_n \Big/ \sum_{n=1}^{N} \Delta T_n \ . \tag{3.26}$$

Special cases:

If the model is horizontally layered angles β_k and β_k' are zero for all values of k, and (3.26) reduces to the expression obtained by Dix (cf. equation (3.19)).

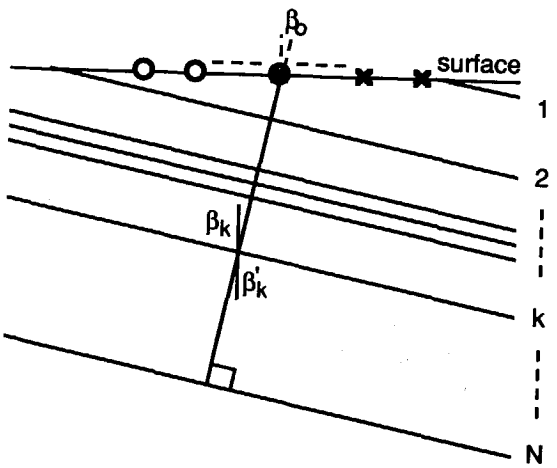

Figure 3.8
Subsurface consisting of a plan parallel system of dipping layers.

For a subsurface consisting of a plan parallel system of dipping layers (Figure 3.8) angles β_k and β_k' are equal. Hence, $\gamma_n = 1$ and equation (3.26) becomes

$$V^2_{nmo,N} = \frac{1}{\cos^2\beta_o} \sum_{n=1}^{N} c_n^2 \Delta T_n \Big/ \sum_{n=1}^{N} \Delta T_n \ ,$$

which is the dip-corrected version of equation (3.19).

Velocity analysis in the τ,p-domain

An appealing approach to velocity analysis on CMP-data is based on τ,p mapping, among others described by Diebold and Stoffa (1981). In this method CMP-data in the traveltime/offset (t,h)-domain are mapped into the intercept-time/ray-parameter (τ,p)-domain where the velocity analysis is performed. For horizontally layered media, the *approximate* hyperbolas in (t,h) coordinates are transformed into *exact* ellipses in (τ,p) coordinates. A discussion of (τ,p) velocity analysis is beyond the scope of this thesis.

Dip moveout

As can be seen from equation (3.6), stacking velocities depend on reflector dips. This implies that the NMO correction applied in the stacking process is *dip selective*. Furthermore, *reflection point smear* occurs for dipping reflectors. As a consequence, in conventional CMP stacking, reflection events related to different reflection points, are stacked. To overcome these problems, it is preferred to remove the dip dependency from the CMP data before velocity analysis and stacking.

Consider the simple subsurface shown in Figure 3.9a. The corresponding CMP-gather contains two moveout curves. The traveltimes in both moveout curves are equal at the indicated offset.

NMO correction for the horizontal reflector would correct the offset traveltime from T(h) to T_0(o) according to

$$T_0^2(o) = T^2(h) - \frac{(2h)^2}{c^2}, \qquad (3.27a)$$

and the resulting trace is positioned correctly at the surface point M. Equation (3.27a) represents the *zero-dip* NMO correction, which is indicated by the subscript "o" in $T_0(o)$.

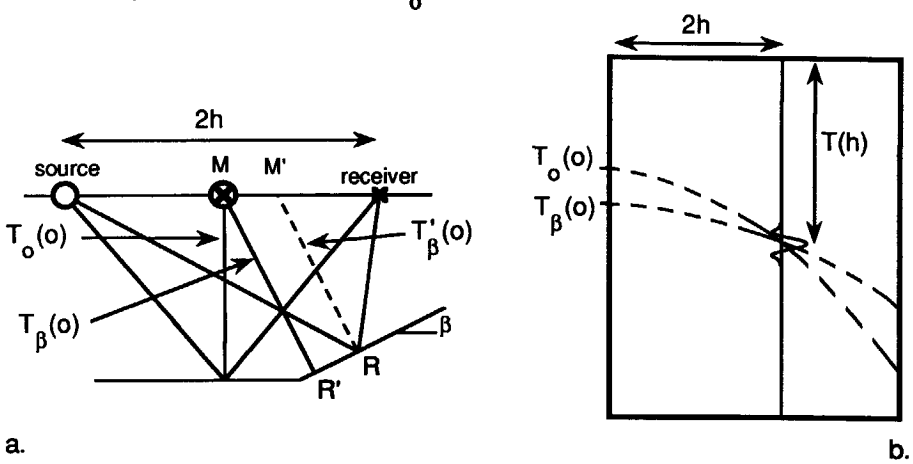

Figure 3.9

a. Simple subsurface geometry containing a horizontal and a dipping reflector. Note that an offset-dependent reflection point smear occurs for the dipping reflector.

b. The traveltimes in both moveout curves are equal at the indicated offset. Zero-dip NMO corrects the offset traveltime T(h) to the zero offset traveltime $T_0(o)$ and positions the result at the surface point M, which is incorrect for a dipping reflector.
DMO correction has two effects:
Firstly, it removes the residual moveout related to the reflector dip. This involves a traveltime correction from $T_0(o)$ to $T\beta(o)$. Secondly, the resulting trace is mapped to the correct zero offset position. This involves an additional traveltime correction from $T\beta(o)$ to $T'_\beta(o)$.

NMO correction for the dipping reflector would correct the offset traveltime from T(h) to $T_\beta(o)$ according to

$$T_\beta^2(o) = T^2(h) - \frac{(2h)^2}{(c/\cos\beta)^2} \qquad (3.27b)$$

and in CMP processing the resulting trace is erroneously positioned at M. Equation (3.27b) represents the NMO correction related to the dipping reflector, which is indicated by the subscript "β" in $T_\beta(o)$. Since the offset traveltime is related to reflection point R the moveout corrected trace should be positioned at M', where

$$MM' = RR'/\cos\beta = \frac{2h^2 \sin\beta}{cT_\beta(o)} \tag{3.28a}$$

and where RR' is the reflection point smear (cf. equation (3.16)). This also means that an additional traveltime correction is needed according to

$$T'_\beta(o) = T_\beta(o) - \frac{2\,RR'tg\beta}{c} = T_\beta(o) - \frac{4h^2 \sin^2\beta}{c^2\,T_\beta(o)}\,. \tag{3.28b}$$

$T'_\beta(o)$ represents the zero offset traveltime to the reflection point R.

Equation (3.27b) can be split into a dip-independent and a dip-dependent part according to

$$T^2_\beta(o) = T^2(h) - \frac{(2h)^2}{c^2} + \frac{(2h)^2}{c^2}\sin^2\beta\,, \tag{3.29a}$$

which is equivalent to

$$T^2_\beta(o) = T^2_o(o) + \frac{(2h)^2}{c^2}\sin^2\beta\,. \tag{3.29b}$$

The first part of the moveout (second term in the right-hand side of (3.29a)) is associated with the zero-dip NMO, while the second part is the moveout related to the reflector dip (third term in (3.29a)). This term is known in the literature as the DMO-term (Dip MoveOut), which is somewhat misleading; DMO not only corrects for the residual moveout, as is suggested by equation (3.29b), but DMO also maps the resulting trace to its correct surface position.

Summarizing,

1. Zero-dip NMO correction removes the moveout for zero-dip. This involves a traveltime correction from T(h) to $T_0(o)$. The result is positioned at the midpoint location M.
2. DMO corrects for two effects:
   Firstly, it removes the residual moveout related to the reflector dip. This involves a traveltime correction from $T_0(o)$ to $T_\beta(o)$. Secondly, the resulting trace is mapped to the correct zero offset position. For the source-receiver pair shown in Figure 3.9a the trace is mapped from M to M'. This involves an additional traveltime correction from $T_\beta(o)$ to $T'_\beta(o)$. The procedure removes the *reflection point smear* and introduces a desired *midpoint smear*. Hence, by applying DMO the data in one CMP-gather are redistributed into neighboring CMP-gathers.

Before applying DMO, the data need to be NMO corrected with the zero-dip NMO velocities. These velocities are not known, since dip dependencies are still present. Hence, the procedure is as follows:

1. Apply an NMO correction (for all offsets), using initial zero-dip stacking velocities, according to (3.27a).
2. Apply a multi-dip DMO correction for all offsets, according to (3.29b) and (3.28b).
3. Apply an inverse NMO correction with the velocities used in step 1, according to (3.27a).
4. Perform velocity analysis on the dip corrected data.

If the velocities used in the first step differ from the zero-dip NMO velocities, steps 1 to 4 may be applied iteratively as to improve the initial NMO velocities (Deregowski, 1986).

The DMO process may be considered as a preprocessing step prior to (zero-dip) velocity analysis. It is based on the assumption that the medium velocity is constant. A macro model driven approach to DMO is common reflection point (CRP) stacking (Van der Schoot, 1989). The CRP method however requires a macro model. Therefore it is not well suited for velocity analysis.

3.2.2 Velocity estimation in horizontally layered media (Dix's method)

For a horizontally layered medium, the traveltime relation for the N^{th} reflector is defined by equations (3.18) and (3.19). Dix (1955) inverted equation (3.19) to arrive at a recursive expression for the interval velocities:

$$c_N^2 = \frac{V_{nmo,N}^2 T_N(o) - V_{nmo,N-1}^2 T_{N-1}(o)}{\Delta T_N} . \qquad (3.28)$$

Hence, when the NMO velocities for interface N and N-1 ($V_{nmo,N}$ and $V_{nmo,N-1}$ respectively) and the corresponding ZO-traveltimes ($T_N(o)$ and $T_{N-1}(o)$ respectively) are known, then the interval velocity in layer N can be obtained from Dix's inversion formula. The interface depth of reflector N (z_N) is then obtained from

$$z_N = z_{N-1} + \frac{1}{2} c_N \Delta T_N , \qquad (3.29)$$

where z_{N-1} is the depth of reflector N-1.

Dix related the medium parameters to the measurable seismic parameters by assuming

$$V_{nmo,n} = V_{st,n} \qquad (3.30)$$

for n =1,...,N.

Upon substitution of V_{st} into equation (3.28) the medium parameters can be obtained. As mentioned before, this method is only valid in a small offset approximation and assumes that the medium is horizontally layered. With these restrictions the traveltime curves may be approximated by hyperbolas, implicitly assuming that the NMO velocities in (3.28) may be replaced by the corresponding stacking velocities.

3.2.3 Velocity estimation with dipping plane interfaces

Shah (1973) and Hubral (1976) extended Dix's method to media containing dipping plane interfaces. For dipping interfaces (3.19) is no longer valid and should be replaced by equation (3.26). In order to be able to estimate the interval velocities from (3.26), not only zero offset traveltimes and stacking velocities must be known. The dips of the interfaces are required also. The reflector dips may be calculated from the time slopes in the stacked section (simulated zero offset section). Hyperbolic moveout is still assumed in their method, which implicitly assumes the equality of V_{nmo} and V_{st}.

3.2.4 Poststack traveltime inversion

In the procedures described above analytic expressions for the moveout curves are used that are based on the hyperbolic moveout assumption. Postack traveltime inversion as described by van der Made (1988) is not restricted to this assumption, i.e. it does not require the equality of V_{nmo} and V_{st} to relate the medium parameters to observed quantities. As opposed to analytically calculating hyperbolic moveout curves, in this method CMP-data are simulated by raytracing through an initial macro model. The simulation is done with the true acquisition geometry. From the simulated data zero offset traveltimes and stacking velocities are derived, which are compared to the (T_{st},V_{st}) values obtained from the measured data. The data mismatch between the computed (T_{st},V_{st}) values and the observed (T_{st},V_{st}) values is used to perturb the input model. Next, the procedure is repeated with the perturbed model until the data mismatch is below a predefined threshold.

An advantage of this method is that the initial model can be more realistic. Furthermore, the measured data and the simulated data are treated by the same fitting process.

3.2.5 Moveout correction with nonhyperbolic traveltime curves

In the poststack traveltime inversion stacking velocities are calculated by hyperbolic moveout corrections. Hadley et al. (1988) describe a method that does not assume hyperbolic moveout. As opposed to the hyperbolic

moveout correction, in this method the moveout curves are computed directly by raytracing through a model. The moveout curves are generally nonhyperbolic. By applying a nonhyperbolic moveout correction according to the simulated moveout curves and assessing which curve best fits the observed moveout, the correct interval velocity may be determined. Using the estimated interval velocity the time horizon under consideration may be depth converted. The procedure is repeated for all macro boundaries, i.e. the method is a top-down approach. The main assumption made in this method is that the estimated interface is locally flat within the length of the reflection point smear. A similar method is proposed by Landa et al. (1988). Gjøystdal and Ursin (1981) and van der Made (1986) also describe a prestack traveltime inversion algorithm. This method does not work directly on the seismic traces (as do the methods of Landa et al. and Hadley et al.), but on picked prestack traveltimes. The picking process can be guided by hyperbolic trajectories derived from stacking information (Geerlings, 1990).

3.2.6 Velocity determination by means of wave field extrapolation of CMP data

Finally, Wapenaar and Berkhout (1985) use a different approach to overcome the problems that are inherent to the hyperbolic assumption. Their technique is based on layer replacement. Velocities in successive layers are replaced by one constant velocity through wave field extrapolation of CMP-gathers. In this way the medium is transformed into a constant velocity system for which the hyperbolic relation holds. This method can be applied in media with arbitrarily curved interfaces. Wave field extrapolation appears to be a powerful method to remove distorting propagation effects from seismic data.

3.3 DEPTH POINT-ORIENTED MACRO MODEL ESTIMATION

Conventional processing techniques based on CMP-stacking and poststack migration break down in situations with complex subsurfaces. This gave rise to the development of depth-oriented techniques such as prestack depth migration and prestack redatuming, which do not have the shortcomings found in poststack methods. Because of the progress in computer technology the use of prestack techniques is feasible now.

However, these techniques are very sensitive to the accuracy of the macro model. Therefore, the philosophy is to use this sensitivity for the estimation of macro models. This concept is nowadays well appreciated and different algorithms have been developed that employ the underlying idea. All of these estimation techniques use depth extrapolation of the prestack surface data to depth points in the subsurface, hence the name *depth point-oriented* techniques. In this section I will discuss these new methods and put them into perspective with each other.

3.3.1 Coherency analysis of CDP-gathers

As was already discussed in Chapter 2 it is possible to generate CDP-gathers by shot record redatuming. In the following I will discuss how CDP-gathers can be used to detect errors in the macro velocity model. Consider the model shown in Figure 3.10. For this simple subsurface shot records were computed.

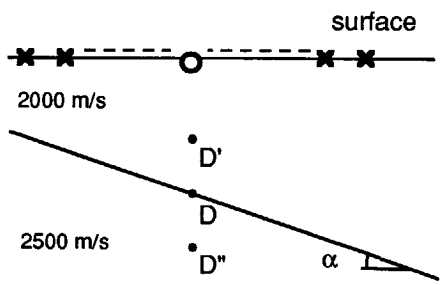

a.

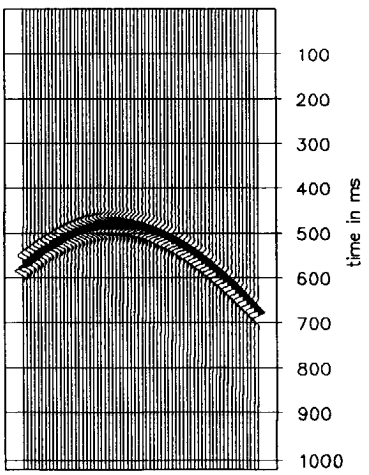

b.

Figure 3.10

a. Model containing one plane dipping interface, which separates two layers with different velocities.

b. Shot record simulated for the model shown in Figure 3.10a.

By shot record redatuming to the indicated depth point D (located at the dipping interface) a CDP-gather may be constructed (Figure 3.11a). Using the correct velocity in the redatuming yields an event in the CDP-gather that is horizontally aligned at t = 0. Consequently, the ZO-trace obtained by CDP-stacking shows a high amplitude event at t=0. This is in accordance

with the physical interpretation of the ZO-trace: zero offset aquisition on top of an interface yields the highest amplitude since no geometrical spreading is involved. Note also that the two-way traveltime of such a ZO-trace equals zero. Hence, after shot record redatuming and CDP-stacking, focusing of the reflection energy occurs at the reflection point and at t=0, if the correct macro model is used.

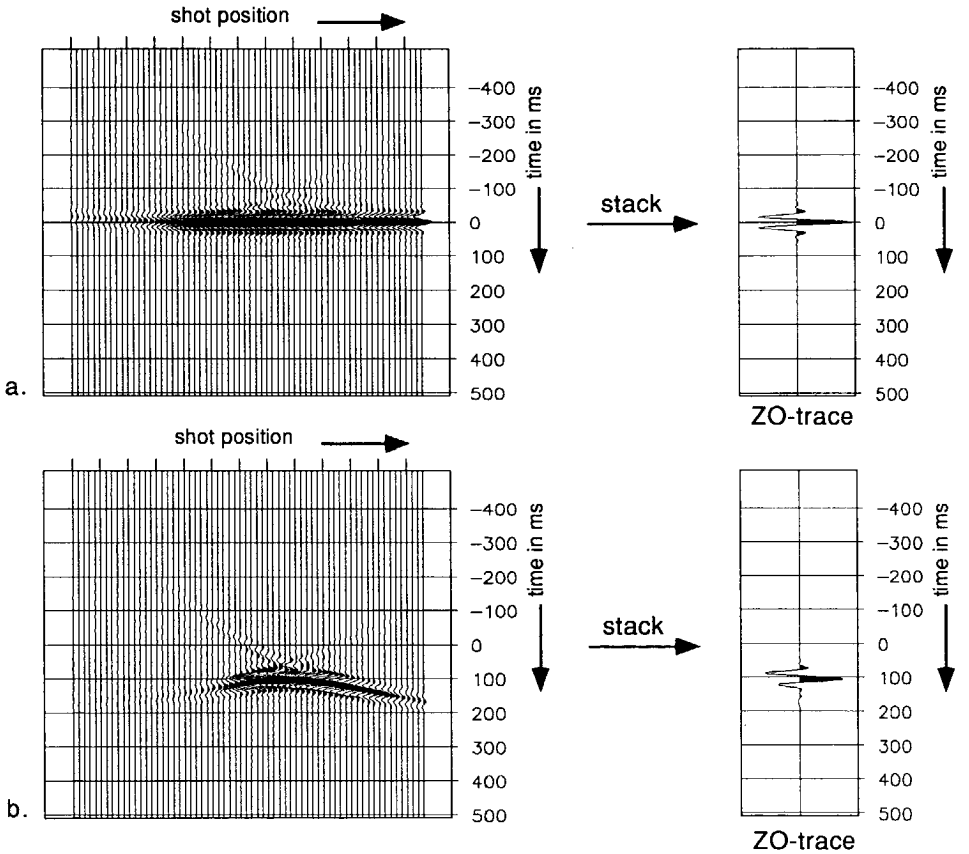

Figure 3.11a, b

a. CDP-gather at depth point D located at the interface. The extrapolation was done with the correct velocity. Alignment occurs at t=0 yielding a high amplitude event after CDP-stacking.

b. CDP-gather at depth point D located at the interface. The extrapolation was done with too high a velocity. No proper alignment occurs. Hence, after CDP-stacking the amplitude has degraded.

When the redatuming is performed with an incorrect velocity the CDP-gather at D exhibits a residual moveout and the CDP-stacked trace shows an event that does not occur at t=0 (Figure 3.11b). Moreover, the amplitude

has degraded. There exists, however, one depth point D', vertically shifted with respect to D, where the CDP-gather is (partly) aligned. At this depth point (cf. Figure 3.10) the velocity error is partly compensated by a depth error introduced at this depth point (Figure 3.11c). The amplitude of the CDP-stacked trace is partly restored, but the event is still located at a time deviating from t=0. The time for which the alignment is optimum is called the focus time t_f. And the depth at which focusing (i.e. alignment) occurs will be called the focus depth z_f. The CDP-gather at D" (Figure 3.11d) results in a ZO-trace that contains an event at t=0. Hence, by imaging at

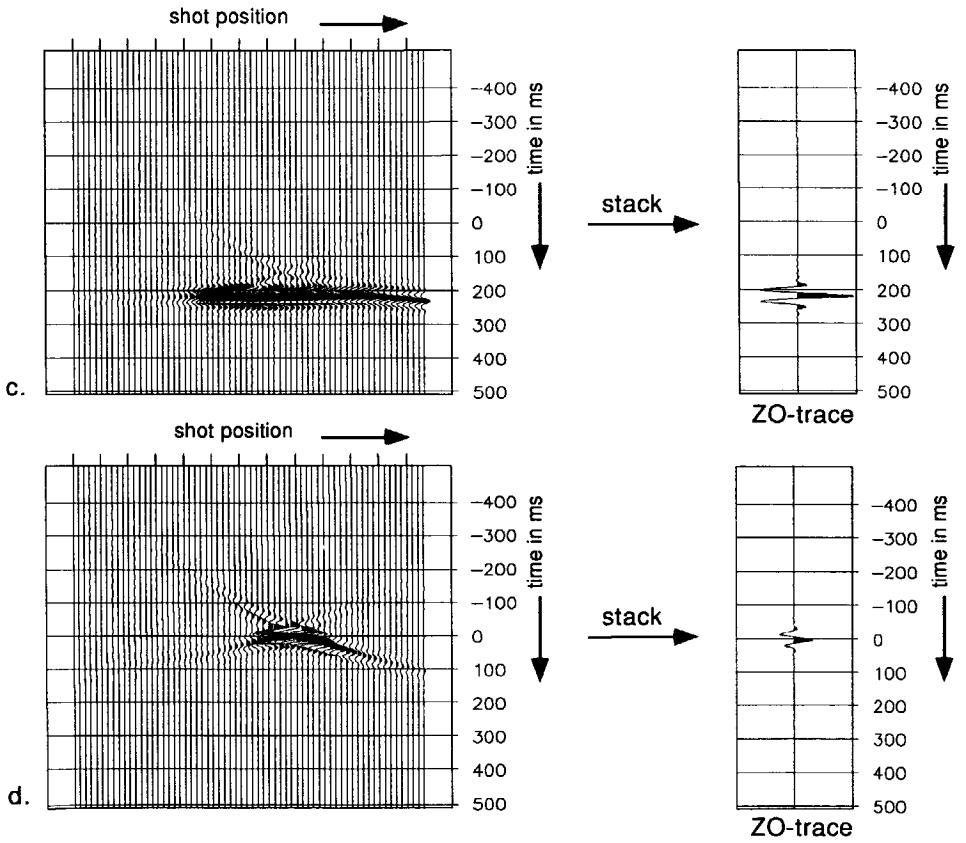

Figure 3.11c, d

c. CDP-gather at depth point D'. The velocity error is compensated by a depth error, yielding alignment (but not at t=0). Alignment occurs at $t \neq 0$ yielding a high amplitude event after CDP-stacking at $t \approx 200$ ms.

d. CDP-gather at depth point D". Imaging at t=0 will position the reflector at D". The amplitude in the migration result will not be optimum due to the imperfect alignment.

t=0 the reflector will be positioned at depth D". Besides that, the amplitude in the migration result will not be optimum due to the imperfect alignment in the CDP-gather.

In the next chapter it will be shown how these two parameters (z_f and t_f) can be used to update the macro model. The problem is to find the depth point at which focusing occurs. Therefore a number of depth points have to be scanned. This is done by redatuming to a range of depth points located on a vertical line as indicated in Figure 3.12. Next, the CDP-stacked traces (ZO-traces) are gathered and displayed in a VSP-like picture, the horizontal axis denoting time-axis and the vertical axis denoting the depth-axis. By contouring the envelopes of these traces the focusing of energy can be elegantly shown. As mentioned before each trace in the focus panel is obtained by stacking the traces of the corresponding CDP-gather. However, any other coherency measure, for instance semblance, may equally well be applied.

If the correct macro model is used in the wave field extrapolation process focusing occurs along the t=0-axis. An incorrect macro model yields a focus panel with focusing occurring off the zero-time axis. By picking each focus, (t_f, z_f)-pairs are obtained that can be used in updating the macro model.

3.3.2 Continuous depth focusing analysis

Faye and Jeannot (1986) presented a depth focusing analysis method based on analysing focus panels. Their technique is the depth-domain description of an earlier publication by Yilmaz and Chambers (1984), which describes focusing in the time-domain. Faye and Jeannot use full prestack migration (S-G migration, Denelle et al., 1985) and analyse the recursively extrapolated data prior to imaging. At each lateral position a focus panel is obtained. In fact a 3-D focus block (x,z,t)-volume can be constructed (Figure 3.13) that contains focus panels, one for each lateral position x. Note that the cross-section at t=0 (imaging) contains the prestack migration result. The 3-D focus block allows for a continuous velocity analysis at each lateral position. However, since the macro interval velocity in a macro layer is only smoothly varying, it is sufficient to inspect only a sparse set of focus panels. This is in analogy with conventional velocity analysis, where a sparse set of CMP-gathers is

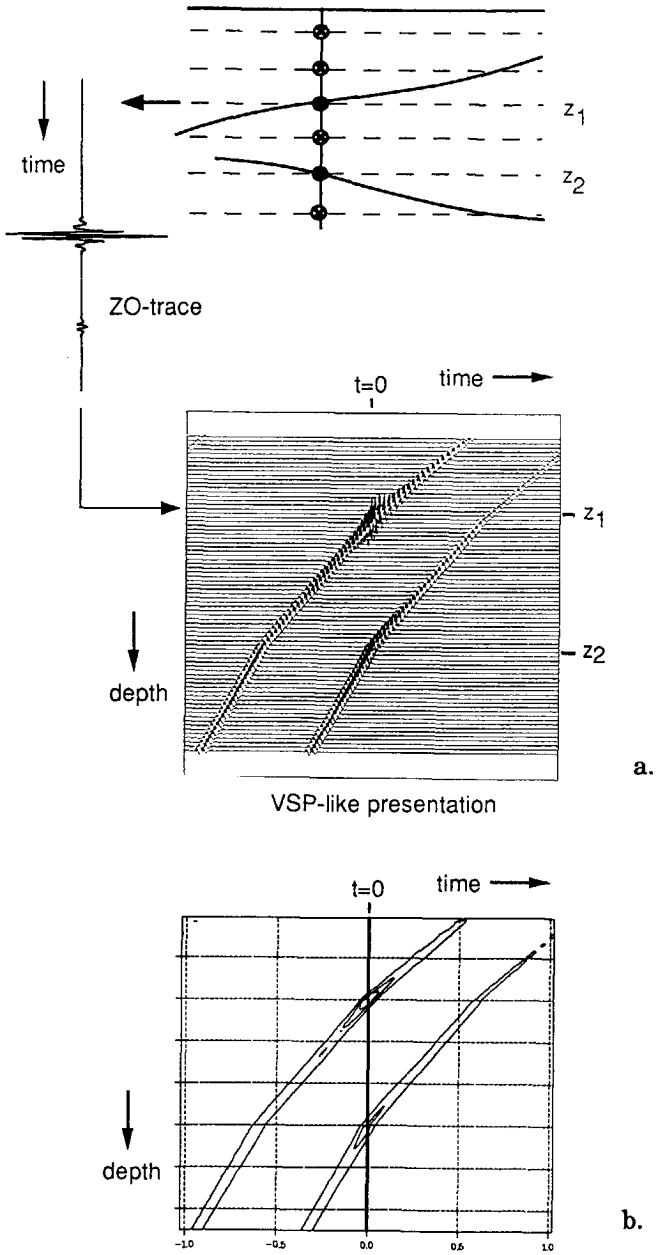

Figure 3.12

a. Redatuming to depth points along the vertical coordinate yields (after CDP-stacking) a panel of zero offset traces that can be displayed in a VSP-like presentation as a function of two-way traveltime (horizontal axis) and depth (vertical axis).

b. Contouring the (envelope of the) data of figure 'a' elegantly visualizes the focusing of energy that occurs due to alignment of events in the corresponding CDP-gathers.

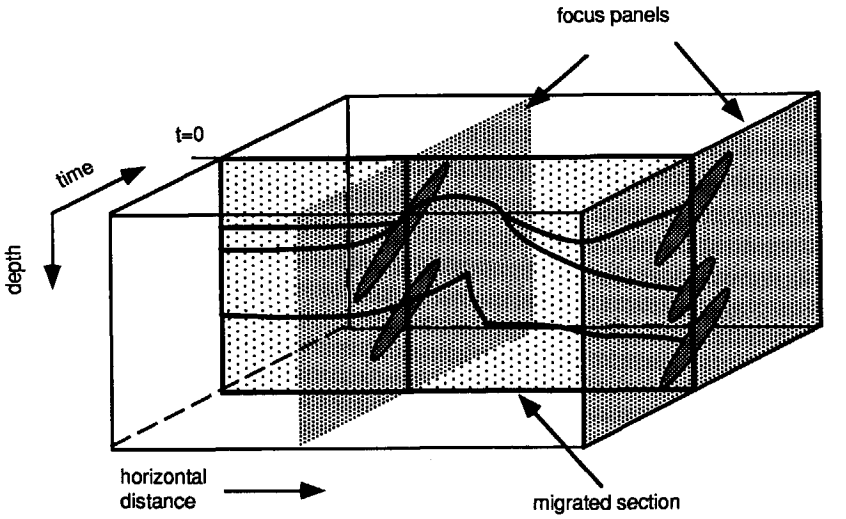

Figure 3.13
A 3-D focus volume. The cross section at t=0 contains the prestack migration result.

analysed. Therefore it is preferred to use a non-recursive extrapolation scheme that allows for extrapolation to depth points that are sparsely sampled in the lateral direction as was already discussed in the previous chapter.

Instead of using a recursive S-G migration scheme Cox et al. (1988) propose a non-recursive shot record redatuming scheme. There are significant advantages of separate extrapolation of shot records. Firstly, it does not require the reordering of the data into common receiver gathers, which is of practical importance in 3-D macro model estimation. Secondly, in the shot record approach it is possible to analyse the extrapolated data prior to CDP-stacking. Furthermore, other measures of horizontal alignment may be used instead of CDP-stacking. Note that in S-G schemes it is not possible to obtain CDP-gathers, since CDP-stacking is done implicitly.

3.3.3 Iterative shot record migration

Apart from the analysis of focus panels and CDP-gathers, image gathers (also called postmigration Common Receiver gather) can be used, as proposed by Berkhout (1984), Al-Yahya (1989) and Van Trier (1988). In this method depth extrapolation is performed by shot record migration. *After*

imaging, the data are reordered into image gathers. An image gather can be obtained from the migrated shot records by collecting the depth traces that are related to one lateral position (Figure 3.14). After migration with the correct macro model, each image in an image gather should be horizontally aligned regardless of the structure in the subsurface (Figure 3.15). It will be shown in section 4.2.3 that the curvature observed in image gathers can be used as an analysis tool to update the macro model.

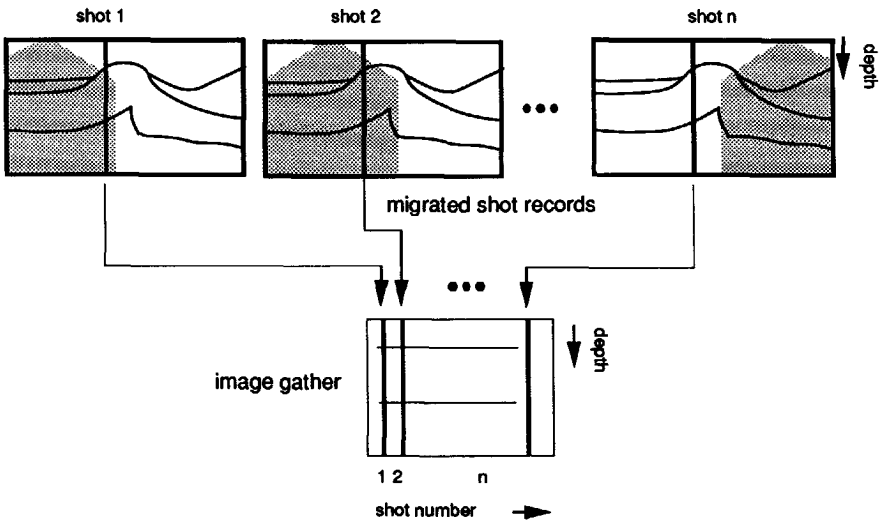

Figure 3.14
An image gather can be extracted from migrated shot records by collecting the depth traces that are related to one lateral position.

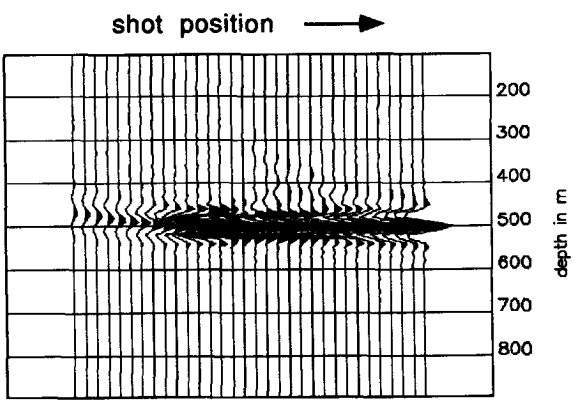

Figure 3.15
Each image in an image gather is horizontally aligned regardless of the structure in the subsurface if the correct macro model is used.

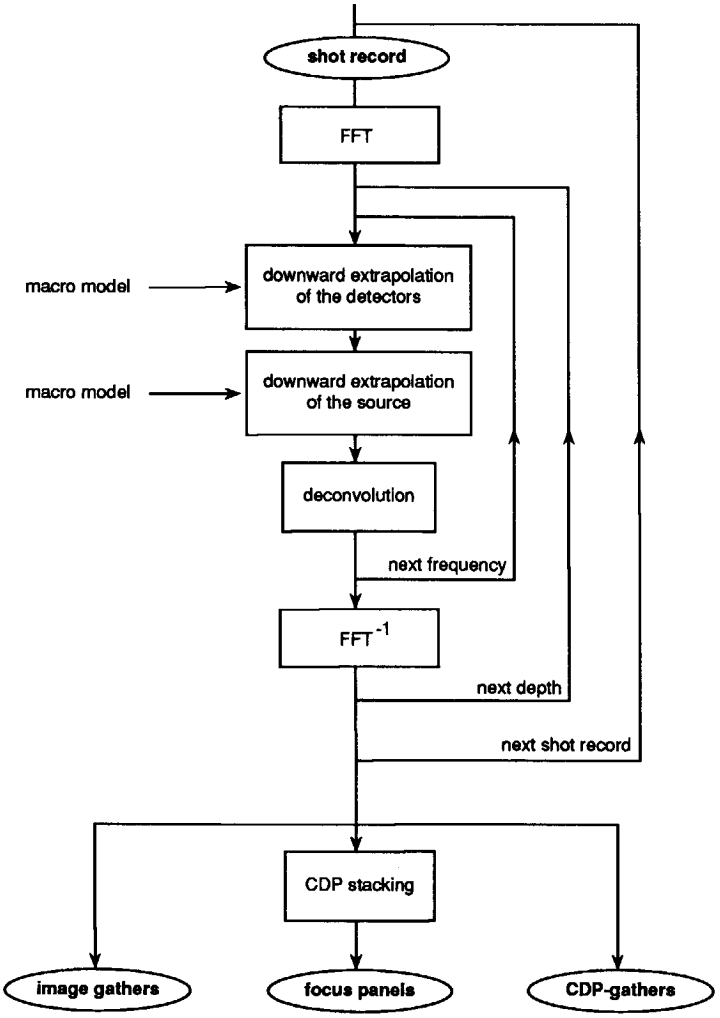

Figure 3.16
Flow diagram of shot record extrapolation. By using shot record extrapolation techniques it is possible to construct CDP-gaters, image gathers and focus panels.

In conclusion, in this section I described three closely related macro model estimation methods. All techniques are depth point-oriented, i.e. the data used in the estimation procedure are related to subsurface depth points. Figure 3.16 shows the flow diagram of a shot record extrapolation procedure. The actual implementation should not necessarily be according to this scheme; it is merely to illustrate the different data volumes that can be obtained.

CHAPTER 4

ESTIMATION OF MACRO VELOCITY MODELS BY WAVE FIELD EXTRAPOLATION

4.1 INTRODUCTION

In this chapter I present the DELPHI method on macro velocity model estimation. As mentioned before, the macro subsurface model defines the traveltimes of the macro boundary reflections. In the following, it is assumed that the *surface-related* processing steps such as decomposition and multiple elimination have already been applied to the surface measurements, as can been seen in the overall processing scheme (Figure 1.3b). The data after surface-related preprocessing are used to separately estimate the P-wave macro velocity model and, if applicable, the S-wave macro velocity model.

As stated before, it is not necessary to do a laterally continuous velocity analysis since within a macro layer the velocity does not change rapidly. The macro boundaries, however, can have sudden changes (e.g. faults). Therefore our approach is to split the estimation of the macro velocity model into two modules:

1. Estimation of the macro interval velocities

This is the most expensive part of the procedure. It involves extrapolation of shot records to grid points (x_d,y_d,z), followed by some coherency analysis. Because the velocity information is contained in the moveout of the data with offset, prestack data with sufficient offset is needed to determine the velocities.

2. Estimation of the macro boundaries

Once the macro interval velocities are known the macro boundaries can be estimated straightforwardly from the traveltimes. At the stage of macro velocity model estimation we are not interested in obtaining true amplitudes but merely in delineating the structure of the macro boundaries. This means that a fast time to depth conversion algorithm can be chosen.

These two estimation modules together define the total macro velocity model estimation procedure. Depending on the objective they can be used in a borehole oriented estimation scheme or in a reservoir oriented scheme. In the first scheme the velocity analysis is done for one lateral position (vertical datum line) at the location of a (potential) well (Figure 4.1a). In the second scheme the velocity analysis is done for a number of lateral positions because of the lateral extent of the problem (Figure 4.1b). In general, the *velocity analysis* locations can be sparsely sampled in the lateral direction of one macro layer (just as with conventional velocity analysis).

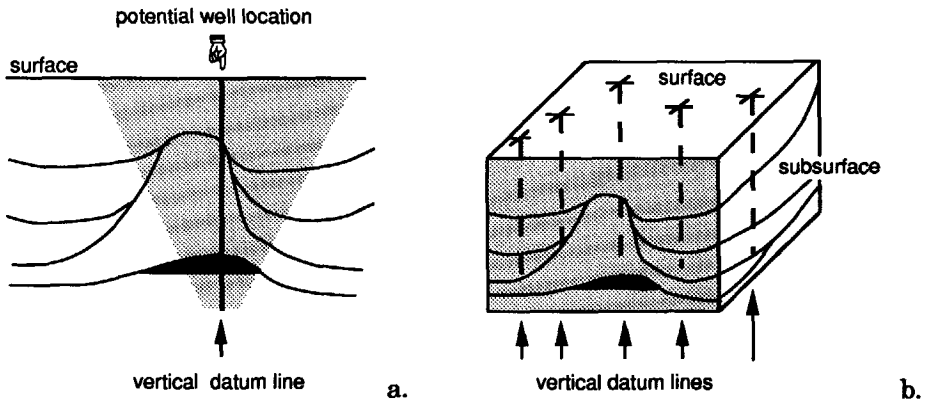

Figure 4.1

a. A borehole oriented estimation scheme involves velocity analysis at a potential well location ('vertical datum line').

b. In a reservoir oriented estimation scheme velocity analysis is done for a number of vertical datum lines, followed by interpolation.

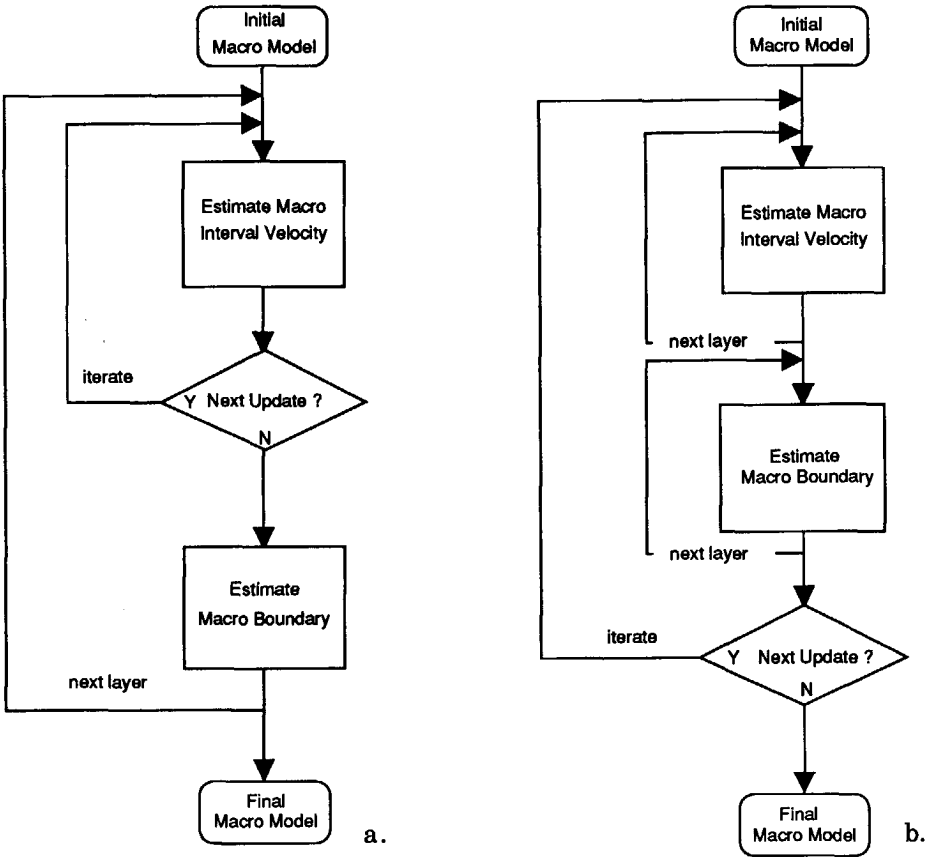

Figure 4.2

a. Borehole oriented estimation scheme in a layer-stripping implementation.

b. Borehole oriented estimation scheme in a multi layer (cascaded) implementation.

The total procedure is preferably implemented in a layer-stripping mode (Figures 4.2a and 4.3a). However, this may not be the most economical implementation as was also recognized by MacBain (1989). In case of simple subsurface geometries the total number of iterations can be reduced by applying a cascaded velocity estimation (Figures 4.2b and 4.3b). Here, per iteration, the interval velocities are estimated for a number of macro layers and although the estimation for a given layer is less accurate if shallower layers still contain errors, the overall number of iterations is reduced. Note that the macro *velocity* estimation is followed by macro *boundary* estimation. In the following the two estimation modules will be discussed in more detail.

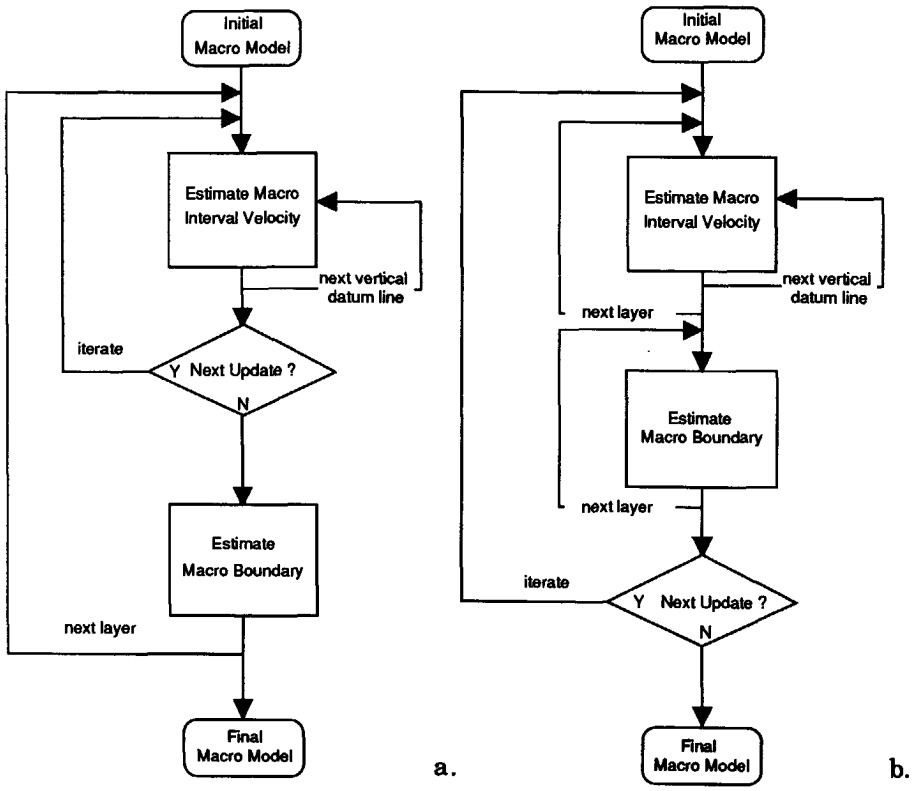

Figure 4.3

a. Reservoir oriented estimation scheme in a layer-stripping implementation.
b. Reservoir oriented estimation scheme in a multi layer (cascaded) implementation.

4.2 ESTIMATION OF MACRO INTERVAL VELOCITIES

The estimation of the macro velocities involves extrapolation of the prestack surface data to predefined vertical datum lines. At each vertical datum line a coherency analysis is performed. The extrapolation is done with a non-recursive shot record redatuming scheme as developed by Kinneging (1989). This scheme is chosen for two reasons:

1. *The redatuming procedure is non-recursive*

   Hence, operators are calculated that describe propagation from the surface to the depth points of the vertical datum line only. The operator calculation is done by raytracing through the macro velocity model that has to be updated. Raytracing contributes to the

efficiency of the algorithm. Moreover, for velocity estimation, amplitudes are of minor importance.

2. *The shot records are redatumed separately*

Unlike S-G schemes this enables us to analyse the redatumed data *before* stacking over all shots. So with a shot record oriented scheme CDP-gathers can be analysed using CMP-like coherency techniques.

4.2.1 Traveltime equation for CDP-gathers in horizontally layered media

To update the macro velocity model, we need a way of relating the traveltimes, observed in CDP-gathers that are obtained by wave field extrapolation, to the medium parameters. We should therefore study what happens if the extrapolation is done with an erroneous macro velocity model. In this section I derive the traveltime equation for CDP-gathers in horizontally layered media. In the next section this equation is used to derive update equations for the macro velocity model. Consider the subsurface in Figure 4.4a. For the moment the subsurface is assumed to be horizontally layered. At the surface a shot record is recorded.

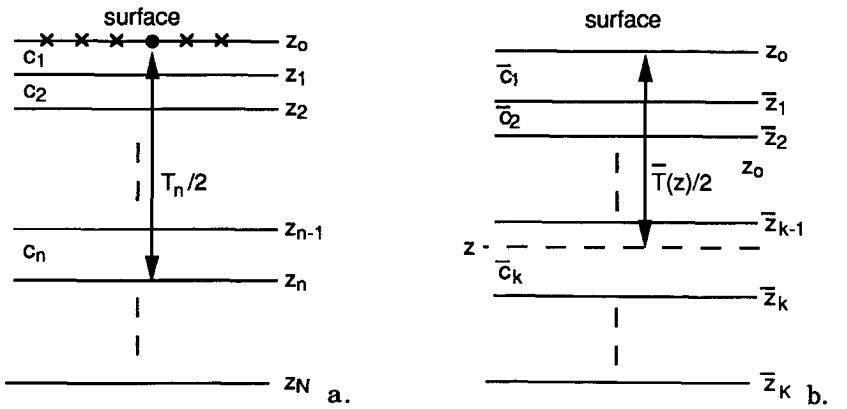

Figure 4.4

a. Horizontally layered medium (true subsurface).

b. Macro velocity model containing erroneous interval velocities and reflector depths.

The observed traveltime function related to the n^{th} reflection, $T_{p,n}(x_s,x,z_o)$, is represented by a MacLaurin series, which may be approximated for small offsets by a hyperbola in the (x-t)-domain according to:

$$T_{p,n}^2(x_s,x,z_0) \approx T_n^2 + ((x-x_s)/V_n)^2 \quad , \tag{4.1}$$

where the subscript "p" denotes that the traveltime is related to the detected wave field, x represents the lateral coordinate of the receiver at the surface and x_s represents the lateral coordinate of the source. T_n represents the vertical two-way traveltime to the n^{th} reflector in the true subsurface (Figure 4.4a):

$$T_n = \sum_{i=1}^{n} \Delta T_i = \sum_{i=1}^{n} \frac{2\Delta z_i}{c_i} \quad , \tag{4.2}$$

where Δz_i and c_i denote the thickness and interval velocity of layer i, respectively. V_n represents the rms velocity down to reflector n:

$$V_n^2 T_n = \sum_{i=1}^{n} c_i^2 \Delta T_i = \sum_{i=1}^{n} 2c_i \Delta z_i \quad . \tag{4.3}$$

Equation (4.1) is exact for a horizontal reflector in a constant velocity medium.

Suppose that the shot record is redatumed, with the macro model shown in Figure 4.4b, to the indicated depth level z. Redatuming involves inverse extrapolation of the detected wave field to depth level z, followed by deconvolution with the source wave field at depth level z (see Chapter 2).

Inverse extrapolation of the detected wave field

After inverse extrapolation of the detected wave field to depth level z, the resulting traveltimes related to reflector n amount to

$$T'^2_{p,n}(x_s,x_d,z) \approx T'^2_n + ((x_d-x_s) / V'_n)^2 \quad , \tag{4.4}$$

where x_d represents the lateral coordinate of the downward extrapolated receiver at depth level z and x_s represents the lateral coordinate of the source. The prime (') denotes that we are dealing with an extrapolated wave field. Furthermore,

$$T'_n = T_n - \bar{T}(z)/2 \tag{4.5}$$

and

$$V'^2_n T'_n = V^2_n T_n - \bar{V}^2(z)\bar{T}(z)/2 \ . \tag{4.6}$$

$\bar{T}(z)/2$ represents the vertical one-way traveltime in the macro velocity model up to the depth level z and is defined by (assuming that the depth level is located in the k^{th} layer in the macro velocity model, cf. Figure 4.4b):

$$\bar{T}(z) = \sum_{i=1}^{k-1} \frac{2\Delta\bar{z}_i}{\bar{c}_i} + \frac{2(z - \bar{z}_{k-1})}{\bar{c}_k} \ , \tag{4.7}$$

where $\Delta\bar{z}_i$ and $\Delta\bar{c}_i$ denote the thickness and interval velocity of the i^{th} layer in the macro velocity model, respectively.

In addition,

$$\bar{V}^2(z)\bar{T}(z) = \sum_{i=1}^{k-1} 2\bar{c}_i\Delta\bar{z}_i + 2\bar{c}_k(z - \bar{z}_{k-1}) \ . \tag{4.8}$$

$\bar{V}(z)$ is the rms velocity in the macro velocity model down to z. Note that equation (4.8) contains the depth z of the new datum level.

Equation (4.4) represents an approximated hyperbola. According to equation (4.5) the apex time of this hyperbola has decreased with respect to the apex time in the surface data. Equation (4.6) implies that the radius of the wavefront has decreased as well. This is in accordance with physical intuition: the geometrical spreading that is observed by downward extrapolated detectors is less than the geometrical spreading observed by detectors at the surface.

Forward extrapolation of the source wave field

Forward extrapolation of the source wave field to depth level z yields, in terms of traveltimes:

$$T'^{2}_{s}(x_s,x_d,z) = (\bar{T}(z)/2)^2 + ((x_d-x_s) / \bar{V}(z))^2 , \qquad (4.9)$$

where the subscript "s" in T'_s denotes that the traveltime is related to the source wave field.

Deconvolution of the detected wave field for the incident source wave field

In terms of traveltimes this deconvolution means that for each depth point the traveltime of the extrapolated source wave field is subtracted from the traveltime of the inverse extrapolated detected wave field:

$$T(x_s,x_d,z) \hat{=} T'_{p,n}(x_s,x_d,z) - T'_s(x_s,x_d,z)$$

$$= \sqrt{T'^{2}_{n} + ((x_d-x_s) / V'_n)^2} - \sqrt{(\bar{T}(z)/2)^2 + ((x_d-x_s) / \bar{V}(z))^2} \quad (4.10)$$

4.2.2 Update equations for CDP-gathers

For fixed x_d and z and for variable x_s, equation (4.10) represents an expression for the traveltime curve of the n^{th} macro reflection in a CDP-gather at (x_d,z). For small offsets the square roots may be approximated and equation (4.10) reduces to

$$T(x_s,x_d,z) \approx \left(T'_n + \frac{(x_d - x_s)^2}{2V'^{2}_{n} T'_n}\right) - \left(\bar{T}(z)/2 + \frac{(x_d - x_s)^2}{\bar{V}^2(z)\bar{T}(z)}\right)$$

$$= T_n - \bar{T}(z) + (x_d - x_s)^2 \left(\frac{1}{2V_n^2 T_n - \bar{V}^2(z)\bar{T}(z)} - \frac{1}{\bar{V}^2(z)\bar{T}(z)}\right) . \qquad (4.11)$$

The objective is to find the position of the grid point (depth point) for which the n^{th} reflection in the corresponding CDP-gather is horizontally aligned. The depth of this particular grid point is called the focus depth (remember that alignment in a CDP-gather results in focusing of the energy after CDP-stacking, hence the name *focus* depth). The focus depth is denoted by

$z_{f,n}$, the subscript n indicating that the focus is related to the n^{th} macro boundary in the true subsurface. The time at which alignment occurs is called the focus time $t_{f,n}$. The alignment occurs in a CDP-gather when equation (4.11) is independent of the source coordinate x_s. Hence, when

$$\frac{1}{2V_n^2 T_n - \bar{V}^2(z_{f,n})\bar{T}(z_{f,n})} - \frac{1}{\bar{V}(z_{f,n})^2 \bar{T}(z_{f,n})} = 0 \ , \tag{4.12}$$

which is equivalent to the condition

$$V_n^2 T_n = \bar{V}^2(z_{f,n})\bar{T}(z_{f,n}) \ , \tag{4.13}$$

where $V_n^2 T_n$ is defined by (4.3). $\bar{V}^2(z_{f,n})\bar{T}(z_{f,n})$ is defined by (4.8) upon substitution of the focus depth $z_{f,n}$ (assuming that the focus depth is located in the k^{th} layer in the macro velocity model), yielding

$$\bar{V}^2(z_{f,n})\bar{T}(z_{f,n}) = \sum_{i=1}^{k-1} 2\bar{c}_i \Delta\bar{z}_i + 2\bar{c}_k(z_{f,n} - \bar{z}_{k-1}) \ . \tag{4.14}$$

The focus time at $z_{f,n}$ amounts to

$$t_{f,n} = T_n - \bar{T}(z_{f,n}) \ . \tag{4.15}$$

Relation (4.3) can be inverted according to (Dix, 1955):

$$c_n^2 = \frac{V_n^2 T_n - V_{n-1}^2 T_{n-1}}{T_n - T_{n-1}} = \frac{V_n^2 T_n - V_{n-1}^2 T_{n-1}}{\Delta T_n} \ . \tag{4.16}$$

ΔT_n represents the vertical two-way traveltime in layer n and may be determined by using equation (4.15):

$$\Delta T_n = T_n - T_{n-1} = \left(\bar{T}(z_{f,n}) + t_{f,n}\right) - \left(\bar{T}(z_{f,n-1}) + t_{f,n-1}\right) \ , \tag{4.17}$$

where $t_{f,n}$ and $t_{f,n-1}$ represent the focus times of foci n and n-1 respectively. Substitution of (4.13) and (4.17) into (4.16) yields a recursive estimation formula for the macro interval velocity:

$$c_n^2 = \frac{\bar{V}^2(z_{f,n})\bar{T}(z_{f,n}) - \bar{V}^2(z_{f,n-1})\bar{T}(z_{f,n-1})}{\left(\bar{T}(z_{f,n})+t_{f,n}\right) - \left(\bar{T}(z_{f,n-1})+t_{f,n-1}\right)} \quad . \tag{4.18}$$

The reflector depth can be recursively estimated from

$$z_n = z_{n-1} + \frac{c_n}{2}\Delta T_n = z_{n-1} + \frac{c_n}{2}\left[(\bar{T}_n+t_{f,n}) - (\bar{T}_{n-1}+t_{f,n-1})\right] \quad . \tag{4.19}$$

Equation (4.18) states that the true interval velocity can be estimated from the macro velocity model parameters and the locations of focus n-1 and focus n, $(z_{f,n-1},t_{f,n-1})$ and $(z_{f,n},t_{f,n})$, respectively. The true reflector depth can then be calculated from (4.19).

Special case:

When the macro velocity model is chosen such that focus n and focus n-1 both occur in the n^{th} macro layer, then equations (4.18) and (4.19) simplify to

$$c_n^2 = \bar{c}_n^2 \Big/ \left(1 + \frac{(t_{f,n} - t_{f,n-1})\bar{c}_n}{2\,(z_{f,n} - z_{f,n-1})}\right) \tag{4.20}$$

and

$$z_n = z_{n-1} + (z_{f,n} - z_{f,n-1})\sqrt{1 + \frac{(t_{f,n} - t_{f,n-1})\bar{c}_n}{2\,(z_{f,n} - z_{f,n-1})}} \quad . \tag{4.21}$$

Note that for a single-layer medium these expressions reduce to

$$c_1 = \frac{\bar{c}_1}{\sqrt{1 + (\bar{c}_1 t_{f,1} / 2z_{f,1})}} \tag{4.22}$$

and

$$z_1 = z_{f,1} \sqrt{1 + (\bar{c}_1 t_{f,1} / 2z_{f,1})} \quad . \tag{4.23}$$

In conclusion, by measuring the focus time and focus depth of the consecutive foci, and by calculation of the parameters $\bar{V}(z_{f,n})$ and $\bar{T}(z_{f,n})$ from the macro velocity model, the updated macro velocity and macro boundary depth can be found. The updating equations are accurate for horizontally layered media in a small offset approximation. In practice these assumptions are not valid, but they become less severe when the focus time deviates only slightly from t=0. Experience has shown that the correction will be in the proper direction, which permits an iterative approach.

Note that in the derivation of the update equations, for notational convenience, it was assumed that the prestack data were recorded along the x-axis (2-D assumption). In 3-D, however, these equations remain exactly the same.

Vertical velocity gradients within a macro layer

In the derivation of equations (4.18) and (4.19) it is assumed that the macro interval velocities are constant within each layer. In practice vertical gradients can occur e.g. due to compaction. Unfortunately vertical velocity gradients can not be accurately estimated from surface reflection data (Gibson et al., 1979). However, if the velocity gradient is known from some other source of information like e.g. a well log or a database, this a priori knowledge can be incorporated in the estimation procedure.

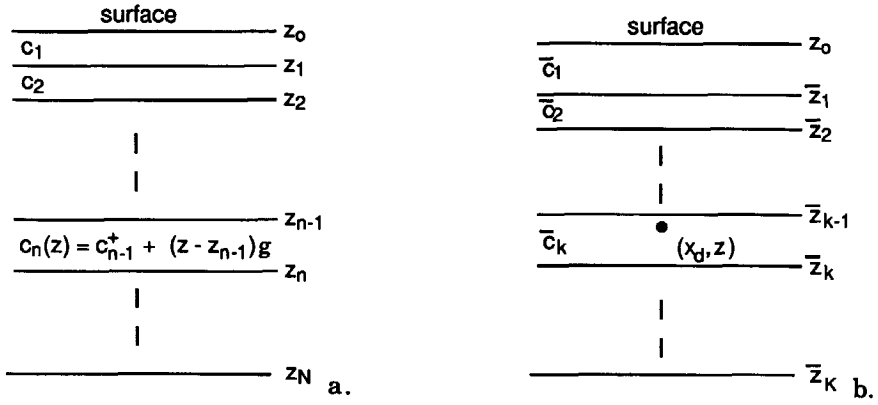

Figure 4.5

a. Horizontally layered medium (true subsurface). Layer n contains a vertical velocity gradient.

b. Macro velocity model containing erroneous interval velocities and reflector depths.

Suppose the macro boundaries and macro interval velocities up to layer n–1 have already been determined. Then the macro velocity in layer n can be estimated by using equation (4.18). In case of a vertical velocity gradient in layer n, c_n no longer represents a constant interval velocity but the rms velocity within the layer. Hence equation (4.18) should be replaced by

$$v_n^2 = \frac{\bar{V}_n^2 \bar{T}_n - \bar{V}_{n-1}^2 \bar{T}_{n-1}}{(\bar{T}_n + t_{f,n}) - (\bar{T}_{n-1} + t_{f,n-1})}, \tag{4.24}$$

where v_n represents the rms velocity within layer n. The velocity function $c_n(z)$ in layer n may be written as

$$c_n(z) = c^+_{n-1} + (z - z_{n-1})\, g, \tag{4.25}$$

where c^+_{n-1} denotes the local velocity just below macro boundary n-1 and g denotes the (known) velocity gradient (Figure 4.5). The rms velocity is related to this velocity function by

$$v_n^2 \Delta T_n = 2 \int_{z_{n-1}}^{z_n} c_n(z)dz = 2(z_n - z_{n-1})c_{n-1}^{+} + (z_n - z_{n-1})^2 g \ . \qquad (4.26)$$

Equation (4.26) contains two unknowns, c_{n-1}^{+} and z_n. Level z_{n-1} is known from the estimation of the macro parameters of layer n-1. The gradient g is known from a priori information and $v_n^2 \Delta T_n$ can be determined from equation (4.24). The layer thickness can be derived from

$$z_n - z_{n-1} = \frac{c_{ave}}{2} \Delta T_n \ . \qquad (4.27)$$

Note that this relation contains the average velocity in layer n, and not the rms velocity. The average velocity in layer n is defined by

$$c_{ave} \triangleq \frac{\text{total path length}}{\text{total two-way traveltime}} = \frac{2 \int_{z_{n-1}}^{z_n} dz}{2 \int_{z_{n-1}}^{z_n} \frac{dz}{c_n(z)}}$$

$$= \frac{z_n - z_{n-1}}{\int_{z_{n-1}}^{z_n} \frac{dz}{c_{n-1}^{+} + (z - z_{n-1})\, g}} = \frac{(z_n - z_{n-1})\, g}{\ln\left(1 + (z_n - z_{n-1}) \frac{g}{c_{n-1}^{+}}\right)} \ . \qquad (4.28)$$

Substitution of (4.28) into (4.27) yields after some calculus:

$$z_n - z_{n-1} = \frac{c_{n-1}^{+}}{g} \left(\exp\left(\tfrac{1}{2} g \Delta T_n\right) - 1\right) \ , \qquad (4.29)$$

where c_{n-1}^{+} is still unknown. Substitution into equation (4.26) results in

$$\left(\exp(\tfrac{1}{2} g\Delta T_n) - 1\right)^2 + 2\left(\exp(\tfrac{1}{2} g\Delta T_n) - 1\right) - g v_n^2 \Delta T_n / (c_{n-1}^+)^2 = 0 \ . \qquad (4.30)$$

The solution of this quadratic equation reads

$$\exp(\tfrac{1}{2} g\Delta T_n) - 1 = -1 \pm \sqrt{1 + g v_n^2 \Delta T_n / (c_{n-1}^+)^2} \ . \qquad (4.31)$$

Rewriting equation (4.31) and taking the positive root eventually yields

$$c_{n-1}^+ = v_n \sqrt{\frac{g\Delta T_n}{\exp(g\Delta T_n) - 1}} \ . \qquad (4.32a)$$

For small $g\Delta T_n$ this equation may be approximated by

$$c_{n-1}^+ \approx (1 - \tfrac{1}{4} g\Delta T_n)\, v_n . \qquad (4.32b)$$

Equations (4.32a and b) state that the local velocity can be estimated from the rms velocity in layer n (which may be determined from (4.24)), the vertical two-way traveltime in layer n (which may be determined from (4.17)) and the known vertical velocity gradient g. The reflector depth may now be determined from equation (4.29). Note that when the gradient g=0, v_n represents the interval velocity c_n in layer n. In this case (4.32) becomes

$$c_{n-1}^+ = c_n \ , \qquad (4.33)$$

which is what we expected.

4.2.3 Update equations for image gathers

As was mentioned in Chapter 3, it is possible to update the macro model from the curvature of the events in an image gather. In this section I derive a relation between the errors in the macro model parameters and the horizontal misalignment in an image gather. Consider again equation (4.10). We have seen that the traveltime curve for the n^{th} reflection in a CDP-gather can be obtained by keeping x_d and z fixed and by

letting x_s vary. We can also derive the curve for the n^{th} reflection in an image gather. In an image gather the imaging is performed at t=0. Hence, the left-hand-side of equation (4.10) should be zero. Consequently,

$$\sqrt{T'^{\,2}_n + (x_d - x_s)^2 / V'^{\,2}_n} = \sqrt{(\bar{T}(z)/2)^2 + (x_d - x_s)^2 / \bar{V}(z)^2} \,. \qquad (4.34)$$

Note that in an image gather both x_s and z vary; x_d is fixed. For a single-layer medium equation (4.34) may be simplified with the following substitutions:

$$\begin{aligned} T'_n &= 2z_1/c_1 - z/\bar{c} \\ \bar{T}(z)/2 &= z/\bar{c} \\ \bar{V}(z) &= \bar{c} \\ V'^{\,2}_n T'_n &= 2z_1c_1 - z\bar{c} \,, \end{aligned} \qquad (4.35)$$

where z_1 and c_1 denote the reflector depth and the true medium velocity, respectively, and z and $\bar{c}$ denote the extrapolation depth and the extrapolation velocity, respectively. Substitution of these relations into equation (4.34), after squaring both sides yields:

$$(2z_1/c_1 - z/\bar{c})^2 + (x_d - x_s)^2 \frac{2z_1/c_1 - z/\bar{c}}{2z_1c_1 - z\bar{c}} = (z/\bar{c})^2 + (x_d - x_s)^2 \frac{1}{\bar{c}^2} \qquad (4.36)$$

The aim is to rewrite this equation in such a manner that z represents a function of x_s. After some calculus, I obtain

$$\left[z - (c_1/\bar{c} + \bar{c}/2c_1)\, z_1\right]^2 = z_1^2 (c_1/\bar{c} - \bar{c}/2c_1)^2 + \frac{1}{2}(x_d - x_s)^2\left[(c_1/\bar{c})^2 - 1\right] \,. \qquad (4.37)$$

Solving this quadratic equation yields:

$$z = (c_1/\bar{c} + \bar{c}/2c_1)\, z_1 \pm \sqrt{z_1^2 (c_1/\bar{c} - \bar{c}/2c_1)^2 + \frac{1}{2}(x_d - x_s)^2 \left[(c_1/\bar{c})^2 - 1\right]} \qquad (4.38)$$

The only valid solution is obtained by chosing the minus sign. This can be easily seen; when the extrapolation velocity equals the true medium velocity, the observed reflector depth "z" should be equal to the true reflector depth "z_1". Note that there were no approximations involved to arrive from equation (4.34) at (4.38). For small offsets (4.38) can be approximated by (chosing the minus sign):

$$z = (\bar{v}/c_1)\, z_1 + \frac{1}{4}(x_d - x_s)^2 \frac{1 - (c_1/\bar{v})^2}{z_1(c_1/\bar{v} - \bar{v}/2c_1)} \tag{4.39}$$

Equation (4.39) predicts the curvature in an image gather, when an erroneous velocity is taken in the extrapolation process. The event is curved upward if the extrapolation velocity is taken too low. Similarly, the event is curved downward if the extrapolation velocity is taken too high. By calculating the coherence in an image gather along curves defined by (4.39), an estimate of the true medium parameters can be obtained.

Likewise Al-Yahya (1989) derived an equation for the curvature of an event in an image gather (in our notation):

$$z = \sqrt{z_1^2\,(\bar{v}/c_1)^2 + (x_d - x_s)^2\left[(\bar{v}/c_1)^2 - 1\right]}\ . \tag{4.40}$$

In Figure 4.6 these two equations are plotted in overlay with an image gather obtained from a horizontal reflector. Note that equation (4.39) best fits the observed image gather. Updating the macro velocity model is an iterative procedure. Hence, both approaches will yield an updated macro model, but updating according to (4.39) will converge faster to the final solution.

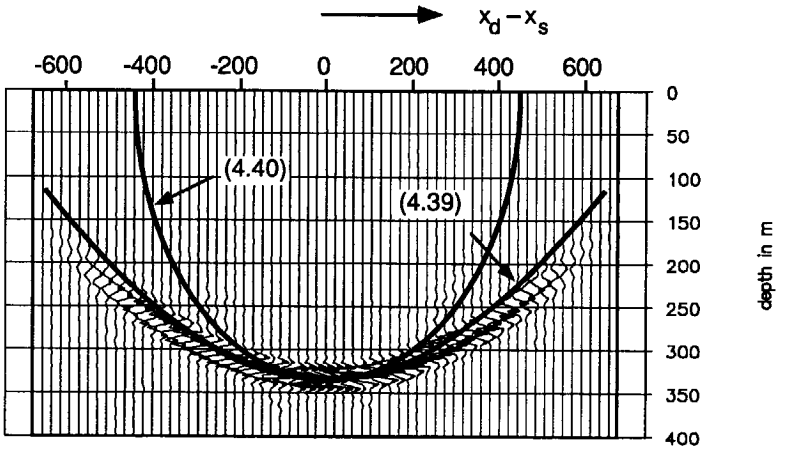

Figure 4.6
Image gather from an horizontal reflector obtained by shot record extrapolation with a velocity that was less than the true medium velocity. Note that the event is curved upward. On top of the image gather the predicted curves (4.39) and (4.40) are plotted. Note that a better fit is obtained with equation (4.39).

4.2.4 Lateral velocity changes within a macro layer

Lateral velocity changes that occur within one macro layer can be easily incorporated. A local estimate of the macro velocities is obtained at each lateral position where a velocity analysis is performed. A spline function can then be defined through the velocities of the macro layer, thus allowing the velocity to change smoothly within the macro layer. Of course, care must be taken, e.g. in the presence of faults, that the velocities through which the spline function is defined belong to one and the same macro layer.

4.3 ESTIMATION OF MACRO BOUNDARIES

4.3.1 Interpolation of macro boundary tie points

At each lateral position where a velocity estimation is performed, also an estimate of the depth of each macro boundary is known (cf. equation 4.19). These estimates are called macro boundary tie points. By spline

interpolation through related tie points, an estimate of the macro boundaries could be obtained (Figure 4.7).

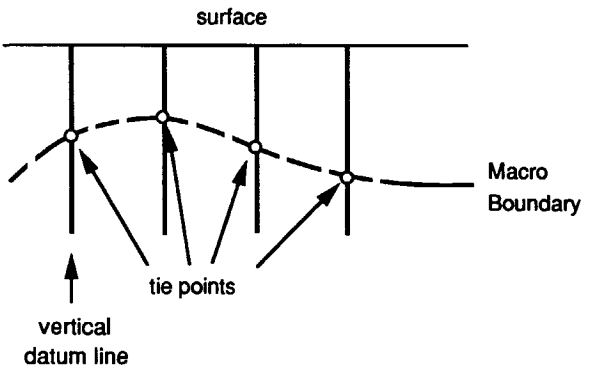

Figure 4.7a
Lateral interpolation of related macro boundary tie points.

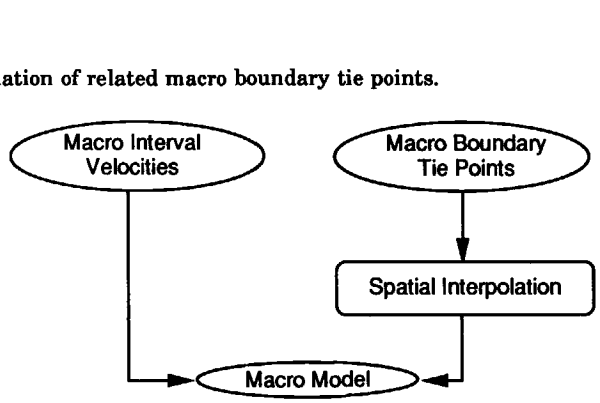

Figure 4.7b
The updated macro velocity model is defined by the interpolated macro boundaries combined with the estimated macro interval velocities.

However, pinch-outs and faults can never be accurately obtained by this splining method. Furthermore, in case of a borehole oriented approach velocity analysis is only done in the vicinity of the well and lateral interpolation is not possible. In general, it is better to use the traveltime information in a direct way to obtain the macro boundaries. Two main strategies can be followed as illustrated by Figure 4.8.

4.3.2 Map migration

The first strategy involves map migration (Figure 4.8a). Input to the map migration algorithm are time tracks that represent zero offset traveltimes. These may for instance be obtained from the stacked data or a

substack (or merely a moveout corrected single offset section). The macro boundaries are tracked in the time-domain, i.e. before depth conversion. The tracked time horizons are then depth converted with a map migration algorithm using the already estimated macro velocities (May and Covey, 1981). This involves inverse zero offset raytracing. For depth conversion of the n^{th} macro boundary it is assumed that the n-1 shallower layers have been determined. The track of the n^{th} tracked time horizon defines the two-way traveltime as a function of lateral distance x,

$$T_n = T_n(x). \tag{4.41}$$

For a surface location the zero offset ray is shot with emergence angle $\beta_{o,n}$. The emergence angle is defined by Tuchel's formula (Tuchel,1943):

$$\frac{dT_n}{dx} = \frac{2 \sin \beta_{o,n}}{c_1}, \tag{4.42}$$

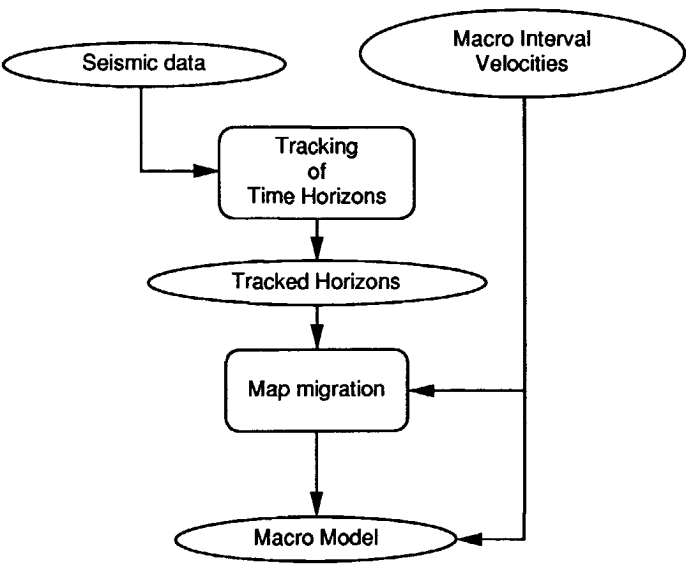

Figure 4.8a
For the estimation of the macro boundaries two methods can be followed, depending on the complexity of the time data. Both methods use the macro velocities that have been previously estimated.
The first method involves tracking of the macro boundaries in a time section. The tracked time horizons are then depth converted with a map migration algorithm.

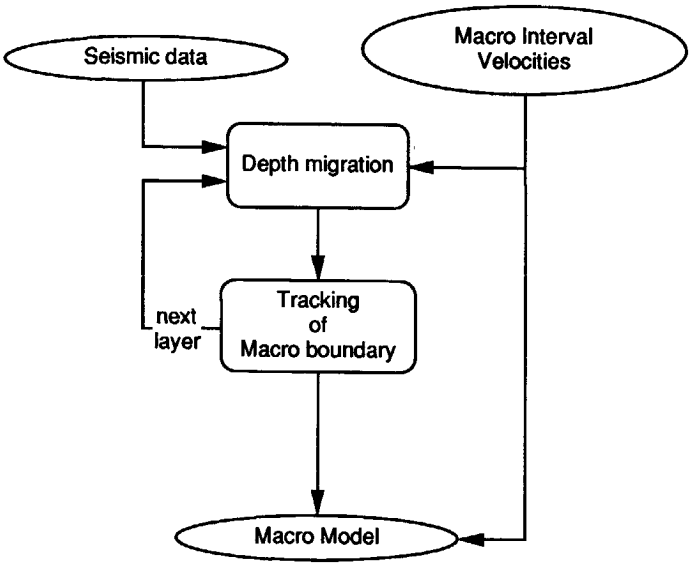

Figure 4.8b
The second method consists of depth migrating the data to just below the bottom of a macro boundary and then tracking the imaged macro boundary.

where c_1 denotes the macro interval velocity at the surface. At each macro boundary the ray is refracted according to Snell's law. The refraction angles are determined by the already estimated macro interval velocities. The raytracing is stopped when the calculated traveltime equals the observed traveltime. The end point of the ray is the normal incidence point to the reflector, so the interface is perpendicular to the end of the ray. The raytracing is done for all surface locations and the calculated normal incidence points are connected to form the n^{th} macro boundary.

This method is very fast, but tracking the macro boundaries before depth conversion may be difficult due to the presence of diffraction energy in the time data. An advantage is that the time horizons have to be tracked only once (since changes in the macro velocity model do not affect the tracked time horizons). Furthermore, after the tracking is done, no user interaction is generally needed in this depth conversion method.

4.3.3 Depth migration

The second strategy of obtaining the macro boundaries involves depth migration (Figure 4.8b). Input to the procedure are the same data as in

the previous method or even the full prestack dataset. These data are then depth migrated, starting with the estimated velocity of the first macro layer, to just below the base of the first macro boundary (until the first macro boundary is completely imaged). This boundary is then tracked and put in the macro velocity model file. Then the procedure is continued, but now the velocity contrast is taken into account and the migration is carried out to just below the next macro boundary which is then tracked, etc. This method is superior over a splining algorithm since the rapid changes of the macro boundaries are correctly taken into account. The advantage of the migration method is that it is very accurate. A disadvantage is that the macro boundaries are tracked *after* depth conversion (migration) which implies that each time the velocities are changed, the depth converted boundaries have to be retracked. Furthermore, the method requires much interaction since the migration can be continued only after the current macro boundary is imaged.

In conclusion, in simple situations the time horizons of macro boundaries can be tracked relatively easily and the map migration method will generally be an adequate method for the macro boundary delineation. However, in complex situations the unmigrated data can be very difficult to interpret, which causes serious difficulties in tracking the macro boundaries in the *time*-domain. Hence, in such cases it is preferred to postpone the tracking procedure until after depth migration, i.e. the tracking is done in the *depth*-domain. From an economical point of view it is not yet feasible to perform a repeated prestack depth migration for the delineation of the macro boundaries. Moreover, by deciding upon the macro boundary algorithm we should bear in mind that here we are only interested in the structure of the macro boundaries and not in true amplitudes. Therefore it is attractive, and often sufficient, to convert the macro boundaries from time to depth by migration of single offset data.

CHAPTER 5

EXAMPLES OF MACRO MODEL ESTIMATION

5.1 INTRODUCTION

In this chapter the macro model estimation procedure is illustrated with examples. In section 5.2 the method is applied to elastic data generated with an elastic finite difference modeling scheme. Estimation of the P-wave macro model and the S-wave macro model is discussed. Section 5.3 shows the method applied to water tank data. Finally, in section 5.4 a real data example is treated. The examples discussed here involve reservoir oriented macro model estimation.

5.2 ELASTIC MACRO MODEL ESTIMATION

In this section the results will be discussed of macro model estimation on simulated elastic data. Shot records were generated with elastic finite difference modeling. The true model is depicted in Figure 5.1. Vertical and horizontal components of the particle velocity were recorded due to vertical and horizontal stress sources.

The data were recorded with the following parameters:

source types	T_{zz} and T_{xz}
receiver types	V_z and V_x
shot spacing	16 m
detector spacing	16 m
number of channels	160

number of shots	128
acquisition geometry	fixed spread
first shot is at	256 m
first detector is at	0 m
sample interval	4 ms
frequency contents	5-70 Hz

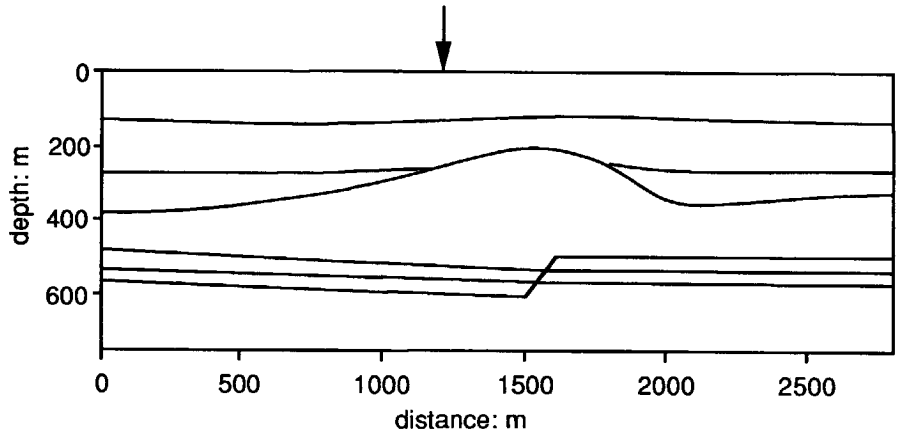

Figure 5.1
2-D inhomogeneous elastic subsurface containing target reflectors below an inhomogeneous overburden.

Figure 5.2 shows one multi-component shot record, the shot location being indicated by the arrow in Figure 5.1. The response of a vertical vibrator, measured by a geophone that records the vertical component of the partical velocity, is generally considered as P-P data (Figure 5.2a). However, from the picture it is clear that these data contain S events as well. Therefore, it is better to refer to these data as pseudo P-P data. After decomposition and elimination of the surface-related multiples, the data shown in Figure 5.3 are obtained. These surface-related processing steps have cleaned up the responses considerably. Furthermore, we can deal with scalar quantities now, and the processing can be split (Chapter 1). The P-P shot records are used to estimate the P-wave macro model. The S-wave macro model can be separately estimated by using the S-S shot records.

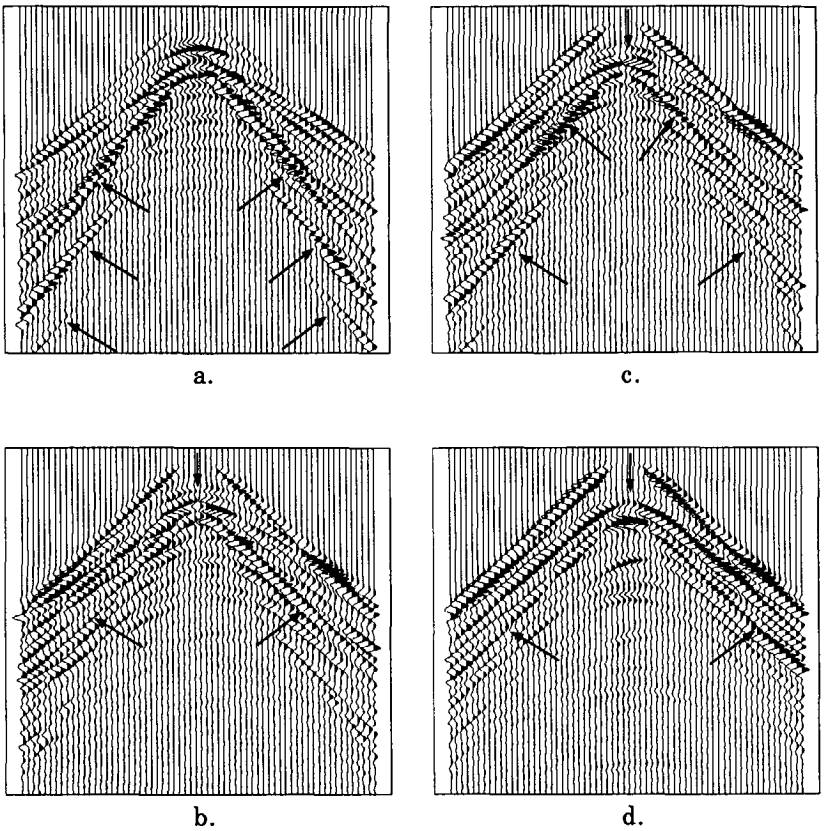

Figure 5.2
Multi-component shot record. The groundroll has already been removed from the data. The arrows indicate spurious events.

a. Pseudo P-P data.
b. Pseudo SV-P data.
c. Pseudo S-S data.
d. Pseudo SV-SV data.

5.2.1 Estimation of the P-wave macro model

Figure 5.4a shows the initial model. In practice conventional velocity analysis has already been done and a better initial estimate may be available. However, to emphasize the convergence of the scheme, this initial model is chosen far from the true model. For estimation of the macro interval velocities the P-P shot records were redatumed to the three vertical datum lines indicated. Two focus panels are shown in Figure 5.4b.

Picking of the foci and application of the update equations results in the following estimated macro interval velocities.

Table 5.1
Updated macro interval velocities in the different layers.

Macro layer	Macro interval velocity [m/s]
1	2275
2	3274
3	2952
4	3955

Since there are three vertical datum lines three estimates of the macro interval velocity are obtained for each macro layer. These were averaged to stabilize the result. So here a priori information, that the macro interval velocities are laterally constant, is used. If a lateral variation would be present, averaging is not allowed and lateral interpolation should be done instead. Note that the number of layers is determined by the number of picked foci and not by the number of interfaces in the initial model.

After the macro interval velocities have been estimated, the macro boundaries have to be converted to depth. From the shot records the zero offset section is extracted (Figure 5.5a) of which the time horizons are tracked. The tracking is done with an automated tracking algorithm (Geerlings, 1990). The tracked horizons (Figure 5.5b) are now depth converted with a map migration scheme (Chapter 4). The map migration procedure is repeated for the next interface until all macro boundaries have been depth converted (Figures 5.6). The macro model (velocities and boundaries) has now been updated. This is the end of the first iteration. The total procedure is repeated with the updated macro model. Again the velocities are estimated from the foci (picked from the new focus panels) and the current macro model (Figure 5.7). Note that the number of vertical datum lines (and their position) is not necessarily the same as in the previous run. Next, the map migration procedure is repeated with the newly estimated velocities resulting in the updated macro model. Note that the time horizons do not have to be retracked.

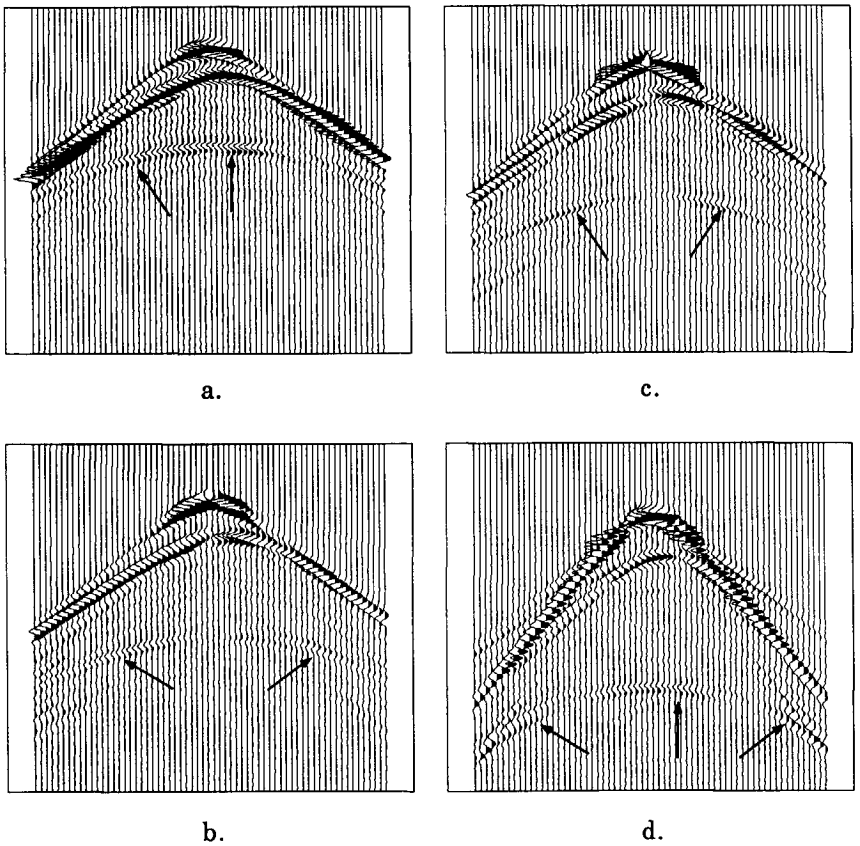

Figure 5.3
Multi-component shot record after elastic decomposition and elastic multiple elimination.
The arrows indicate the response of the target reflectors below z_t = 450 m.
a. True P-P data.
b. True SV-P data.
c. True S-S data.
d. True SV-SV data.

When all foci are located at zero-time (or if the focus times are within some threshold value) the iteration can be stopped. After three iterations the final macro model is obtained (Figure 5.8). The correctness of the model is verified by:

1. Focus panels containing foci at t=0 (Figure 5.8b).
2. CDP-gathers related to a reflector depth point containing a horizontally aligned event at t=0 (Figure 5.8c).
3. Image gathers containing horizontally aligned events at the depth of the reflectors (Figure 5.8d).

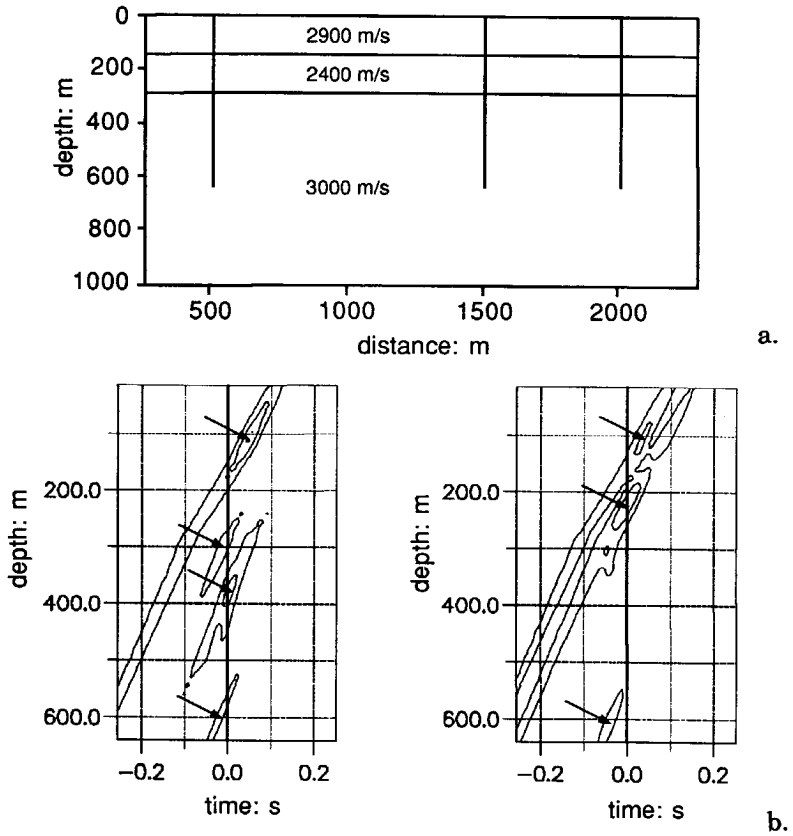

Figure 5.4

a. Initial P-wave macro model.

b. Focus panels at x=500m and x=1500m.

5.2.2 Estimation of the S-wave macro model

By taking a Poisson ratio of 0.25 the P-wave macro model was converted to a rough estimate of the S-wave macro model. This serves as an initial model (Figure 5.9a). Estimation of the S-wave macro model is done with the S-S shot records in analogy with the P-wave macro model. Redatuming to the vertical datum line yields the focus panel shown in Figure 5.9b. It can be seen that there is an ambiguity in picking the first focus. To investigate this problem redatuming was done with the true macro model. In this panel (Figure 5.10a) we would expect a focus at the reflector depths and at t=0. As can be seen from the picture this is not the case. Instead we can observe two foci around the correct depth location. By inspecting the CDP-gather at the correct depth it is immediately clear

what is the cause of this anomaly (Figure 5.10b). The event of the reflector is perfectly aligned at t=0 (as could be expected since the model was correct) but due to the polarity reversal in the wavelet along the event, stacking of this CDP-gather will not yield a high amplitude. The polarity reversal is caused by the angle-dependent reflection coefficient. By comparing the P-P reflection coefficient and the S-S reflection coefficient of this particular interface (Figure 5.11) it becomes clear that in the S-S data a polarity reversal occurs whereas in the P-P data this is not the case. Therefore, this problem did not occur in estimating the P-wave macro model.

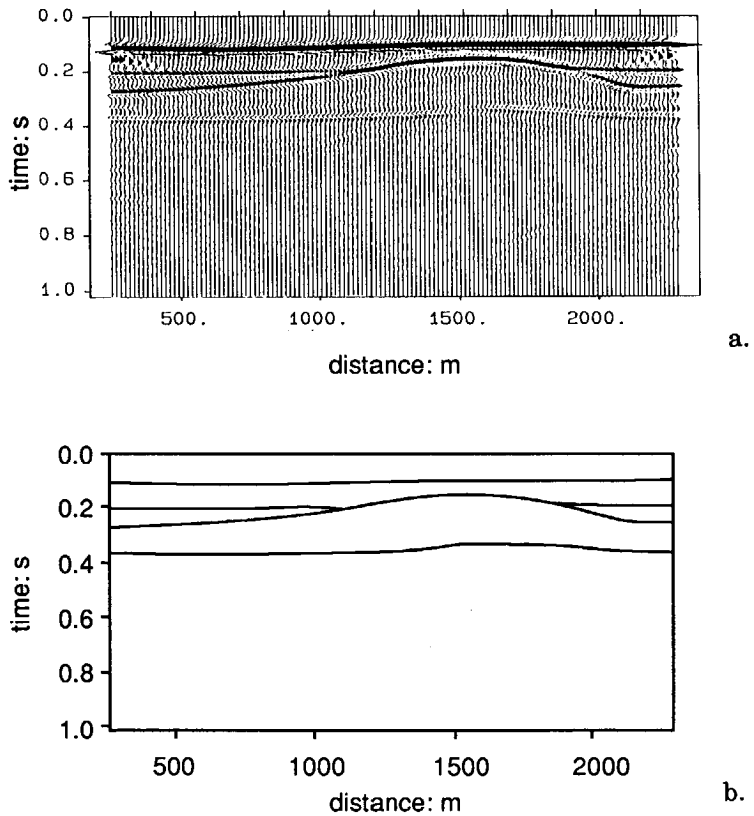

Figure 5.5

a. P-P zero offset section.

b. Tracked horizons from the zero offset section.

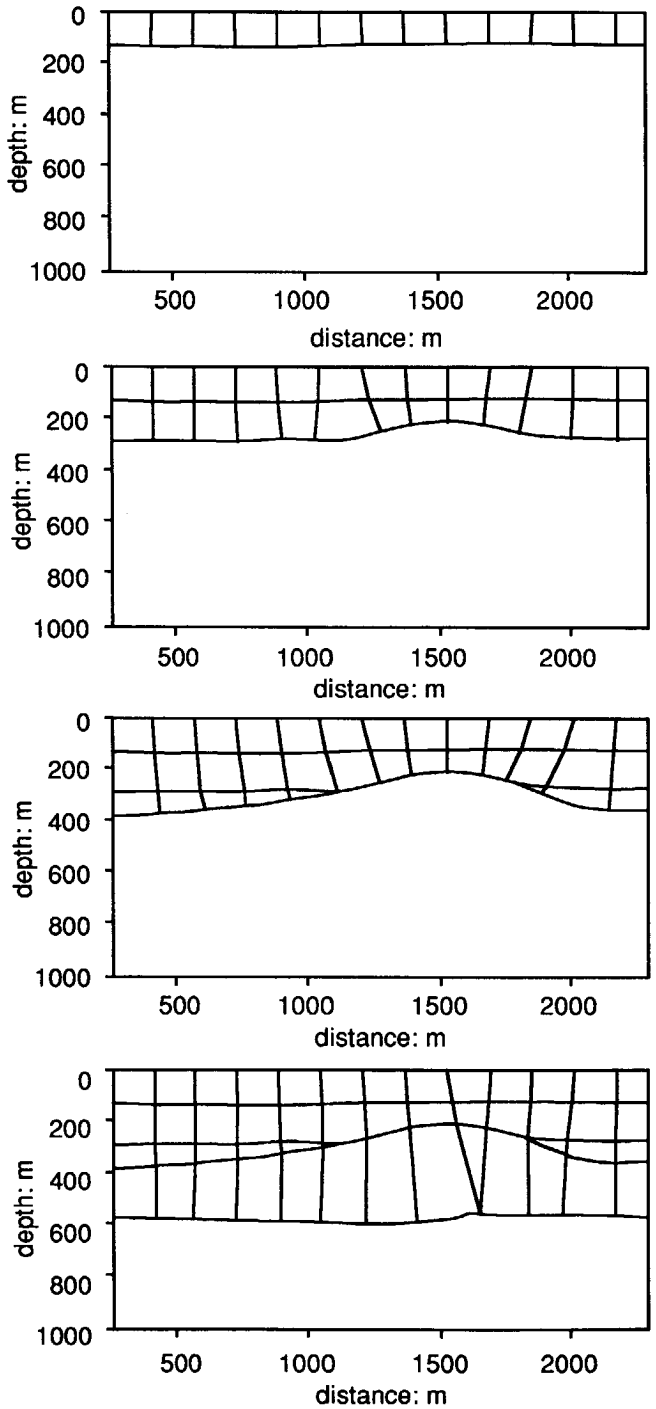

Figure 5.6
Depth conversion of the tracked time horizons by map migration is a top-down approach.

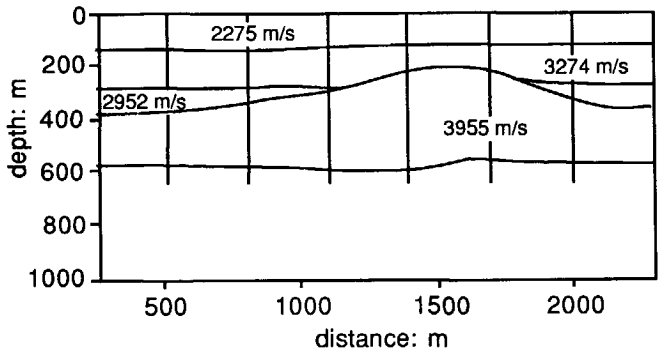

a.

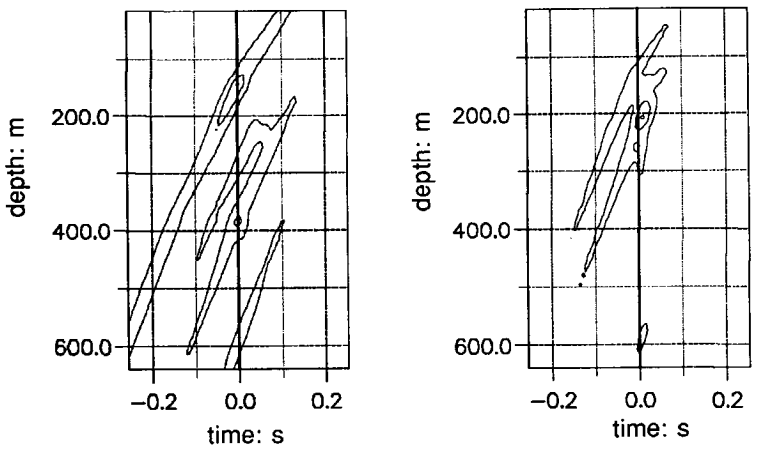

b.

Figure 5.7

a. The procedure is repeated with the updated macro model. Redatuming is done to the vertical datum lines indicated, resulting in the focus panels shown in Figure 5.7b.

b. Focus panels at x=500m and x=1400 m.

So, stacking the CDP-gathers may not always be the best way to determine alignment and therefore we have to look for different alignment measures. Here the advantage of shot record oriented processing becomes clear. By taking the envelope of the individual CDP-traces, the stacked trace no longer suffers from phase changes of the wavelet. The resulting focus panel is now shown in Figure 5.12. It can be seen from the picture that the resolution has slightly degraded by taking the envelope first. The final S-wave macro model is obtained in one iteration (Figure 5.12a).

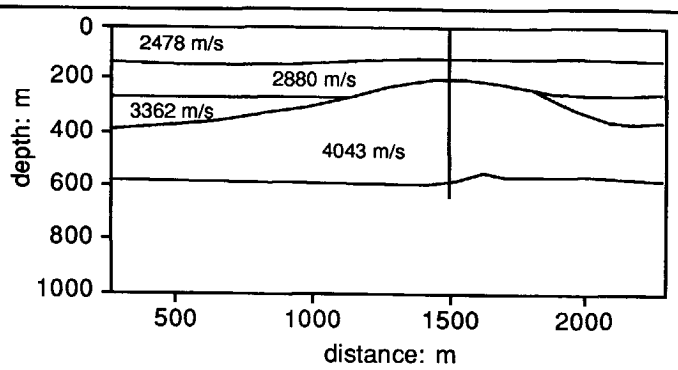

a.

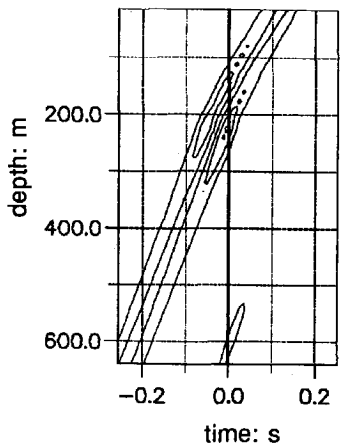

b.

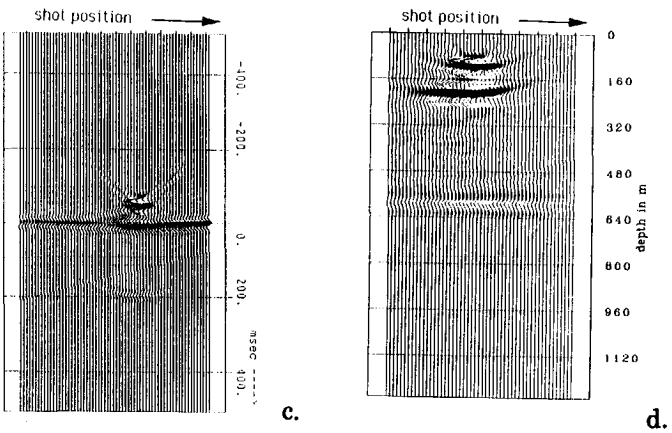

c. d.

Figure 5.8

a. The final estimated P-wave macro model is obtained after three iterations. The correctness of the model is verified by :

b. Focus panels containing foci at t=0.

c. CDP-gathers related to a reflector depth point containing a horizontally aligned event at t=0.

d. Image gathers containing horizontally aligned events at the depth of the reflectors.

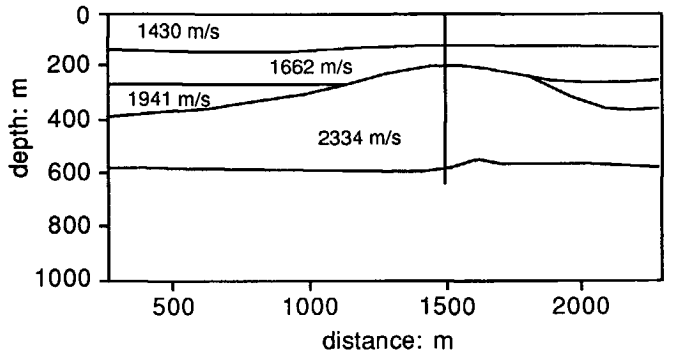

a.

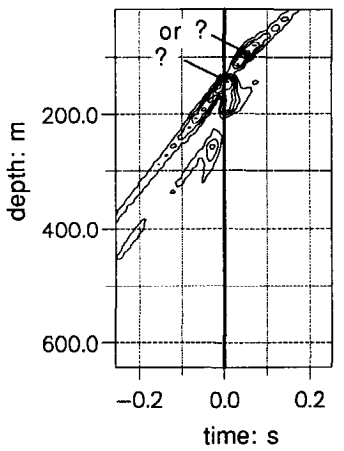

b.

Figure 5.9

a. By taking a Poisson ratio of 0.25 the P-wave macro model was converted to a rough estimate of the S-wave macro model.

b. Focus panel at x=1500 m.

5.2.3 Importance of surface-related preprocessing

In this section the importance of the surface-related preprocessing is illustrated. Redatuming was done to a vertical datum line using the shot records with vertical vibrators and geophones as well (pseudo P-P data, see Figure 5.2a). From these data only the groundroll was removed but no decomposition or multiple elimination was applied. The unprocessed data still contain S-events. Also very strong surface-related multiples are present. The redatuming is done with the true model resulting in the focus panel shown in Figure 5.13. Note that the redatuming process treats the data as if they were pure P-P data. By comparing this result with

Figure 5.8b it becomes clear that the focus panel is severely degraded by the presence of multiples and S-events.

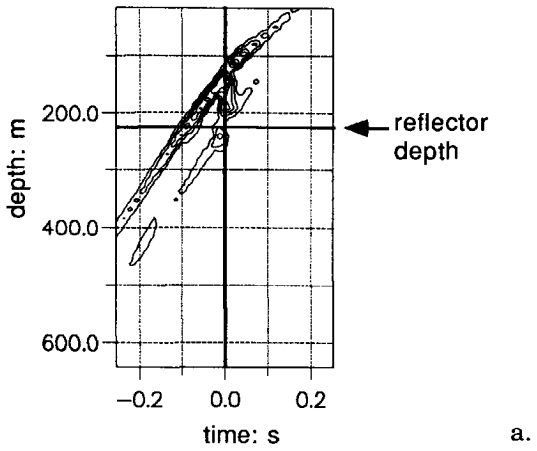

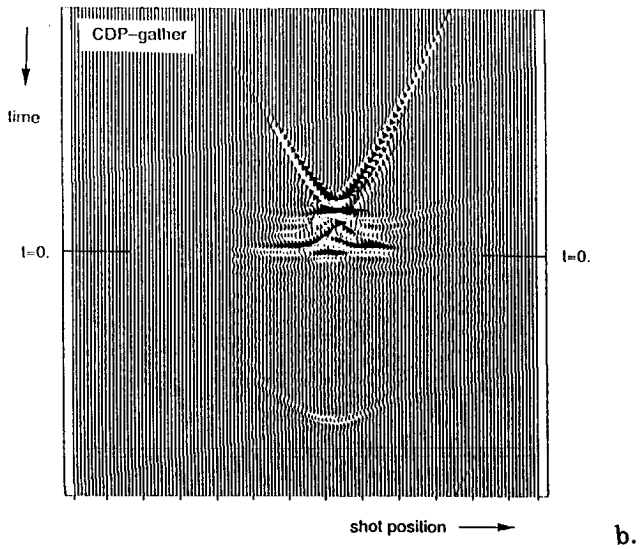

Figure 5.10

a. Focus panel at x=1500 m for true macro model.

b. CDP-gather at x=1500 m, z=208 m (related to a grid point on the second reflector).

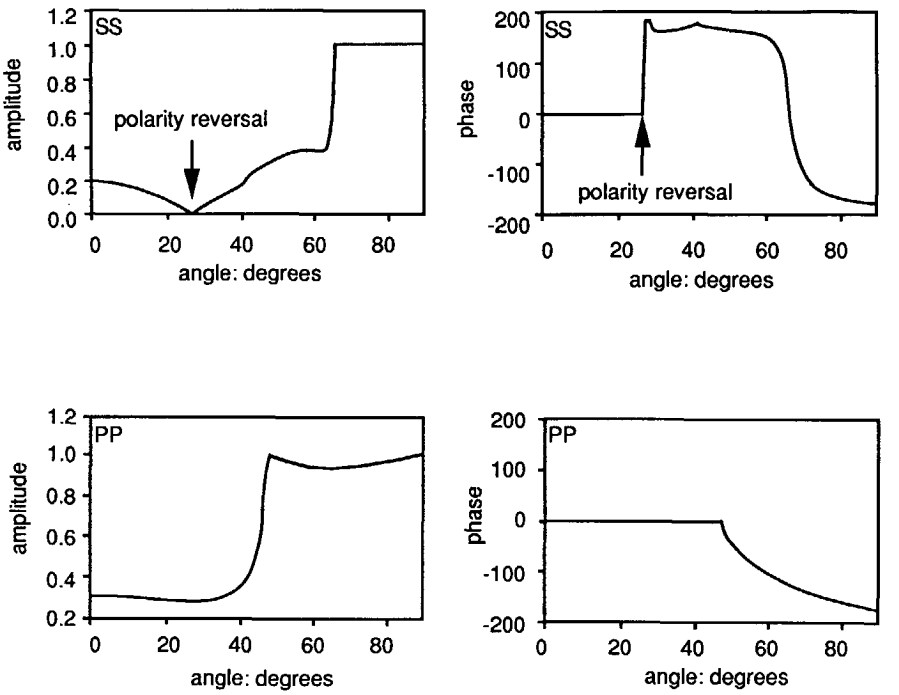

Figure 5.11

a. The angle-dependent S-S reflection coefficient shows a polarity reversal.
Amplitude versus angle (left).
Phase versus angle (right).

b. Angle-dependent P-P reflection coefficient.
Amplitude versus angle (left).
Phase versus angle (right).

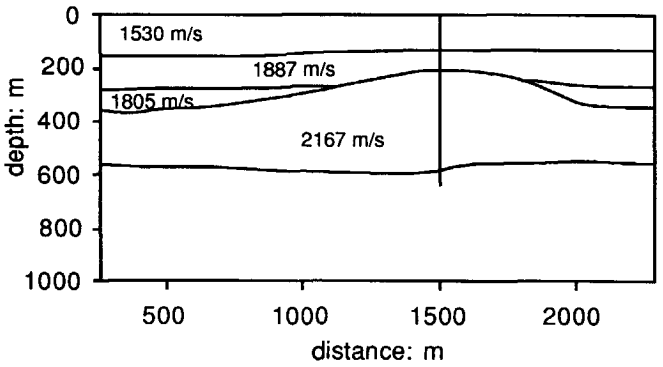

a.

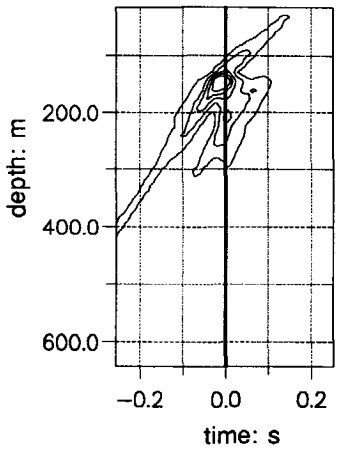

b.

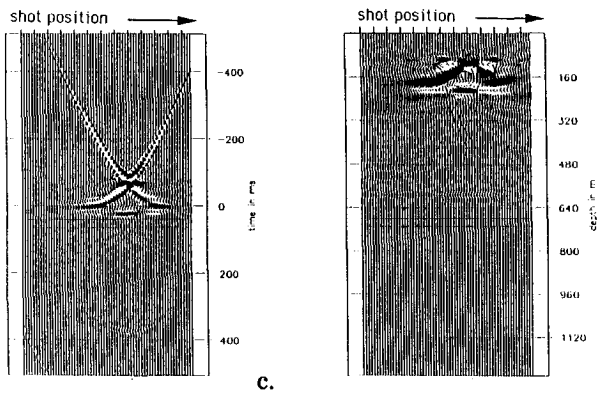

c. d.

Figure 5.12

a. **The final estimated S-wave macro model is obtained after three iterations.**

The correctness of the model is verified by :

b. **Focus panels containing foci at t=0.**

c. **CDP-gathers related to a reflector depth point containing a horizontally aligned event at t=0.**

d. **Image gathers containing horizontally aligned events at the depth of the reflectors.**

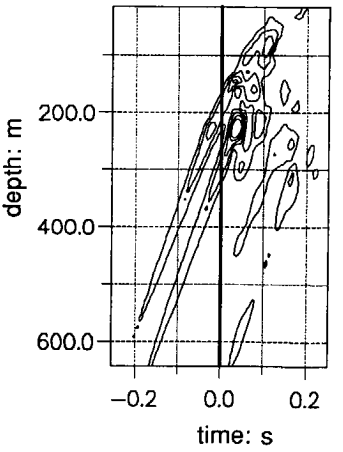

Figure 5.13
Focus panel obtained by redatuming the raw (pseudo P-P) shot records to a vertical datum line (x=1100 m) using the correct macro model. Note that the quality of the panel has degraded due to the absence of preprocessing; some foci occur off the t=0 line, due to the S-events and multiples that are in the data.

5.3 ESTIMATION OF A MACRO VELOCITY MODEL FROM PHYSICAL MODEL DATA

In this section I will discuss the estimation of a macro velocity model from prestack data obtained from a scale model in the water tank of the SAL (Seismic Acoustic Laboratory) in Houston. The deconvolved data were provided by Marathon Oil. The water layer above the scale model was very thick, so that no surface-related multiples were present in the recorded data. The transducers were positioned close to the surface of the model. Only the recorded shot records were available (Figure 5.14). It turned out that conventional velocity analysis based on stacking of CMP-gathers did not produce satisfactory results. This was due to non-hyperbolic moveout in the CMP data (Figure 5.15). So no conventional result was available that could serve as an initial model.

The data were recorded with the following parameters:

shot spacing	24.384 m (80 ft)
detector spacing	24.384 m (80 ft)
number of channels	48
number of shots	296
acquisition geometry	end-off spread
first shot is at	0 m
first detector is at	243.84 m (800 ft)
sample interval	4 ms
frequency contents	5-70 Hz

The values listed above were scaled to seismic dimensions. The scale factors used by SAL were: 1 mm in model dimensions corresponds to 12 m in seismic dimensions and 1 ms corresponds to 5 s. Hence, due to the different scaling factors used in time and distance, the water velocity (1500 m/s) is scaled to 3600 m/s.

From the shot records (Figure 5.14) I extracted the near offset section (Figure 5.16). Zero offset traces were not present in the recorded data. After deconvolution the data were very nearly zero phase, apart from the first event which has some serious ringing.

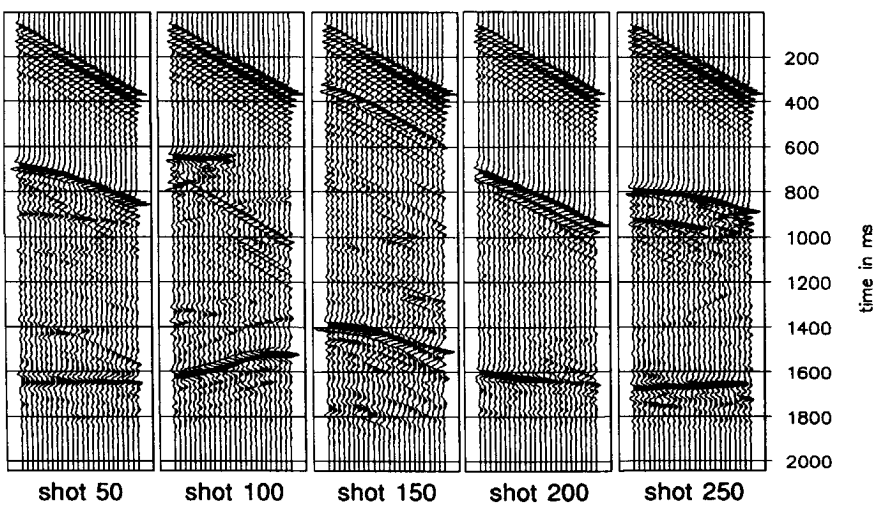

Figure 5.14
Some shot records from the watertank experiment.

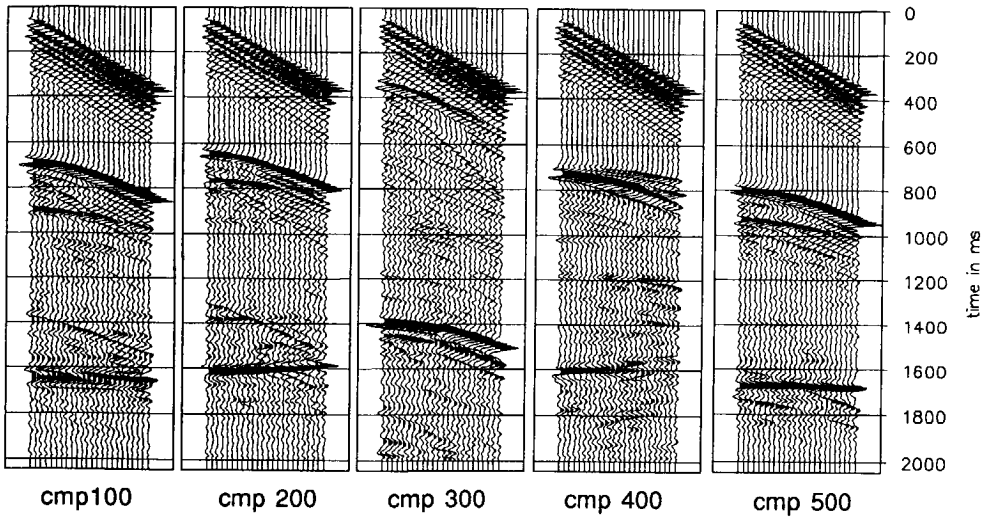

Figure 5.15
CMP-gathers showing non-hyperbolic moveout.

The near offset section shows that the first interface is horizontal and very shallow. The wavelet for this event deviates from the other events. This is mainly due to the fact that energy sent under large emergence angles results probably in a deviating wavelet. Since the first interface is horizontal, the velocity of the first layer, which is the water layer, can be

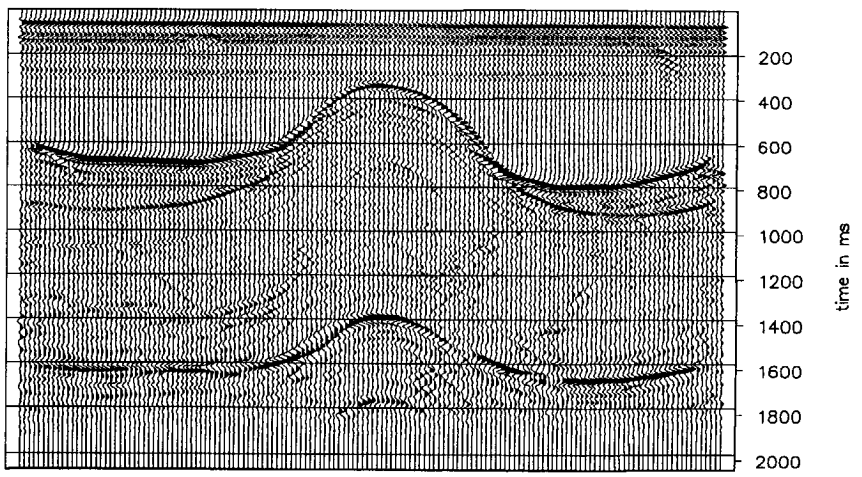

Figure 5.16
Near offset section.

estimated from the moveout in the shot records. The (scaled) water velocity was estimated at 3700 m/s. In the estimation procedure a constant macro interval velocity was assumed for all other macro layers as well (a priori knowledge).

The initial model was taken to be homogeneous (with the estimated water velocity of 3700 m/s, Figure 5.17a). The shot records were redatumed to the twelve indicated vertical datum lines. One of the twelve resulting focus panels is shown in Figure 5.17b. The first focus is already at zero-time. Hence, the first layer indeed has a velocity of 3700 m/s. The second focus is not even close to the zero-time axis and since it occurs at positive times the velocity that was used in extrapolation was much too high for the second layer. After four iterations the second macro interval velocity was estimated at c_2=2500 m/s. For the moment the macro boundary is determined by lateral interpolation of the twelve macro boundary tie points (an improved solution is discussed below).

With the derived model (Figure 5.18a) the next interface was estimated. From the focus panel of Figure 5.18b it is clear that the velocity in this layer must be lower than the one used in the macro velocity model (5525 m/s). From the vertical datum lines in the middle of the model there were no foci for this interface. This fact indicates a pinch-out structure which could easily be seen in the near offset section.

I allowed for the two pinch-outs to have different velocities resulting in the model shown in Figure 5.19a. Again the macro boundary was obtained by interpolation of the macro boundary tie points available from the focusing analysis. This was the sixth iteration. The next estimated interface is a faulting structure (Figure 5.20a) derived from the focus panels as shown in Figure 5.19b. The fault in the macro velocity model could be sharper if there would have been a denser lateral sampling of the vertical datum lines.

The model in Figure 5.20a was obtained after eight iterations. From the next focusing analysis, shown in Figure 5.20b, it becomes clear that there exists at least one other interface. This interface should image between 3300 m and 3400 m, since the event crosses the zero-time axis between those depths. On this event focusing analysis failed because of the lack of

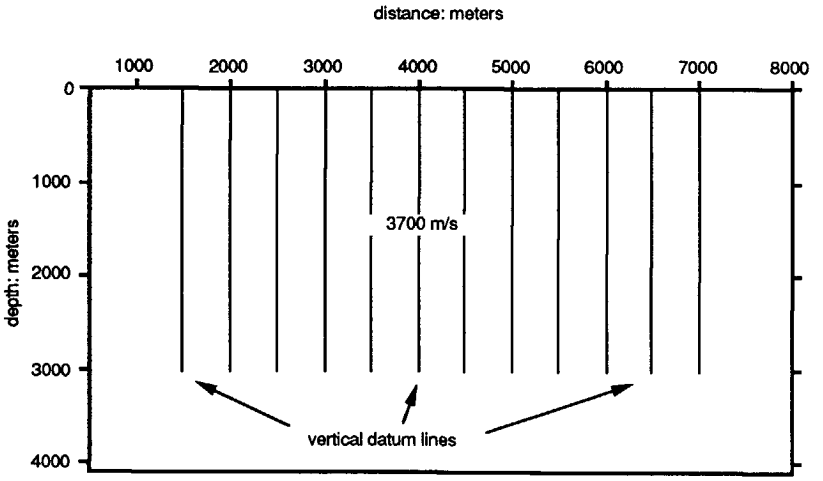

a.

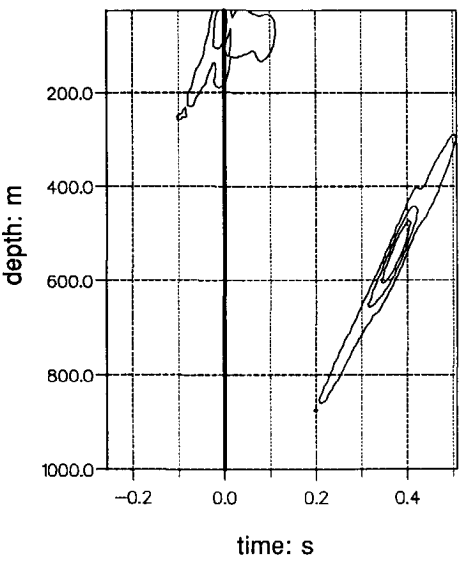

b.

Figure 5.17
a. Initial model.
b. Focus panel at x=1500 m.

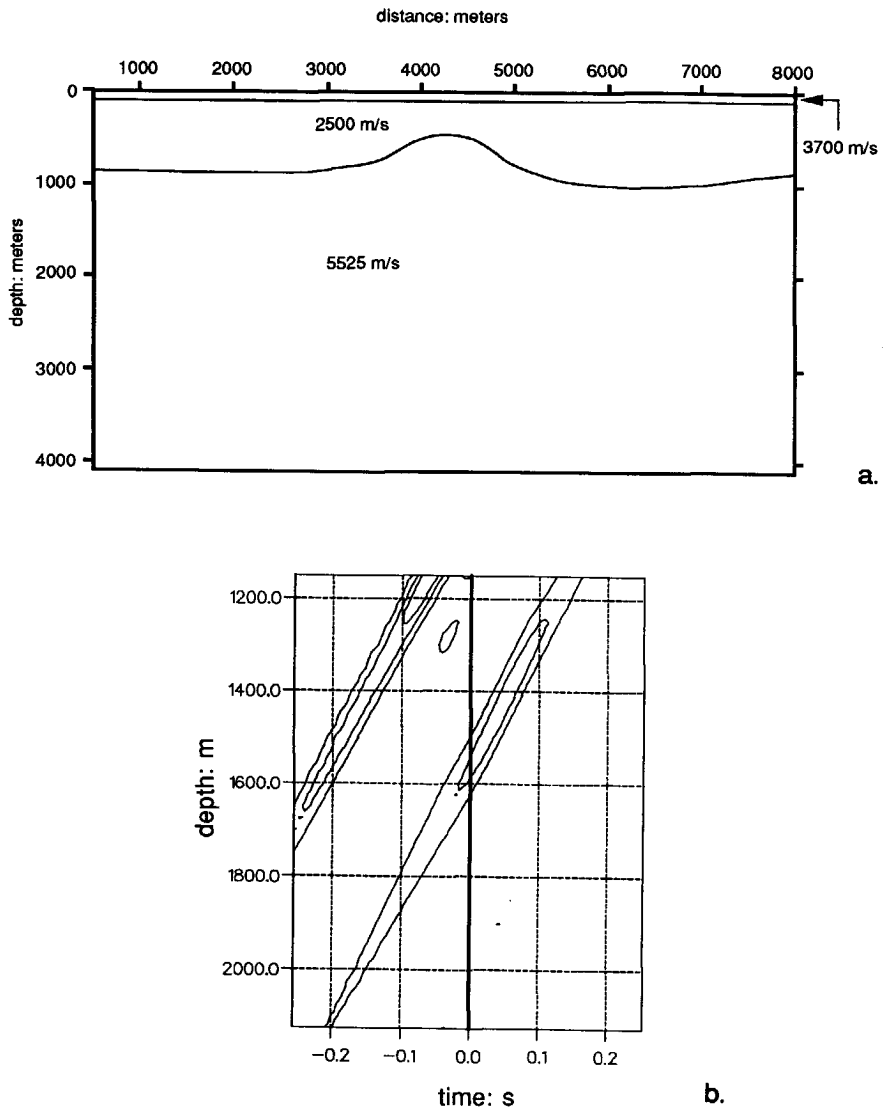

Figure 5.18

a. **Macro velocity model after four iterations.**

b. **Focus panel at x=1500 m.**

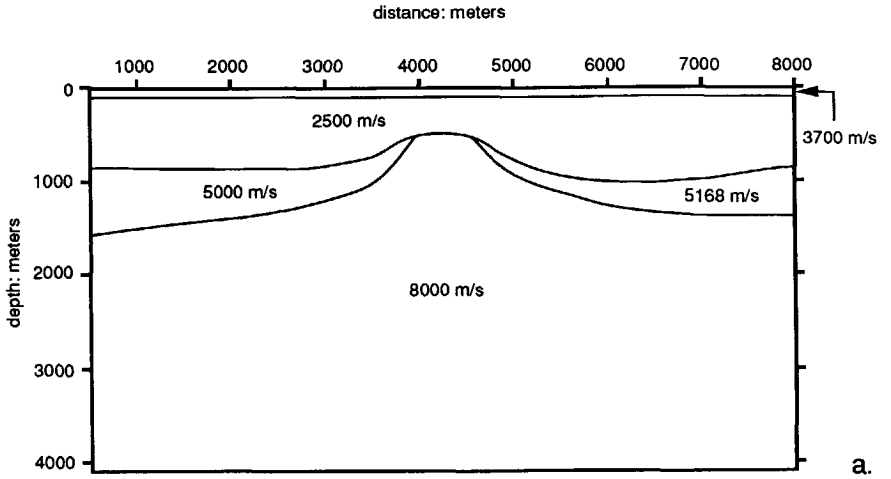

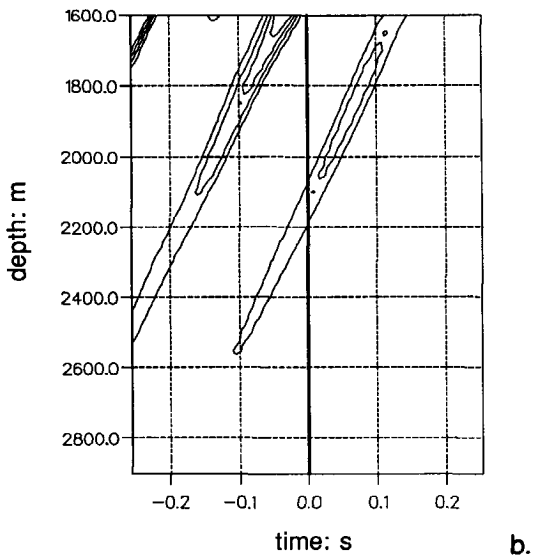

Figure 5.19

a. **Macro velocity model after six iterations.**

b. **Focus panel at x=1500 m.**

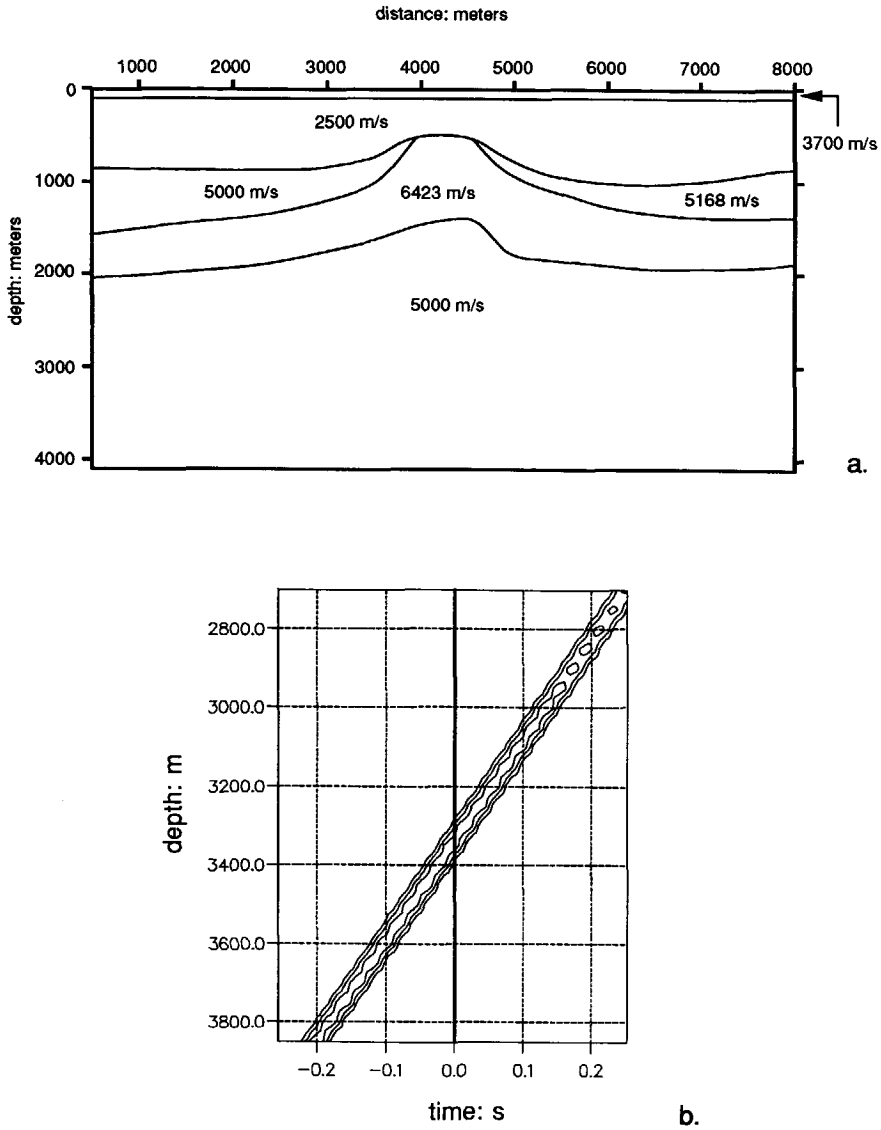

Figure 5.20

a. Macro velocity model after eight iterations.

b. Focus panel at x=1500 m.

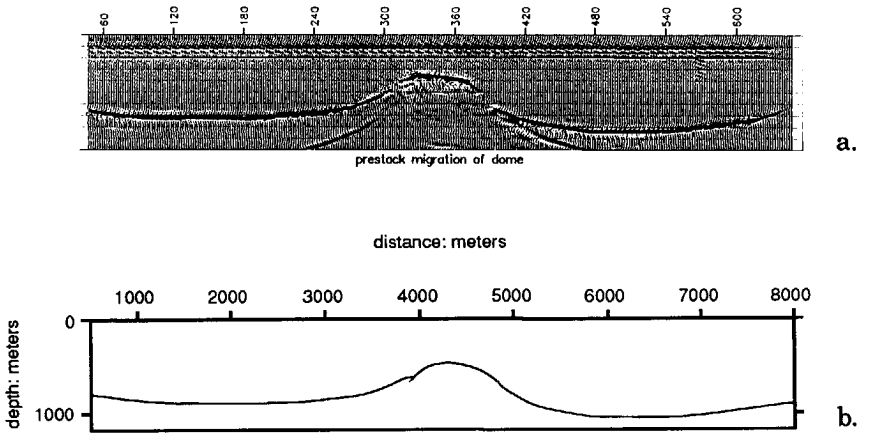

Figure 5.21

a. Prestack migration result to delineate the dome structure.

b. The imaged dome is tracked and stored in the model.

resolution. As in conventional velocity analysis deeper structures will yield less resolution than shallower structures.

As was mentioned in Chapter 4, sudden lateral changes in the macro boundaries cannot be estimated accurately by interpolation of the macro boundary tie points. Hence, depth migration was used to improve the definition of the pinch-outs and the faulting reflector below the dome structure. With the estimated velocities above the dome a prestack migration was performed (Figure 5.21a). By tracking the imaged dome structure the improved macro boundary was determined and stored in the model (Figure 5.21b). Next, the prestack migration was repeated with the new model, in order to image and track the next macro boundary and so on. The final model is shown in Figure 5.22. Note that the pinch-out structures and the faulting reflector below the dome have improved considerably. The focus panel and the related image gather verify the correctness of the macro velocity model.

Figure 5.23b shows the prestack migrated section with the final model. From this figure it can be seen that even the fault blocks below the faulting reflector are imaged well (arrows). To show the effect of prestack depth migration the near offset section is displayed as well (Figure 5.23a).

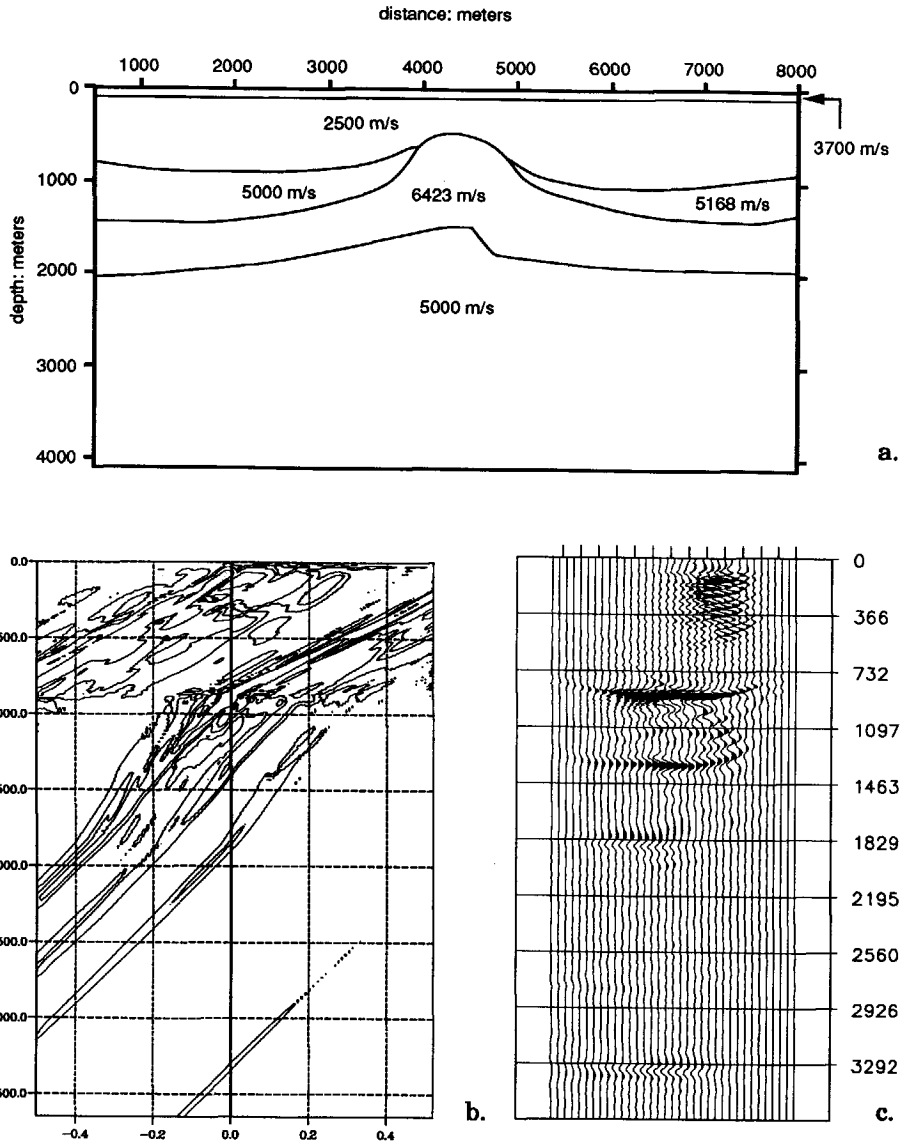

Figure 5.22

a. Final model.

b. Focus panel at x=2000 m. To show all relevant foci the logarithm of the data are displayed.

c. Image gather at x=2000 m.

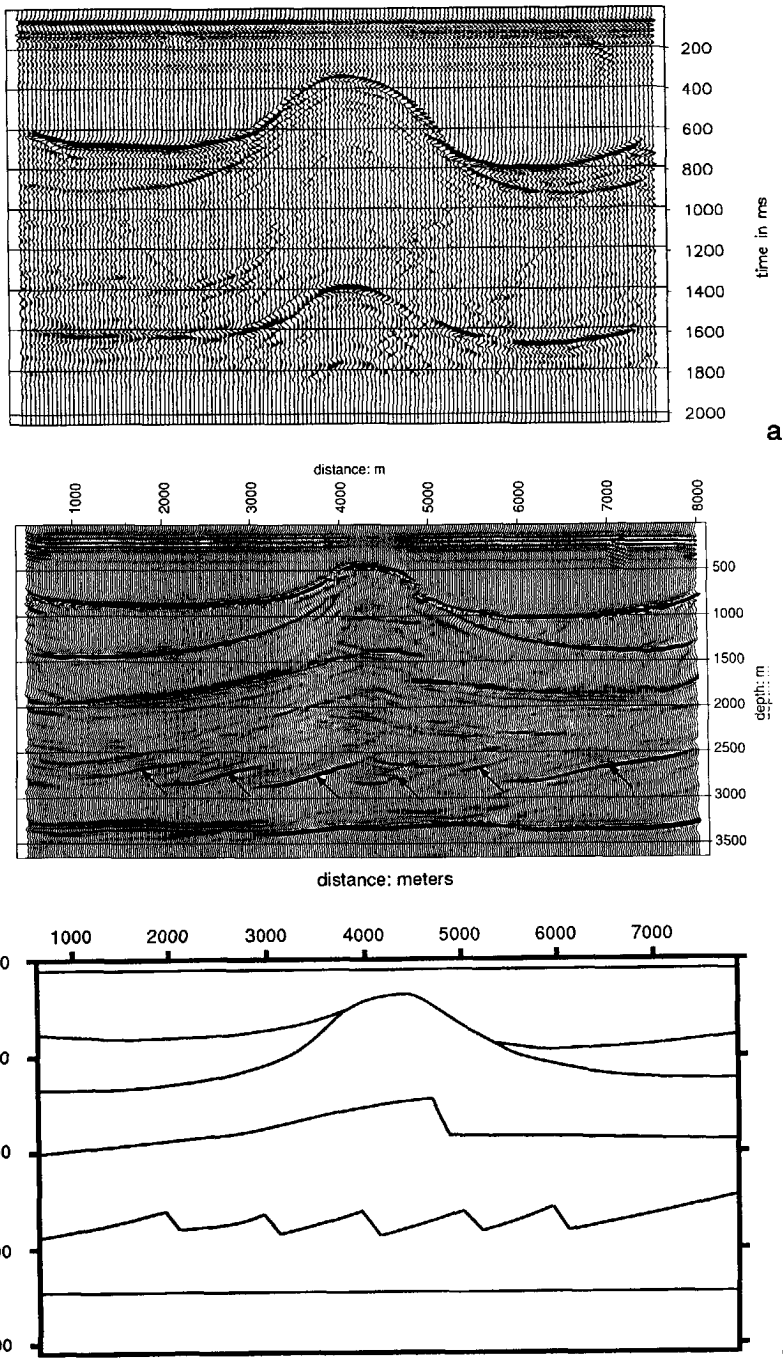

Figure 5.23

a. Near offset section.

b. Prestack migration with the final model.

c. "Blue-print" that was used to build the physical model.

The results were compared to the results presented at the SEG conference in Los Angeles by Postma and Jeannot (1988). The velocities turned out to be less than 7% off compared to the true velocities given in the paper. Jeannot, who uses an S-G based macro velocity model estimation technique, obtained the same accuracy. In Figure 5.23c the "blue-print" is shown that was used to build the physical model. The dome structure and the pinch-out structures were estimated slightly deeper than the corresponding events in the "blue-print". By reinspection it turned out that the physical model was constructed with slight differences from the design documents (Postma and Jeannot, 1988).

5.4 ESTIMATION OF A MACRO VELOCITY MODEL FROM REAL DATA

This section discusses the estimation procedure of a macro velocity model from real data obtained by marine acquisition[1].

The dataset was recorded with the following parameters:

shot spacing	25 m
detector spacing	25 m
number of channels	96
number of shots	332
acquisition geometry	end-off spread
first shot is at	3950 m
first detector is at	1375 m
minimum offset	200 m
sample interval	4 ms
frequency contents	5-70 Hz

From these data an initial model was available, as shown in Figure 5.24a. This type of geology is quite common in the North Sea area. The model contains strong vertical gradients within the macro layers. The major horizons and velocity distributions are given in Table 5.2.

[1]courtesy Placid International Oil, LTD.

Table 5.2
Major horizons and velocity distributions of the initial model. The velocities given in this table represent the propagation velocity at the top of each macro layer.

macro layer	starting velocity m/s	vertical gradient s^{-1}
surface – base Tertiary	1690	0.5
base Tertiary – base Chalk	3660	1.2
base Chalk – top Zechstein	3810	0.4
top Zechstein –>	4500	constant

The gradients were derived from a velocity log that was measured in a nearby well (off the acquisition area). As was already discussed in section 4.2.2 vertical gradients can not be accurately determined from surface measurements. Hence, the gradients were included as a-priori knowledge in the estimation procedure. The stacked section (Figure 5.24b) was obtained after DMO correction. Figure 5.25 shows three common offset sections. As can be seen the far offsets are contaminated with noise and therefore these offsets did not contribute positively to the quality of the stack.

First the initial model was used to depth migrate the poststack section. This provides a preview of the subsurface under consideration (Figure 5.24c). Next, the shot records were extrapolated using the initial model. The prestack depth migration (Figure 5.26b), as well as the focus panels and image gathers (Figures 5.26c and d), were obtained with a shot record extrapolation algorithm. To reduce the computation time, only a part of the shot records is used (12.5%), which corresponds to a shot sampling of 200 m. This reduction gives satisfactory results for the migrated section, but the focus panels suffer from the sparse shot sampling. This can be explained in the following way. When the model is correct, the primary reflections in the CDP-gathers will be horizontally aligned at t=0. Hence, if the initial macro model is already close to the true macro model, spatial aliasing of primary energy will only occur away from the "t=0"-axis. The effect is visible in Figure 5.27a where additional

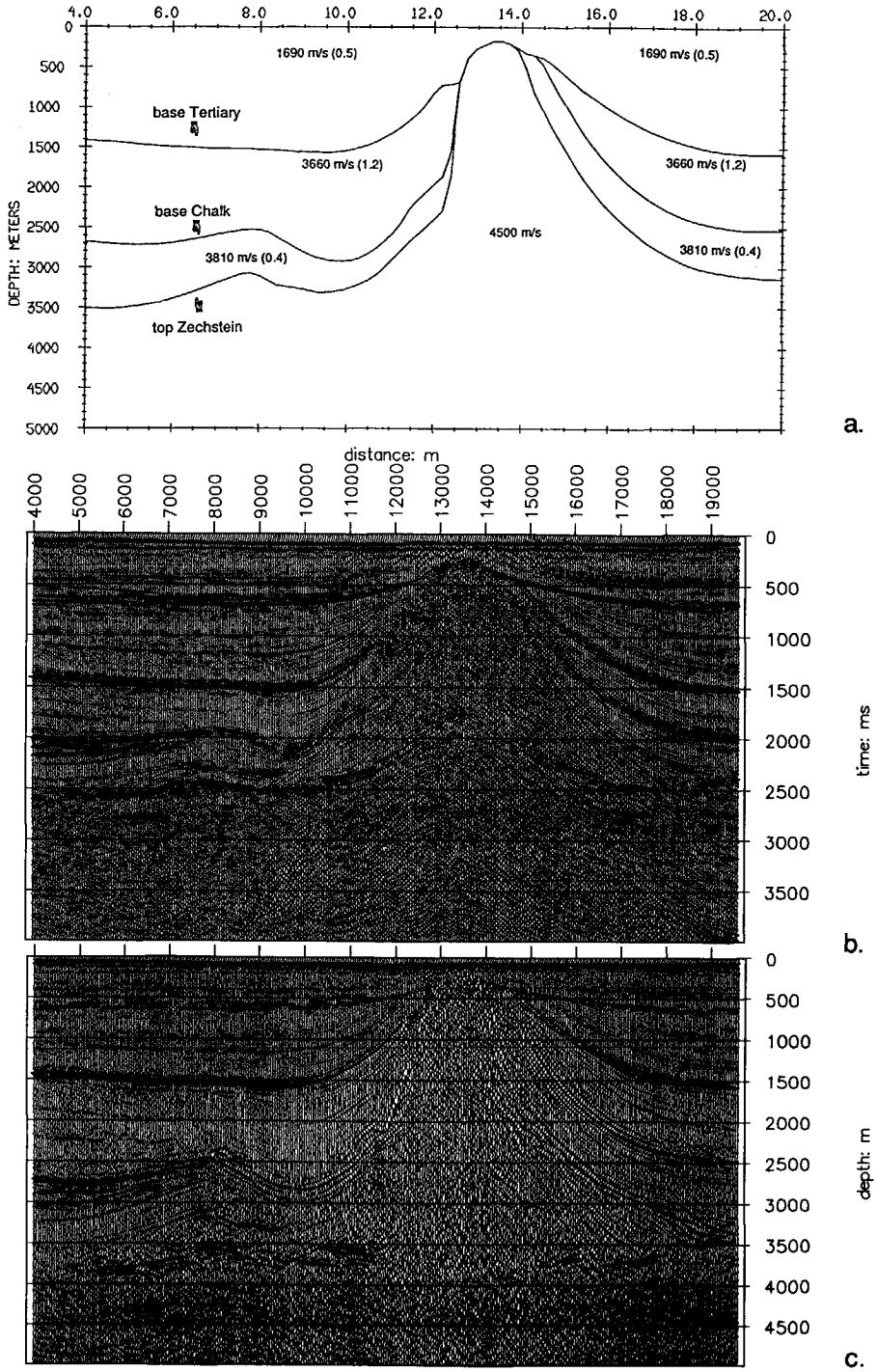

Figure 5.24

a. Initial model. The velocities given in this figure represent the propagation velocity at the top of each macro layer. Note that these starting velocities are laterally constant. The vertical gradients are displayed between brackets ( ).

b. Stacked section (after DMO correction).

c. Depth migration of the stacked section.

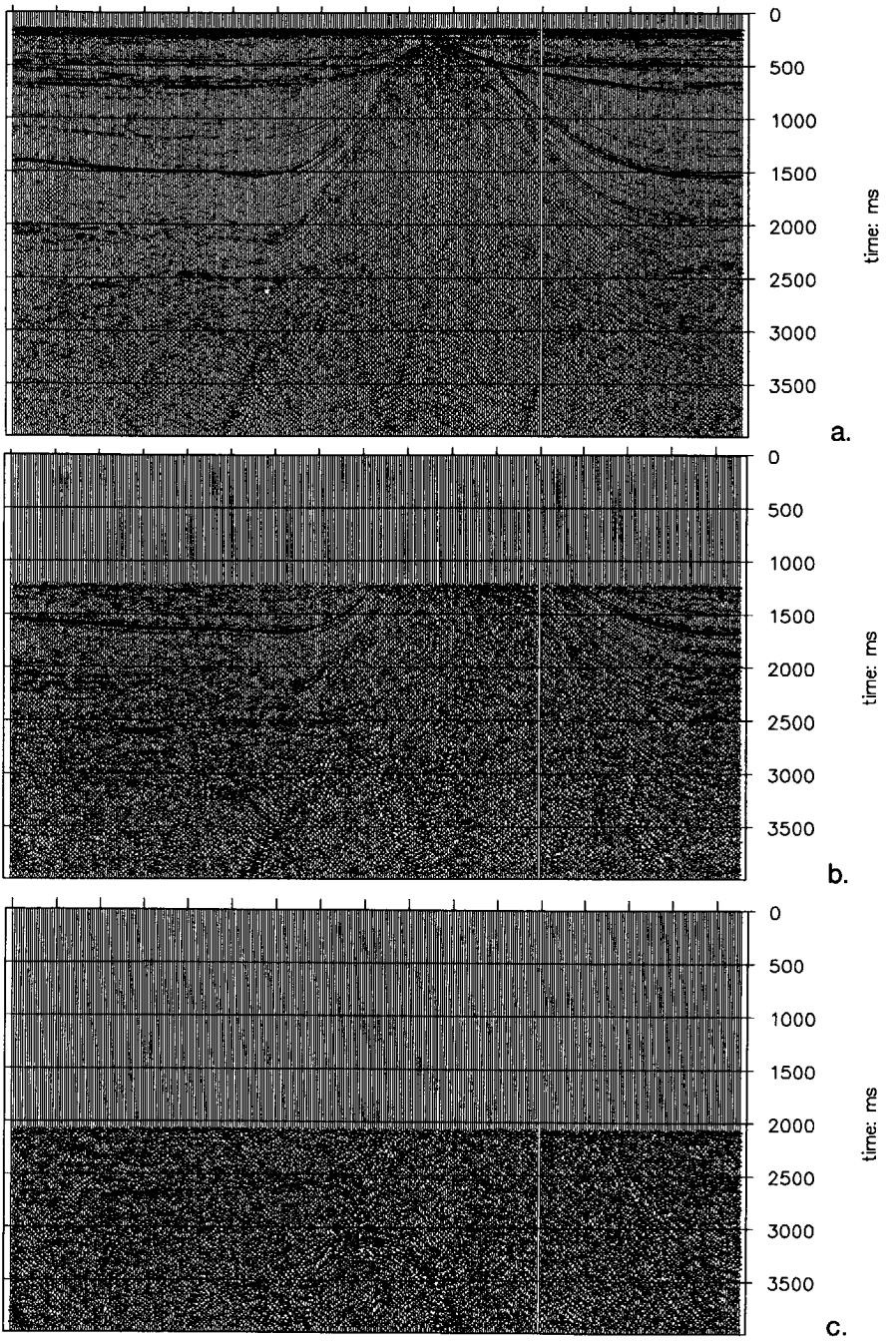

Figure 5.25

a. Near offset section (200 m.).

b. Middle offset section (1375 m.).

c. Far offset section (2575 m.).

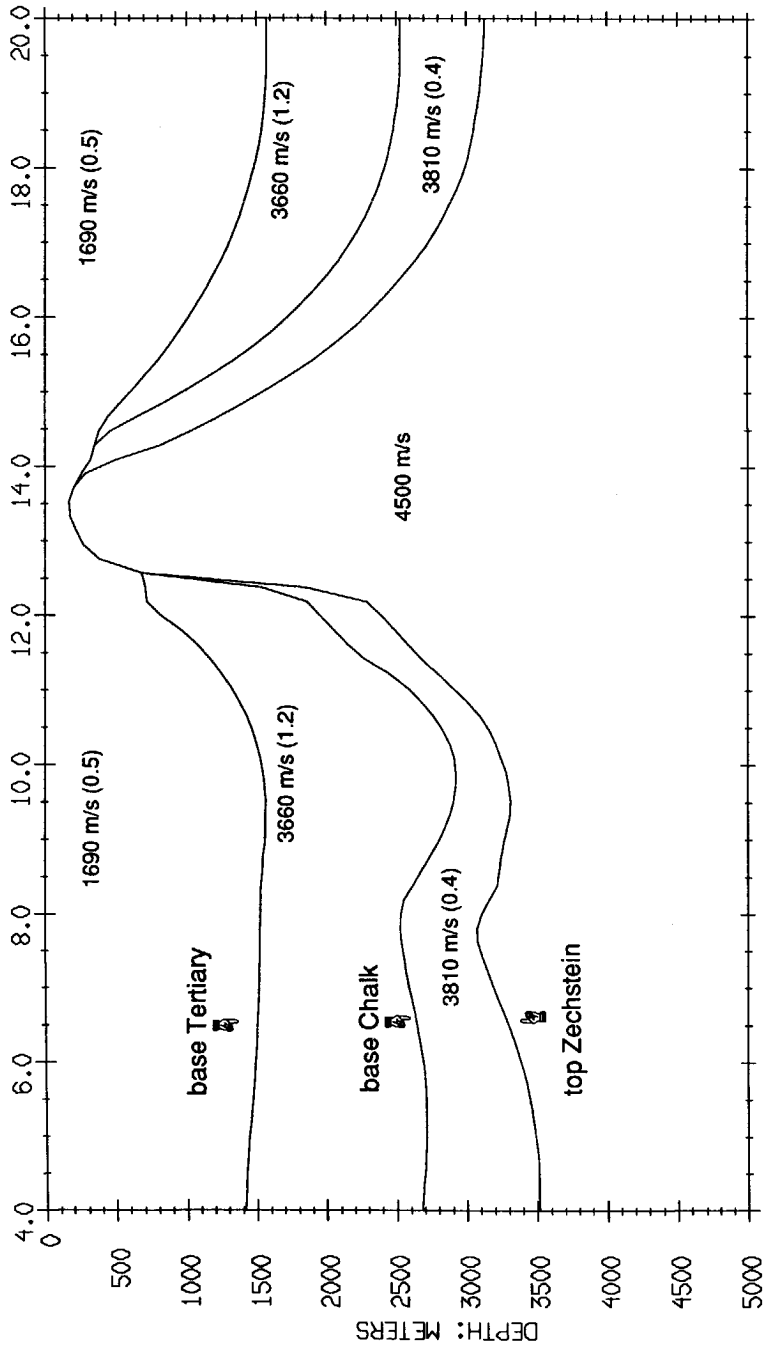

Figure 5.26a
Initial model (rescaled for convenience).

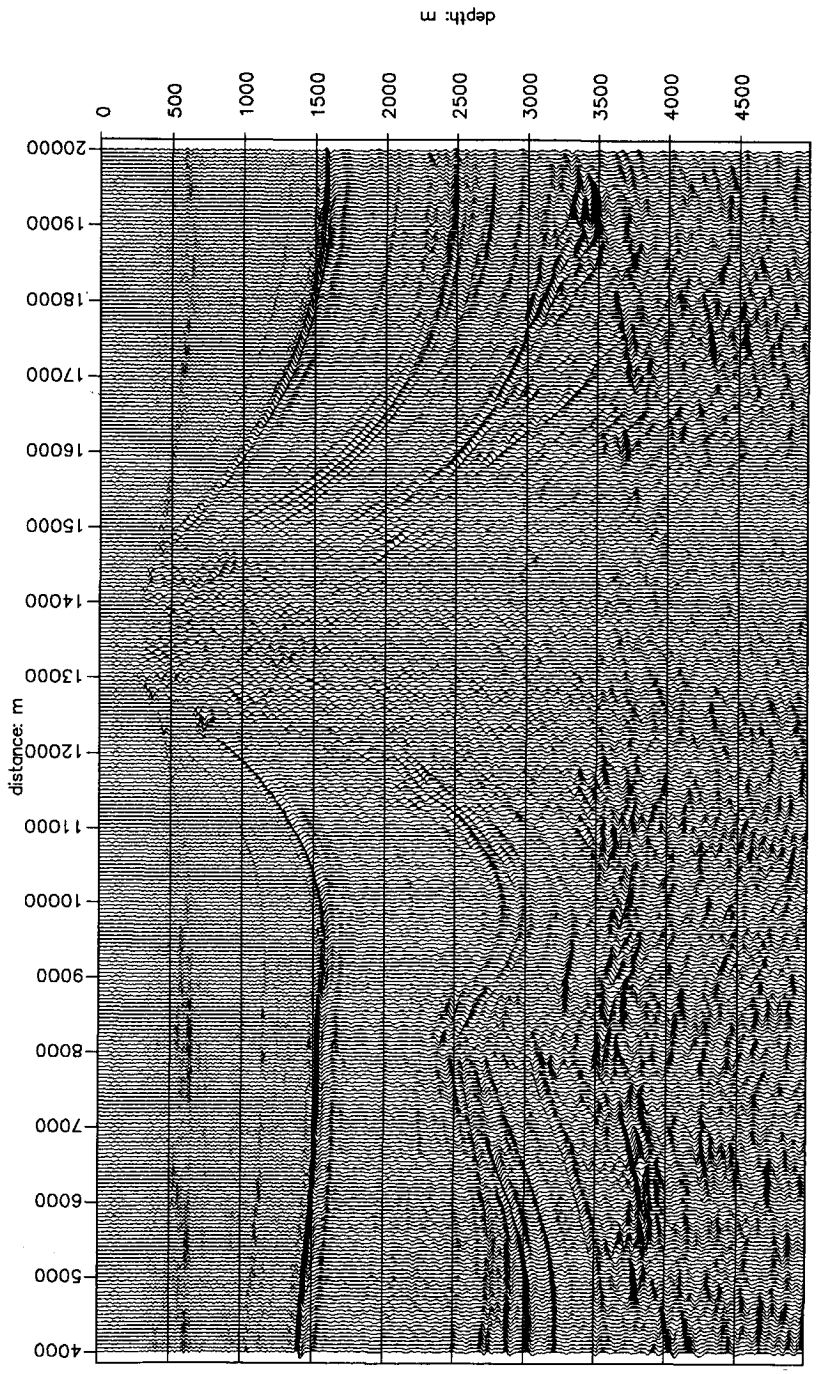

Figure 5.26b
Prestack depth migration with the initial model.

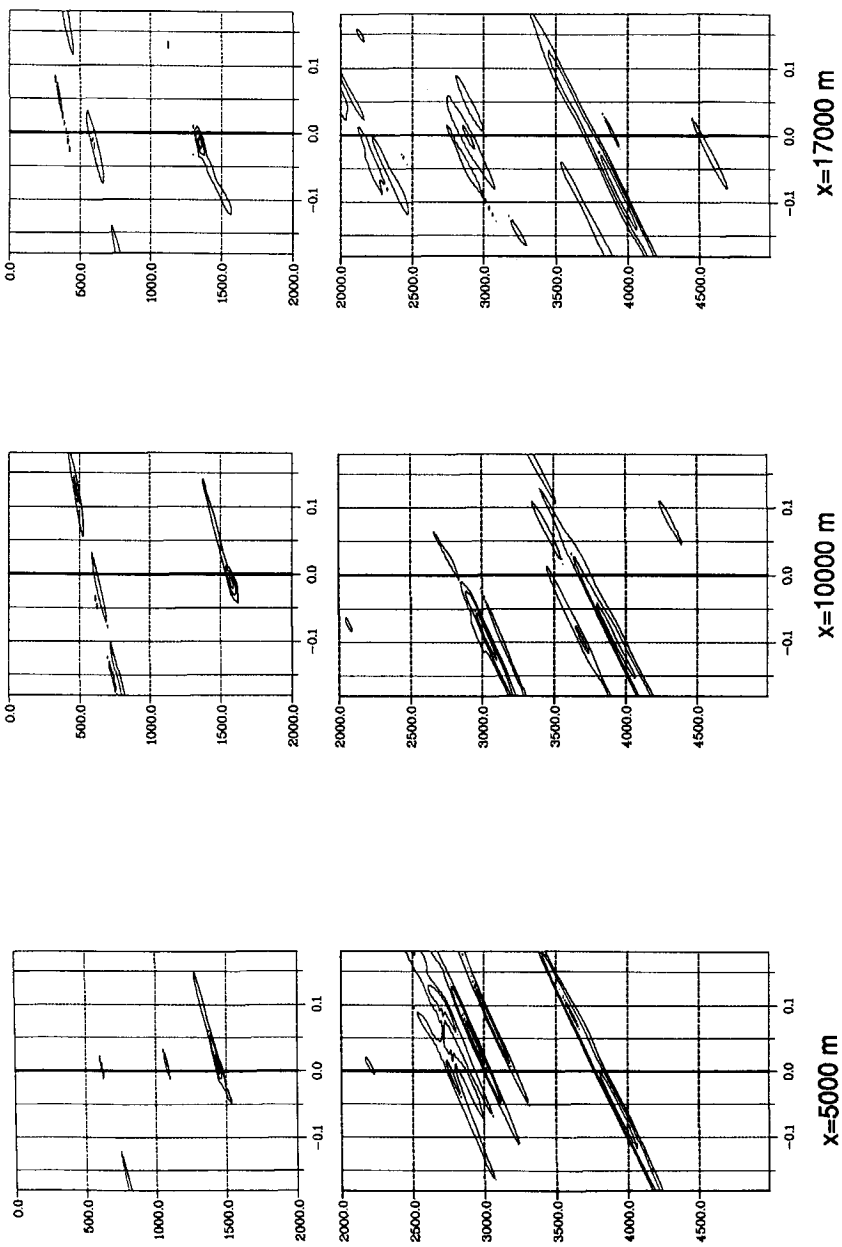

Figure 5.26c
Focus panels corresponding to different lateral positions.

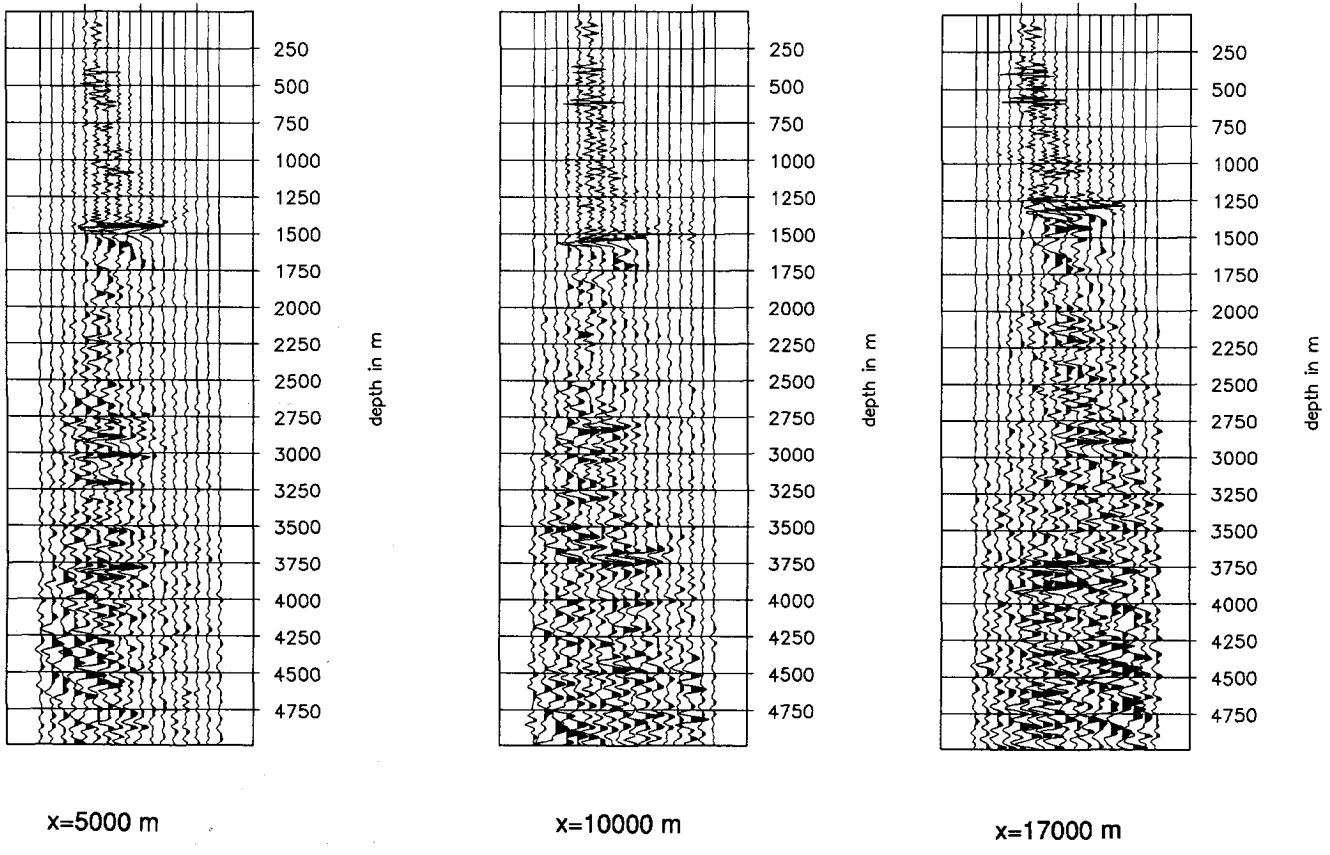

Figure 5.26d
Image gathers corresponding to different lateral positions.

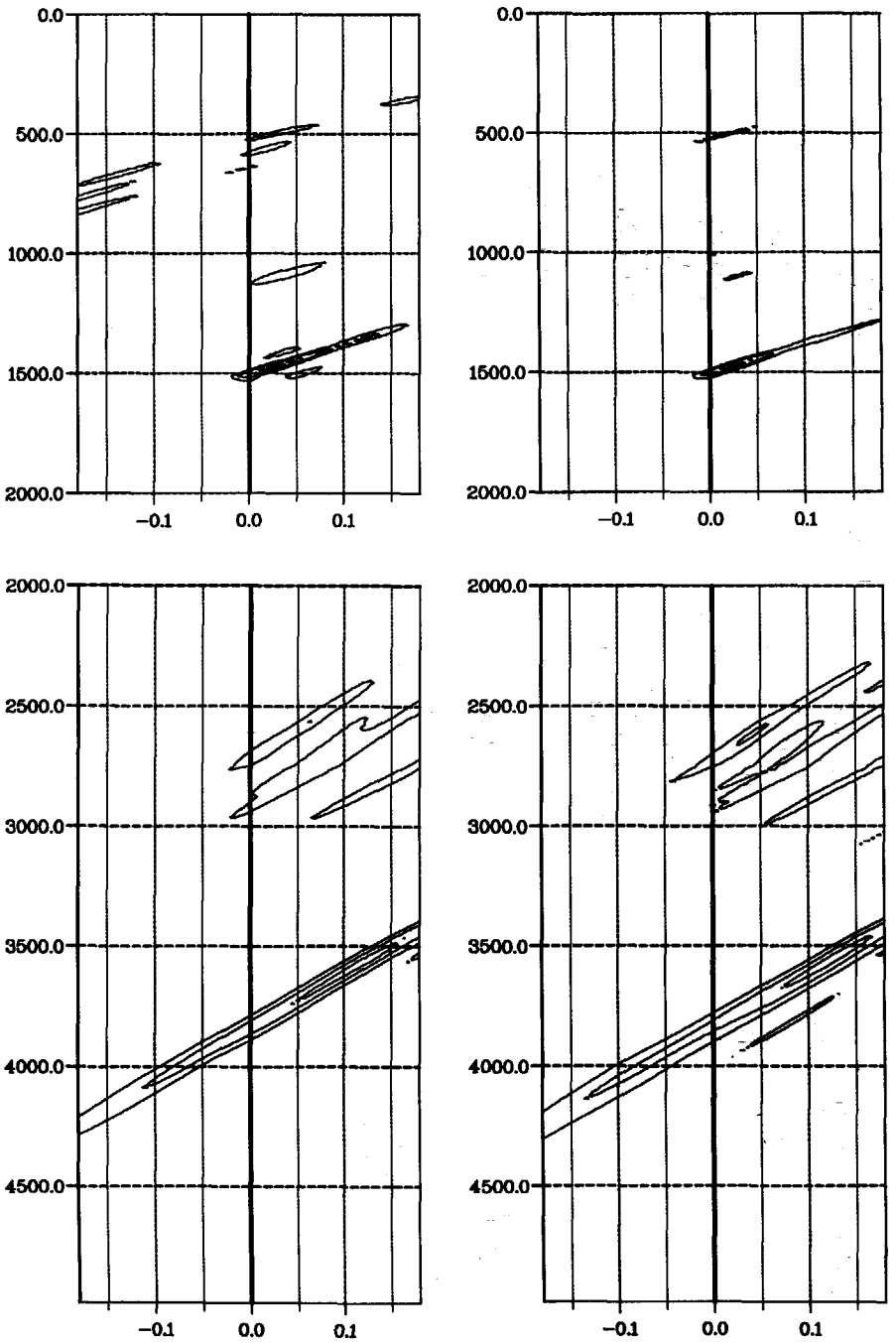

Figure 5.27

a. Focus panel at x=6000 m obtained with 12.5% of the shot records.

b. Focus panel at x=6000 m obtained with 25% of the shot records.

foci are present. These spurious foci only occur in the shallow part of the focus panel, because of the large incidence angles involved. As can be seen in Figure 5.27b the spurious events have vanished when using 25 % of the shot records. Hence, in the next iterations 25% of the shot records were used, which corresponds to a shot sampling of 100 m. In the remainder the macro velocity model was refined from x=4000 m until x=13000 m (for economical reasons).

In the previously discussed examples (sections 5.2 and 5.3) the a-priori knowledge was used of constant macro interval velocities within the macro layers. In this real data example the macro interval velocity may vary in a single macro layer, both in the lateral direction as in the vertical direction. Therefore, the estimated macro interval velocities can not be represented by a single (averaged) macro interval velocity per macro layer. A 5-point moving average filter was applied to stabilize the velocity estimates. The final model is shown in Figure 5.28a. As can be seen in the prestack migrated section (Figure 5.28b), the first interface (at z≈1500 m) is better imaged, as well as the layers in the left part (between z=2750 m and z=3250 m). Also the synclinal structure below x=1000 m (at z≈3000 m) is imaged deeper with respect to the initial model. Although the corresponding focus panels have improved, it can be seen that not all foci are located at the zero-time axis. Also the image gathers still contain curved events. Hence we may conclude that the macro model can still be improved upon.

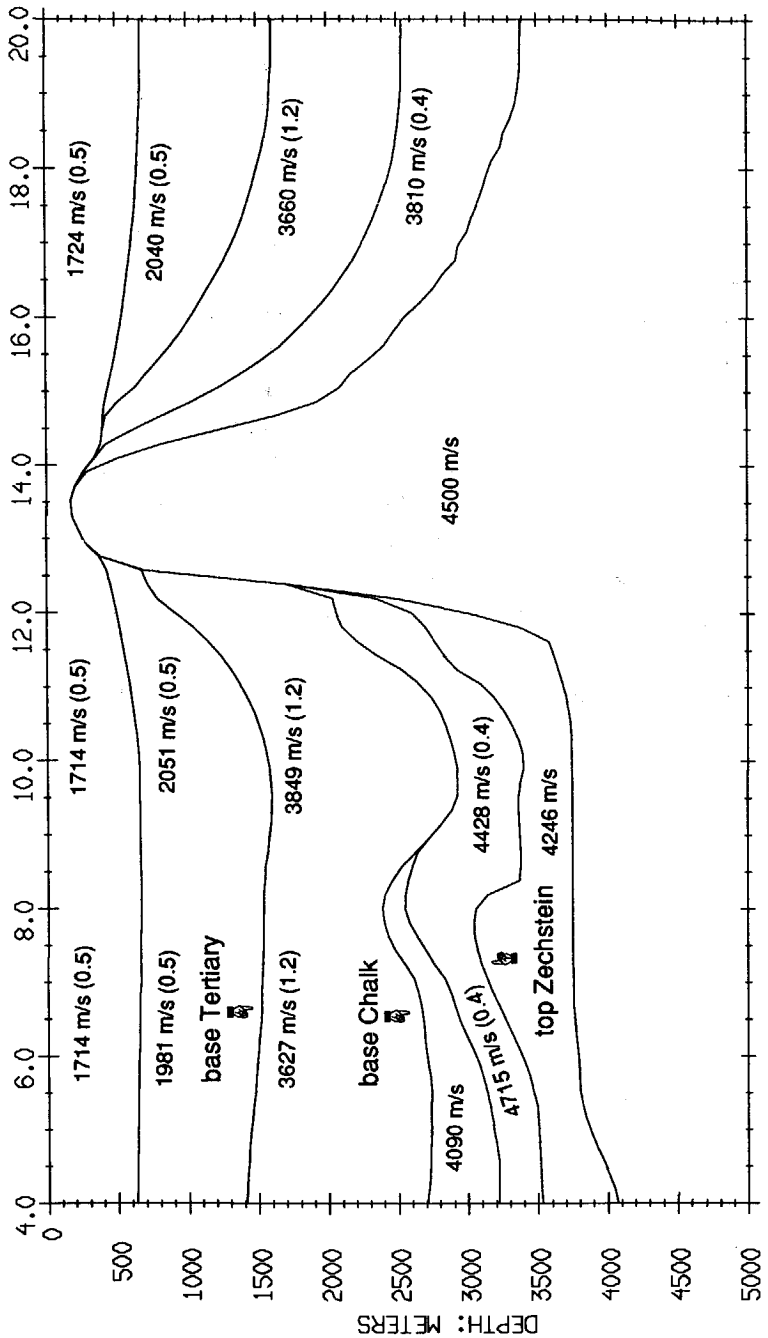

Figure 5.28a
Final macro model. The velocities given in this figure represent the propagation velocity at the top of each macro layer. Note that these starting velocities vary laterally. The vertical gradients are displayed between brackets ( ).

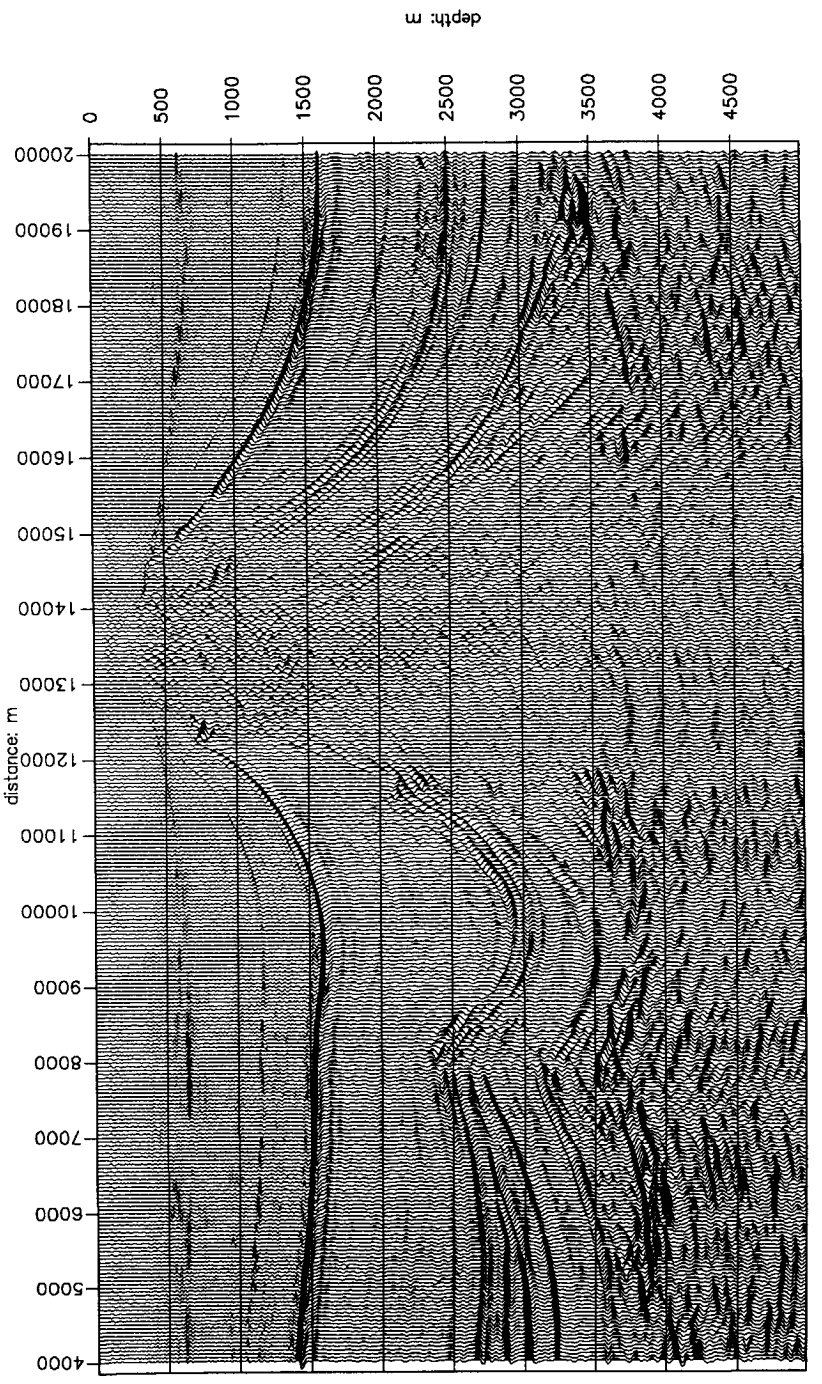

Figure 5.28b
Prestack depth migration with the final model.

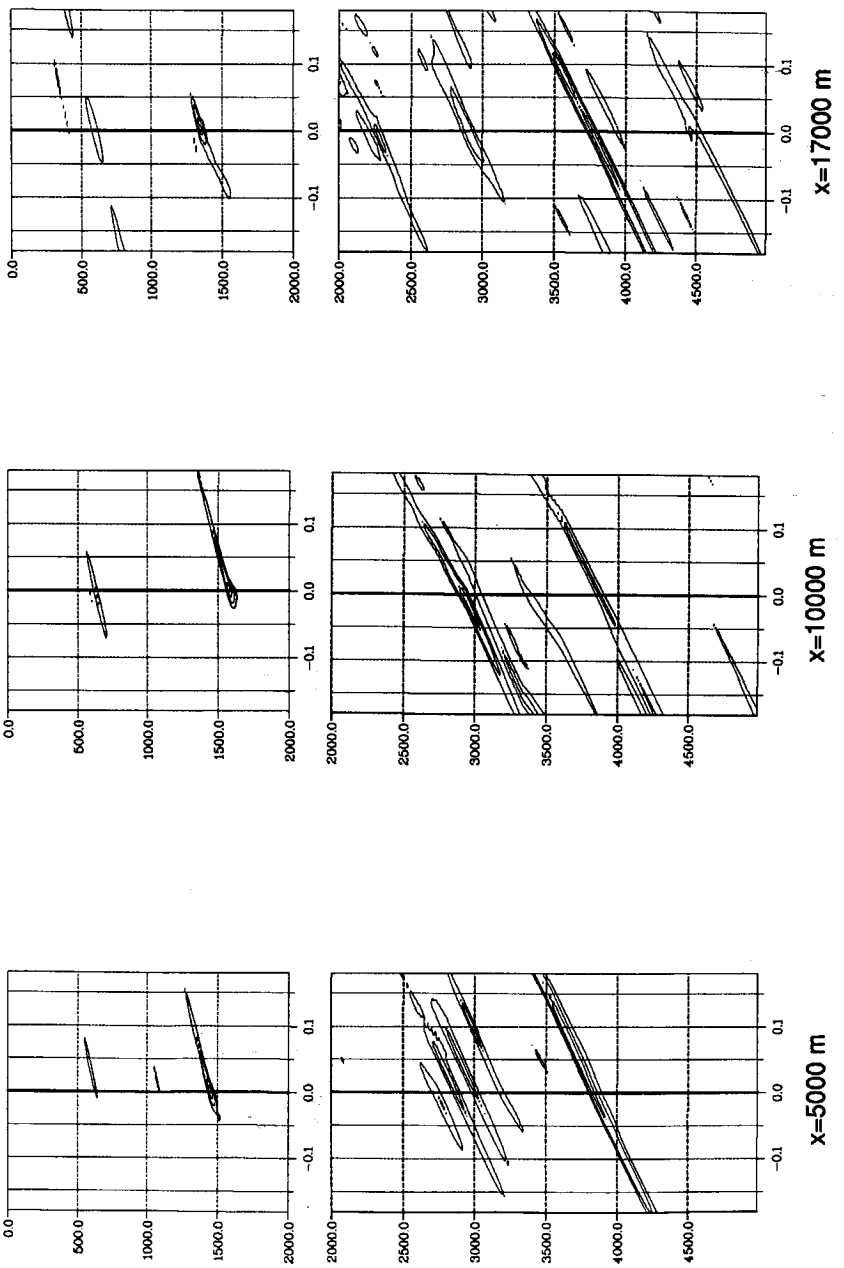

Figure 5.28c
Focus panels corresponding to different lateral positions.

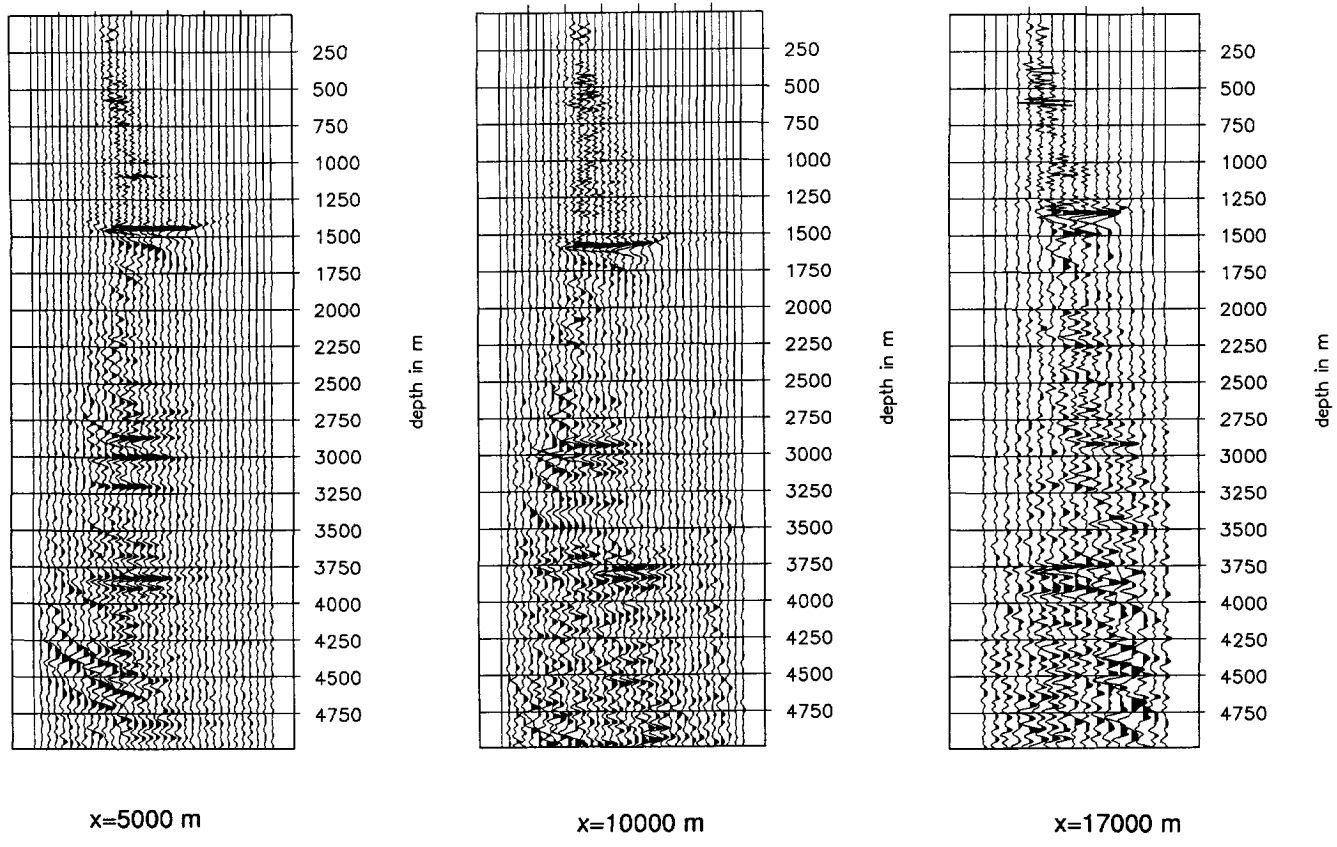

Figure 5.28d
Image gathers corresponding to different lateral positions.

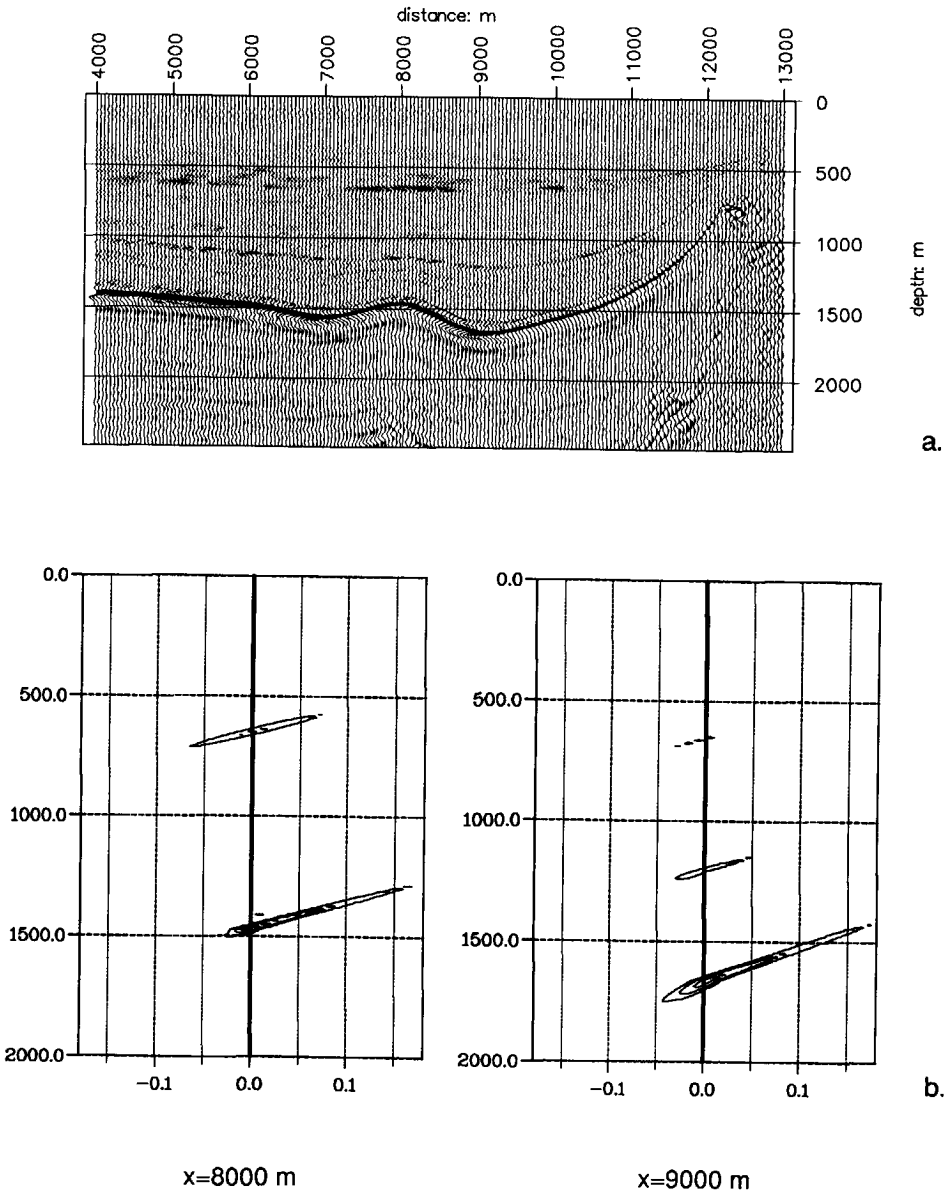

Figure 5.29

a. Prestack migration with a macro model where the estimated velocities were not constrained.

b. Focus panels at x=8000 m and x=9000 m.

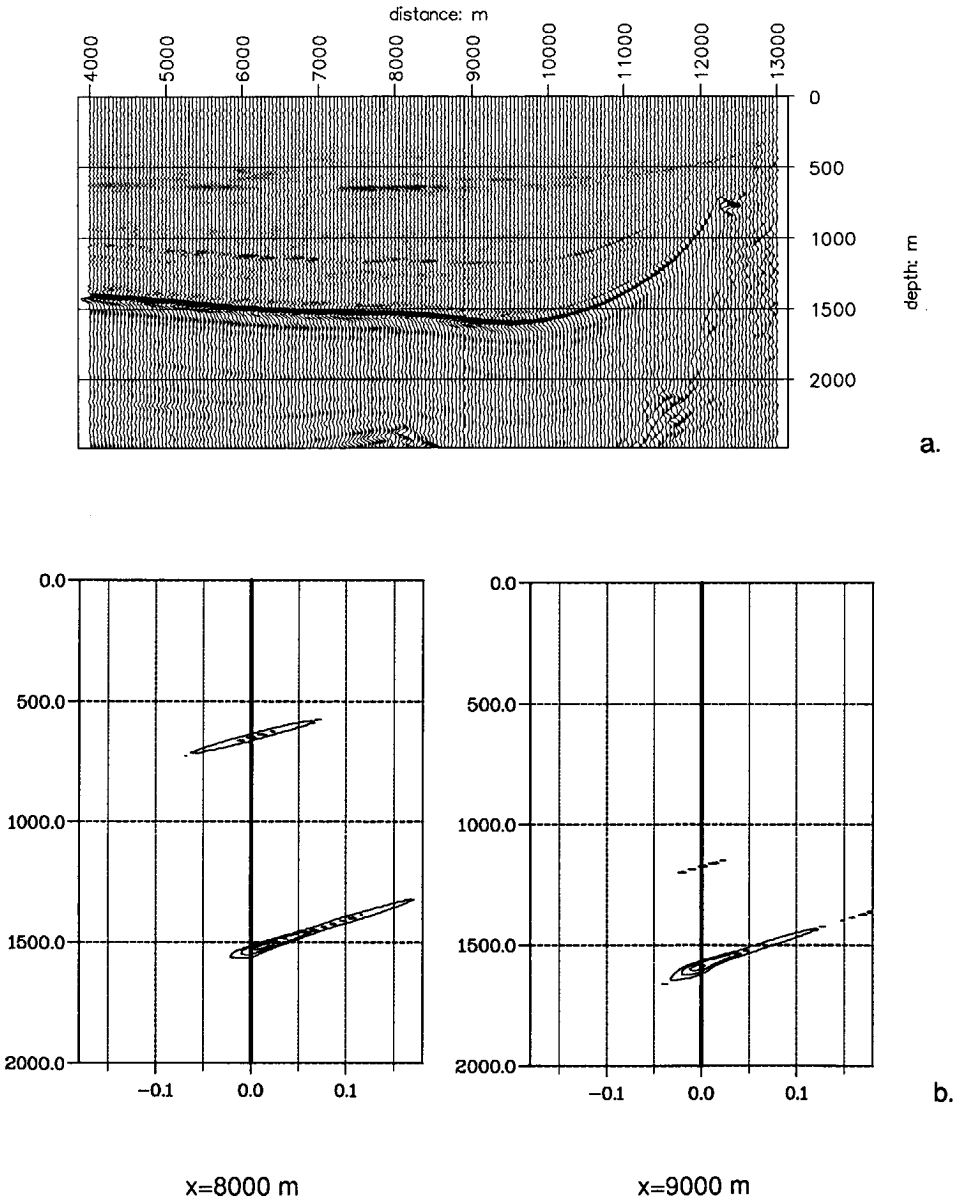

Figure 5.30

a. Prestack migration with the final macro model where the estimated velocities were constrained by a 5-point moving average filter.

b. Focus panels at x=8000 m and x=9000 m.

Discussion

The importance of stabilizing the velocity estimates is illustrated in Figure 5.29. This figure shows the migrated section of the first major interface on the left side of the salt dome. Here no moving average was applied to the velocity estimates, but the velocities in the macro model were obtained by applying a spline interpolation to the derived estimates. From the migrated section (Figure 5.29a) it can be seen that the first major interface contains a curvature that could not be observed in the stacked section. The focus panels at x=8000 m and x=9000 m (Figure 5.29b), however, show foci located at t=0. For comparison the migration result of the final model (Figure 5.30a) and the corresponding focus panels are displayed (Figure 5.30b). As can be seen, also in this figure the foci are located at t=0, but at a different depth. Therefore we must conclude that there exists a non-uniqueness problem: apparently when lateral velocity changes are allowed velocity errors are exchanged by depth errors. To overcome this problem the lateral variations in the velocities must be constrained by incorporating geologic knowledge of the layer. In the example the lateral velocity variations were constrained by the moving average filter.

CHAPTER 6

DISCUSSION AND RECOMMENDATIONS

6.1 DISCUSSION

This thesis describes a new method of estimating the macro velocity model. The method is based on wave field extrapolation of prestack surface data (shot records) to depth points in the subsurface. The extrapolation algorithm uses a macro velocity model. As the extrapolation is done per (2-D) shot record, a 4-dimensional data volume is involved. The four dimensions are: the lateral depth point coordinate, the vertical depth point coordinate, time, and shot number. Such an enormous data volume cannot be studied easily. However, inspection of different cross-sections supplies information about the errors in the macro velocity model. Generally, the extrapolated data are inspected at a number of lateral positions. This is in analogy with conventional velocity analysis on CMP data, where the moveout corrected data are inspected at a number of CMP locations.

Three types of output sections play an important role in the described method: CDP-gathers, image gathers and focus panels. These are obtained by reordering the extrapolated data (Figure 6.1):

1. A *CDP-gather* is the collection of traces related to one common depth point in the subsurface. Each CDP-trace is the result of the extrapolation of one individual shot record to the depth point of interest. Hence, a CDP-gather contains a 2-D cross section of the 4-D data volume at one depth point in the subsurface. The two dimensions are shot number and time.

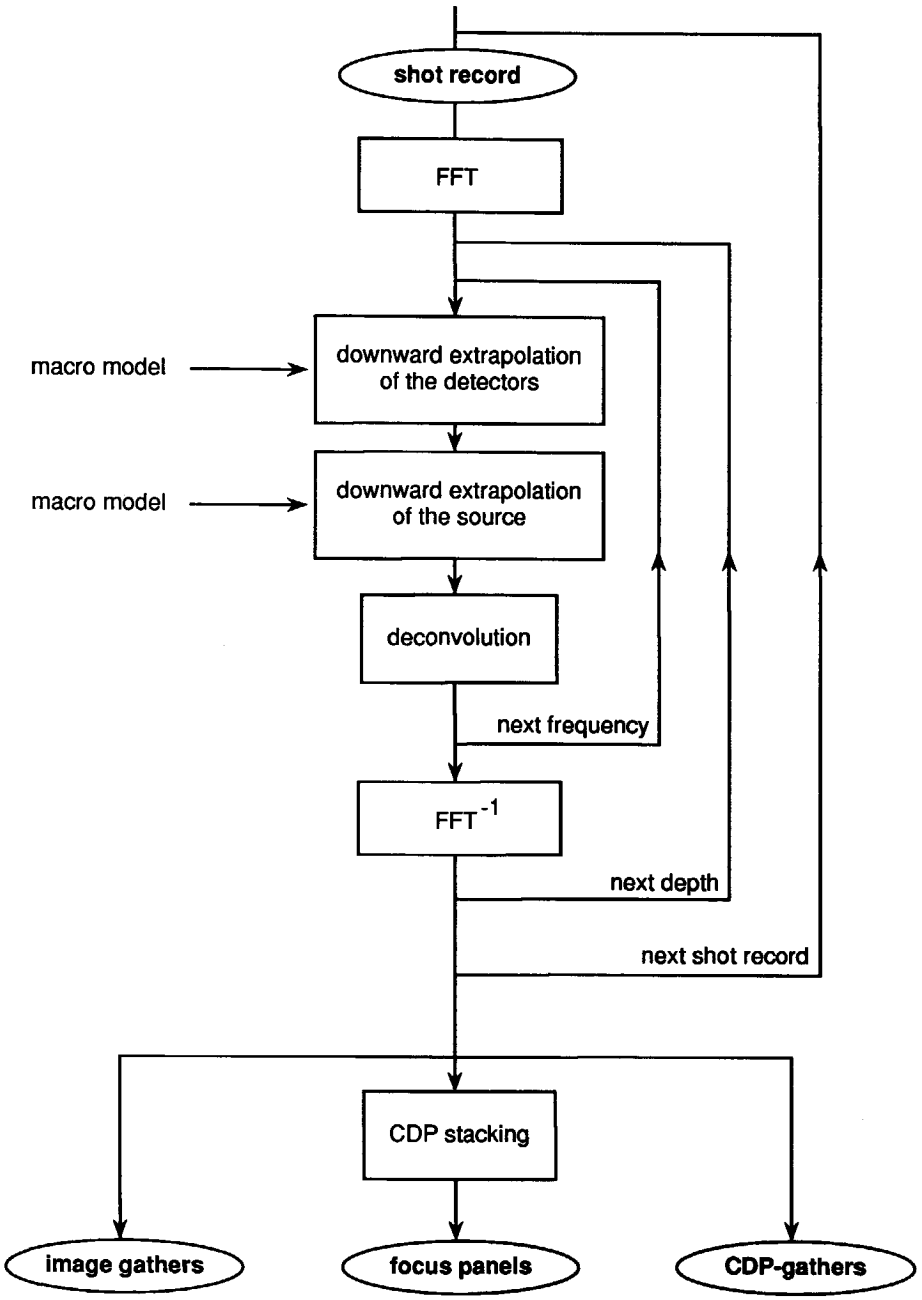

Figure 6.1
By wave field extrapolation of shot records different output sections may be obtained by reordering the extrapolated data.

Horizontal alignment in a CDP-gather should occur at t=0 when the depth point is located on a macro boundary. If alignment occurs at t≠0, this indicates an error in the macro velocity model. For a chosen depth point the time at which alignment occurs is used to quantify the error in the macro velocity model and to update the macro interval velocity accordingly. Note that, in case of a correct macro model, a stacked CDP-gather simulates a zero offset trace with source and detector at the depth point.

2. An *image gather* is the collection of traces of migrated shot records that belong to the same lateral position. It contains a 2-D cross section that can be obtained from the 4-D volume, by considering only one lateral position and by imaging at t=0 for all depth levels. The two dimensions are shot number and depth. An image gather should contain horizontally aligned events at all depth levels. The curvature of the events in an image gather is a measure for the error in the macro velocity model. A *generalized image gather* is obtained if imaging is performed at t≠0. Note that, in case of a correct macro model, a stacked image gather represents one prestack migration trace.

3. The horizontal alignment in CDP-gathers can be quantified with a coherence measure. This can be done by simply stacking the CDP-traces, yielding one stacked trace. Other coherence measures, such as semblance, can also be used. The latter is not possible with S-G oriented extrapolation techniques, since CDP-stacking is done implicitly in this type of schemes. By gathering the CDP-stacked traces for different depth points below one lateral position, a *focus panel* is obtained (after contouring). The two dimensions are time and depth. Foci occurring at t≠0 indicate the errors in the macro velocity model. Figure 6.2 shows how CDP-gathers, generalized image gathers and focus panels are related.

The update equations for the macro velocity model are derived from the traveltime curves of the macro reflections in CDP-gathers. From aligned events in a CDP-gather time-depth pairs can be obtained that are used to update the macro velocity model. The update equations are derived for horizontally layered media. If the medium is not horizontally layered an iterative approach is needed. Experience has shown that in this situation the iterative scheme will converge to the correct macro velocity model. From image gathers it is also possible to estimate the errors in the macro

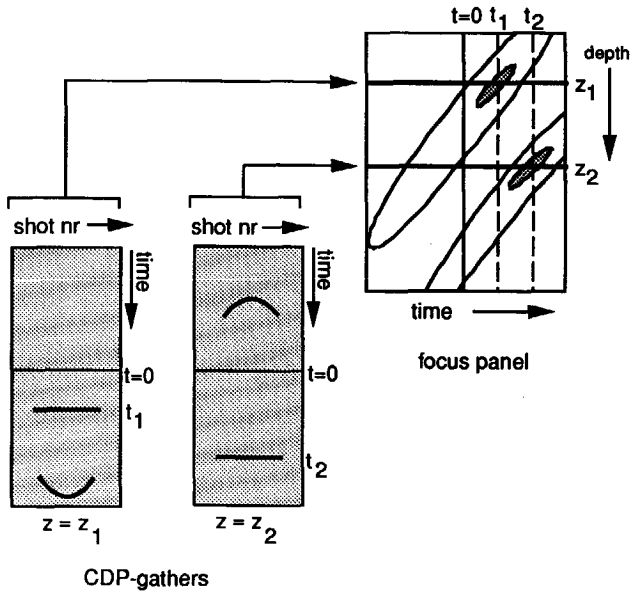

Figure 6.2a
Each time trace in a focus panel is obtained by stacking the traces in a CDP-gather. The CDP-gathers that are used to construct one focus panel are related to one lateral position.

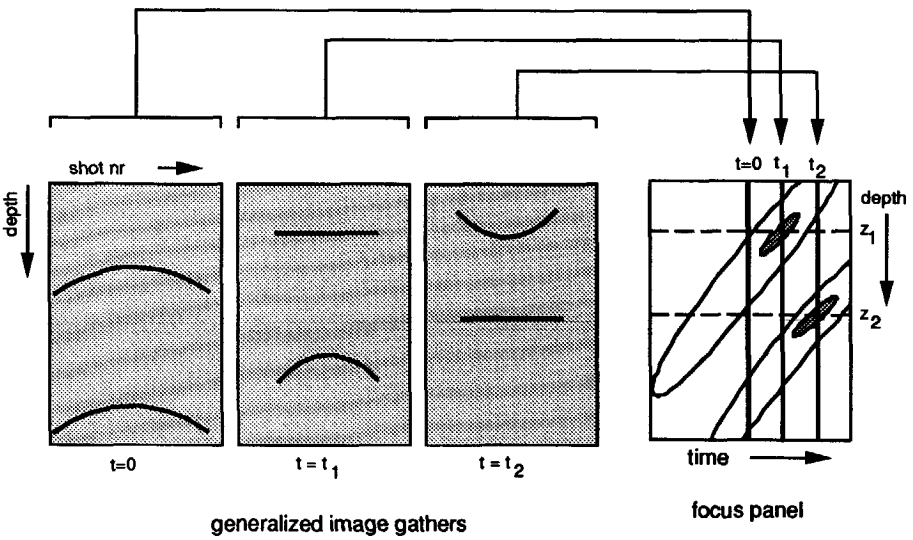

Figure 6.2b
Each depth trace in a focus panel is obtained by stacking the traces in a generalized image gather. The generalized image gathers that are used to construct one focus panel are related to one lateral position. Three generalized image gathers are shown, obtained by imaging at t=0, $t=t_1$, $t=t_2$.

model. By calculating the coherence in an image gather along curves defined by equation (4.39), an estimate of the true medium parameters can be obtained.

6.2 3-D GENERALIZATION

In 3-D data processing an enormous data volume is involved. In order to reduce the total amount of data, the acquisition is generally performed such that the detectors are closely sampled in one direction (henceforth referred to as x-direction) whereas they are sparsely sampled in the perpendicular direction (henceforth referred to as y-direction). This means that in the latter direction the data are spatially aliased. The shots are densely sampled in the y-direction and sparsely sampled in the x-direction. Because of the advantages for the data handling and due to the irregular sampling of shots and receivers, processing per shot record is required (Figure 6.3).

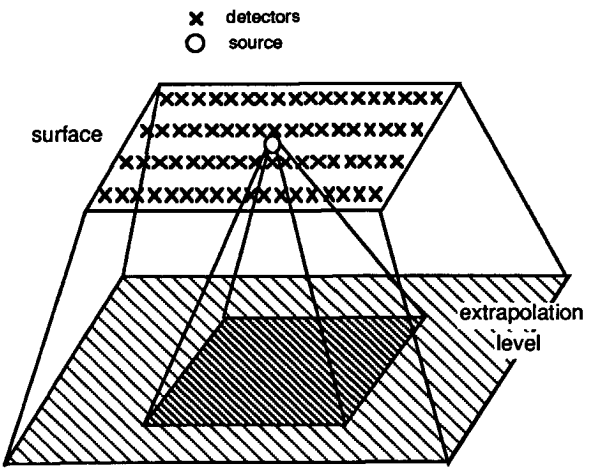

Figure 6.3
Wave field extrapolation of a 3-D shot record to one extrapolation level involves: downward extrapolation of the receivers and downward extrapolation of the source followed by deconvolution in the overlap area.

In this section I discuss a simple example on 3-D macro velocity model estimation. With the model shown in Figure 6.4 3-D shot records were generated with a 3-D raytracing algorithm. The first interface is dipping in the x-direction. The second interface is dipping in the y-direction. The

velocity in the first layer is c_1=1500 m/s and the velocity in the second layer is c_2=2500 m/s.

The data were generated with the following parameters:

shot spacing in x-direction	25 m
spacing of shot lines in y-direction	250 m
spacing of detector lines in x-direction	250 m
detector spacing in y-direction	25 m
total number of channels	205 (5*41)
total number of shots	205 (41*5)
acquisition geometry	fixed spread
first shot is at	(x=500 m, y=500 m)
first detector is at	(x=500 m, y= 500 m)
sample interval	4 ms
frequency contents	5-50 Hz

The acquisition parameters (and Figure 6.4) show that the detectors are closely sampled in the y-direction and sparsely sampled in the x-direction

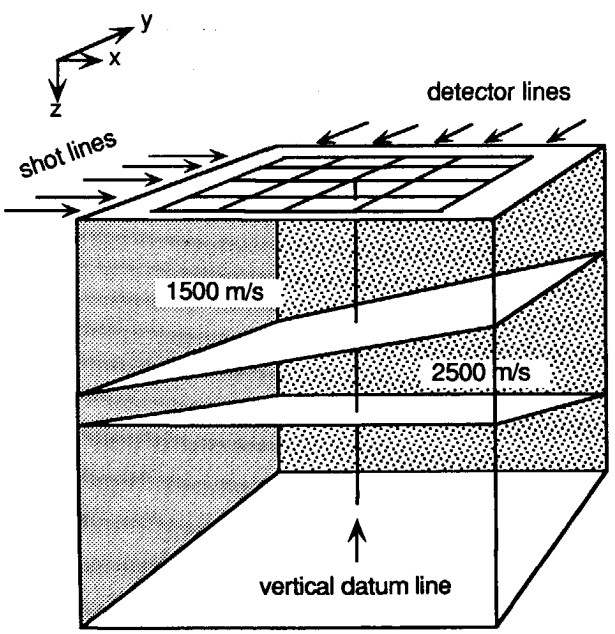

Figure 6.4
The 3-D subsurface contains two plane dipping interfaces. The first interface is dipping in the x-direction. The second interface is dipping in the y-direction. The velocity in the first layer is c_1=1500 m/s. The velocity in the second layer is c_2=2500 m/s.

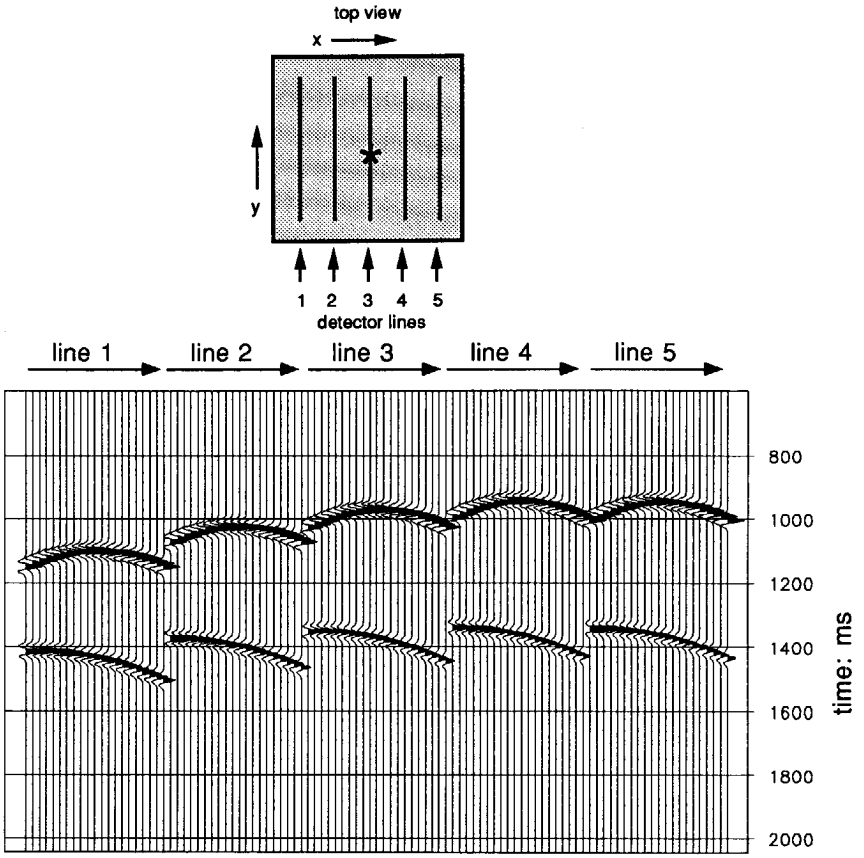

Figure 6.5
For the subsurface of Figure 6.4 a 3-D seismic survey was simulated by generating shot records with raytracing. This figure shows one 3-D shot record for a shot located at (x=1000 m, y=1000 m).

(in accordance with reality). Hence, in the shot records spatial aliasing occurs in the x-direction. Figure 6.5 shows the 3-D shot record for a shot located at the surface at (x=1000 m, y=1000 m). The shots are closely sampled in the x-direction and sparsely sampled in the y-direction. All shot records were redatumed to the vertical datum line at (x=1000 m, and y=1000 m). For the redatuming a non-recursive 3-D shot record redatuming algorithm was used (Kinneging, 1989). When the correct macro velocity model is used in the redatuming process CDP-gathers are obtained as shown in Figure 6.6. These figures show only those traces of the (3-D) CDP-gathers that are related to shot locations on shot line 3. In each CDP-trace the influence of the sparse detector sampling is expressed as separate events (arrows). If no spatial aliasing were present only one

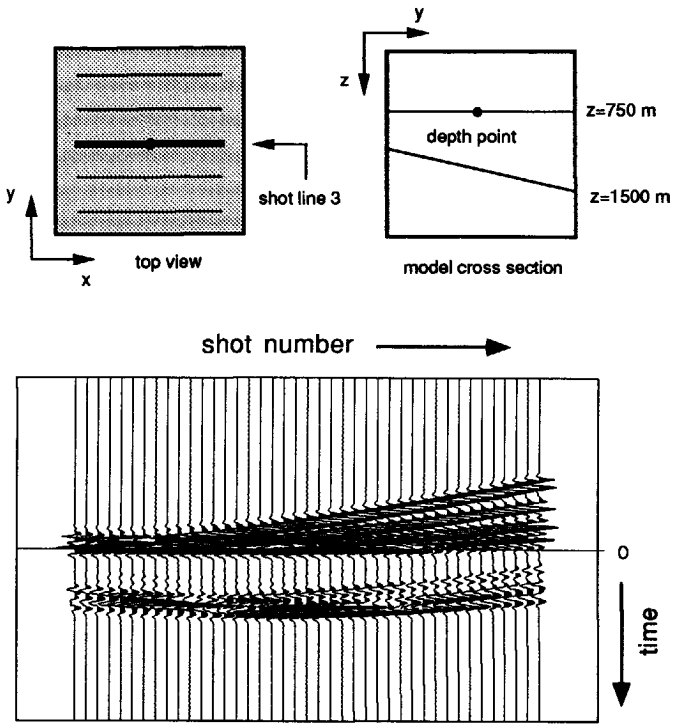

Figure 6.6a
All 3-D shot records were redatumed to the vertical datum line indicated in Figure 6.4. At each depth point on this line a 3-D CDP-gather is constructed (x_s,y_s,t).
CDP-gather for a depth point located on the first interface. Only the traces related to shot line 3 are displayed.

event would remain for each reflector. Similar to the 2-D case, stacking of all traces in the (3-D) CDP-gather yields one zero offset trace at the considered depth point and a focus panel can be constructed by doing this for all depth points on the vertical datum line (Figure 6.7). Note that, although the surface data were spatially aliased, the focus panel still looks acceptable. If the second macro velocity is too high (τ_2=3000 m/s), the second focus occurs at positive times as shown in Figure 6.8.

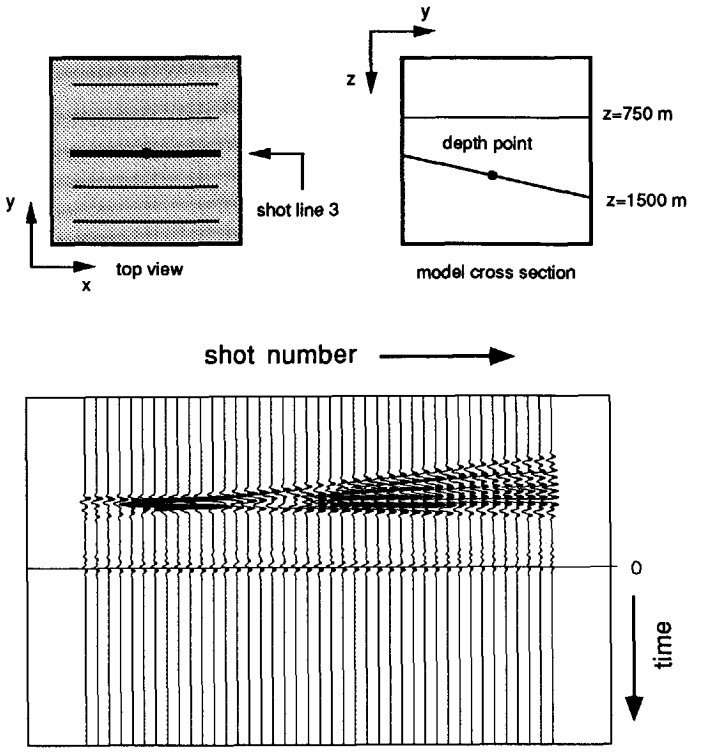

Figure 6.6b
CDP-gather for a depth point located on the second interface. Only the traces related to shot line 3 are displayed.

Discussion

Due to sparse sampling in 3-D acquisition, spatial aliasing will occur in the CDP-gathers, which makes it difficult to interpret them. The focus panels obtained after CDP-stacking still contain well defined foci. This is due to the chosen acquisition geometry: sparse sampling of the detectors and dense sampling of the sources in one direction, dense sampling of the detectors and sparse sampling of the sources in the other direction. However, a false focus occurs at negative times in both focus panels. Therefore, further research is needed to determine the requirements of 3-D acquisition parameters for 3-D velocity analysis by wave field extrapolation.

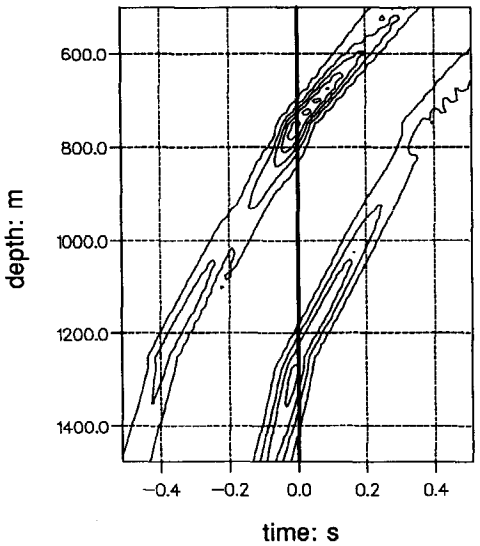

Figure 6.7
Focus panel at (x=1000 m, y=1000 m) for the correct macro subsurface model.

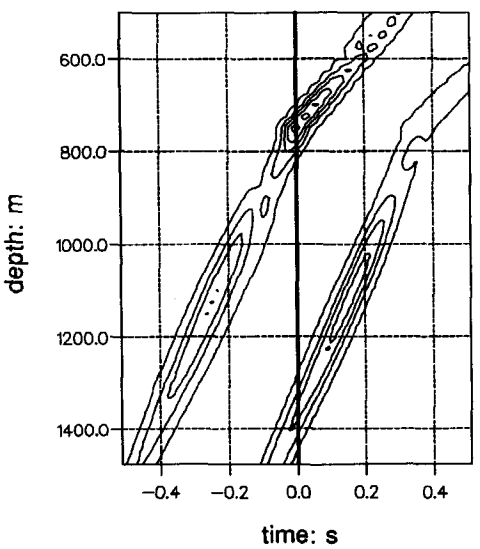

Figure 6.8
Focus panel at (x=1000 m, y=1000 m) for the erroneous macro subsurface model ($\bar{\tau}_2$=3000 m).

6.3 RECOMMENDATIONS

The correctness of the macro velocity model is verified by the consistency of the images for different shots after wave field extrapolation. Based on this principle and on the experience gained in the development of the method I list below a number of considerations that could be taken into account when developing an improved estimation method for the macro velocity model, based on wave field extrapolation.

–Research remains to be done on the requirements of 3-D acquisition parameters if prestack depth migration is to be performed. Spatial aliasing may seriously trouble the estimation of 3-D macro velocity models by wave field extrapolation.

–In this thesis horizontal alignment in CDP-gathers is quantified by measuring amplitudes after CDP stacking. As was mentioned before this may not always be the best way to determine horizontal alignment (section 5.2). Further research is needed to investigate different coherence measures (e.g. semblance) as well.

–To obtain optimum stacking velocities it is common practice to visually inspect the alignment in moveout corrected CMP-gathers in addition to inspection of *semblance panels*. The reason for this is that visual inspection is sometimes easier than focus picking on semblance panels. Similarly, the foci in focus panels may be difficult to pick because of the elongated contours. An alternative to focus picking on focus panels is visual inspection of generalized image gathers. As illustrated in Figure 6.2b the second focus occurs at ($t=t_2, z=z_2$). From visual inspection of the image gathers it follows that alignment of the second event occurs at $z=z_2$ in the generalized image gather obtained by imaging at $t=t_2$. Although no research has been done on this topic, joint inspection of focus panels and generalized image gathers may prove to be a powerful tool.

–For the updating of the macro model user interaction is required after each run of the wave field extrapolation algorithm. In this stage all possible output sections should be available to the user to decide how the macro velocity model should be updated. It should be possible to display focus panels, generalized image gathers, the macro model and the depth migrated section. Hence, storage of these different data sets in a relational

data base system seems a natural way to perform such an analysis. This part is well suited for implementation on an interactive workstation with good graphics capabilities.

–Although it is possible to simultaneously estimate the macro interval velocities in consecutive macro layers, experience has shown that in complex situations it is preferred to estimate the macro velocity model in a top-down approach. Furthermore, depth migration of a common offset section is generally sufficient to delineate the macro boundaries.

–In complicated situations focus panels can be very difficult to interpret. Hence, it is impossible to converge to the correct solution with focus panels only. The process should be guided by macro geologic models of the area. In addition, it is an advantage to inspect focus panels along "geology-adapted" datum lines as is illustrated in Figure 6.9.

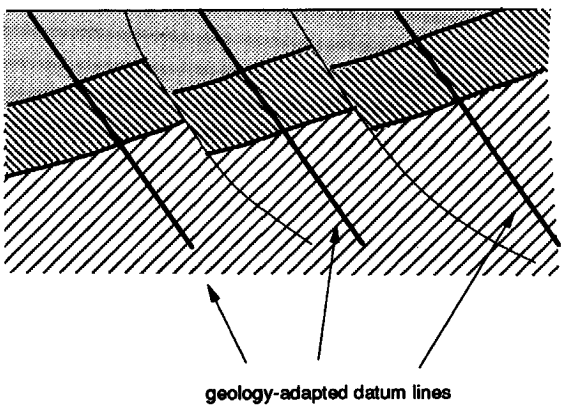

Figure 6.9
With "geology-adapted" datum lines it is possible to position the datum line perpendicular to the macro boundaries and to keep the datum lines within a fault block.

When the datum line is located in a fault block, the macro boundaries are generally perpendicular to the datum line. The advantage is that the update equations have faster convergence for datum lines that are perpendicular to the macro boundaries. Furthermore, the focus panels will be easier to interpret when the datum lines are located within a fault block. Future research will have to prove the validity of this approach.

APPENDIX A

THE CONVOLUTIONAL MODEL FOR THE OBLIQUE PLANE WAVE RESPONSE OF A 1-D SUBSURFACE

In this appendix the convolutional model is derived for the response of a plane wave in a 1-D subsurface.

For a 1-D medium the linearized equation of motion and the linearized equation of continuity are given (in the wavenumber-frequency) domain by

$$\frac{\partial \tilde{P}}{\partial z} = -j\omega\rho\tilde{V}_z \tag{A.1a}$$

and

$$\frac{\partial \tilde{V}_z}{\partial z} = \frac{1}{j\omega\rho}(k^2 - k_x^2)\tilde{P} = \frac{-j}{\omega\rho}(\frac{1}{c^2} - p^2)\tilde{P} \ , \tag{A.1b}$$

respectively. Let us now introduce a new "depth" variable according to

$$\zeta = \int_0^z \frac{2dz'}{c_z(p,z')} \ , \tag{A.2a}$$

with

$$\frac{1}{c_z} = (\frac{1}{c^2} - p^2)^{1/2} \ . \tag{A.2b}$$

Note that this "depth" variable has the dimension of time. With this definition the basic equations can be restated in terms of ζ according to

$$\frac{\partial \tilde{P}}{\partial \zeta} = \frac{-j\omega\rho}{2} Z \tilde{V}_z \qquad \text{(A.3a)}$$

and

$$\frac{\partial \tilde{V}_z}{\partial \zeta} = \frac{-j\omega}{2Z} \tilde{P} \ , \qquad \text{(A.3b)}$$

with the "impedance" Z being given by

$$Z = \rho c_z \ . \qquad \text{(A.3c)}$$

This leads to the following wave equation:

$$\frac{\partial^2 \tilde{P}}{\partial \zeta^2} + (\frac{\omega}{2})^2 \tilde{P} = \frac{1}{Z} \frac{\partial Z}{\partial \zeta} \frac{\partial \tilde{P}}{\partial \zeta} \ , \qquad \text{(A.4a)}$$

with $\tilde{P} = \tilde{P}\,(p,\zeta,\omega)$.

Next we define a Green's function according to

$$\frac{\partial^2 \tilde{G}}{\partial \zeta^2} + (\frac{\omega}{2})^2 \tilde{G} = -\delta\,(\zeta - \zeta') \ , \qquad \text{(A.5a)}$$

with $\tilde{G} = \tilde{G}\,(p,\zeta,\zeta',\omega)$.

Note that

$$\tilde{G} = \frac{e^{-j\frac{\omega}{2}|\zeta - \zeta'|}}{j\omega} \ ; \zeta = \zeta(p),\ \zeta' = \zeta'(p) \ . \qquad \text{(A.6)}$$

Now assume that the upper half space is homogeneous, i.e. $\frac{\partial Z}{\partial \zeta} = 0$ for $\zeta \leq 0$. Then the "source term" in (A.4a) is restricted to the area $0 < \zeta < \infty$. Hence, for the scattered field in the upper half space we may write

$$\tilde{P}^{-}(p,\zeta,\omega) = -\int_0^{\infty} \left(\frac{1}{Z}\frac{\partial Z}{\partial \zeta'}\frac{\partial P}{\partial \zeta'}\right)(p,\zeta',\omega)\, \tilde{G}(p,\zeta,\zeta',\omega)\, d\zeta' \quad . \tag{A.7}$$

Using the Born approximation, we replace $P(p,\zeta',\omega)$ in the integral by the incident wave field

$$\tilde{P}(p,\zeta',\omega) \approx \tilde{W}(p,\zeta',\zeta,\omega)\, \tilde{P}^{+}(p,\zeta,\omega) \quad , \tag{A.8a}$$

where the wave field extrapolation operator is defined as

$$\tilde{W}(p,\zeta',\zeta,\omega) = 2\frac{\partial \tilde{G}(p,\zeta',\zeta,\omega)}{\partial \zeta} \quad . \tag{A.8b}$$

Hence, for $\zeta \leq 0$

$$\tilde{P}^{-}(p,\zeta,\omega) \approx$$
$$-2\left[\int_0^{\infty} \left(\frac{1}{Z}\frac{\partial Z}{\partial \zeta'}\right)(p,\zeta')\, \frac{\partial^2 \tilde{G}(p,\zeta',\zeta,\omega)}{\partial \zeta' \partial \zeta}\, \tilde{G}(p,\zeta,\zeta',\omega)\, d\zeta'\right] \tilde{P}^{+}(p,\zeta,\omega) \quad , \tag{A.9a}$$

or upon substitution of equation (A.6) we obtain for $\zeta = 0$

$$\tilde{P}^{-}(p,\zeta{=}0,\omega) \approx \left[\frac{1}{2}\int_0^{\infty} \left(\frac{1}{Z}\frac{\partial Z}{\partial \zeta'}\right)(p,\zeta')\, e^{-j\omega\zeta'}\, d\zeta'\right] \tilde{P}^{+}(p,\zeta{=}0,\omega) \quad . \tag{A.9b}$$

Note that the integral represents a Fourier transform from ζ' to ω. Therefore (A.9b) may be written as a multiplication:

$$\tilde{P}^{-}(p,\zeta{=}0,\omega) \approx \tilde{R}(p,\omega)\, \tilde{S}(p,\omega) \quad , \tag{A.10a}$$

where

$$\tilde{R}(p,\omega) = \frac{1}{2}\left(\frac{1}{Z}\frac{\partial Z}{\partial \zeta'}\right)(p,\omega) \tag{A.10b}$$

represents the Fourier transform of $\frac{1}{2}\left(\frac{1}{Z}\frac{\partial Z}{\partial \zeta'}\right)(p,\zeta')$, and

$$\tilde{S}(p,\omega) = \tilde{P}^{+}(p,\zeta=o,\omega) \qquad \text{(A.10c)}$$

represents the source wave field at $\zeta=0$. Finally, the inverse Fourier transform of equation (A.10a) reads

$$\tilde{P}^{-}(p,\zeta=o,\zeta') \approx \tilde{R}(p,\zeta') * \tilde{S}(p,\zeta') \ , \qquad \text{(A.11a)}$$

where

$$\tilde{R}(p,\zeta') = \frac{1}{2}\left(\frac{1}{Z}\frac{\partial Z}{\partial \zeta'}\right)(p,\zeta') \ , \qquad \text{(A.11b)}$$

and $*$ denotes convolution along the ζ'-axis. Equations (A.11) represent the convolutional model for the oblique plane wave response of a 1-D medium. Finally, renaming ζ' by τ in equation (A.11a) and omitting $\zeta=o$ and the superscript "-" in $\tilde{P}^{-}(p,\zeta=o,\zeta')$ yields equation (1.4a).

APPENDIX B

MATRIX NOTATION

B.1 INTRODUCTION

In this appendix I discuss the derivation of the matrix notation for wave fields and operators from the Rayleigh integral, as introduced by Berkhout (1985). The formulation is generalized for 2-D and 3-D applications. The matrix notation suits very well with the seismic situation, were we always deal with sampled wave fields of finite duration. Furthermore, with this notation we can easily describe inverse extrapolation. In the derivation I will mainly follow Wapenaar and Berkhout (1989).

B.2 MATRIX NOTATION FOR WAVE FIELDS

If we consider one frequency component ω_i, then the discretized version of a 2-D wave field measured at a constant depth level as a function of lateral position, $p(x,z_0;\omega_i)$, can be represented by a *vector* according to

$$\mathbf{P}(z_0) = \begin{bmatrix} P(-K\Delta x,z_0;\omega_i) \\ \vdots \\ P(k\Delta x,z_0;\omega_i) \\ \vdots \\ P(K\Delta x,z_0;\omega_i) \end{bmatrix}, \qquad \text{(B.1)}$$

where Δx is the distance between the receivers.

For the seismic situation this vector represents one Fourier component of the data in one common shot record. This vector may be written symbolically as

$$\mathbf{P}(z_0) = \begin{bmatrix} P_{-K} \\ \vdots \\ P_k \\ \vdots \\ P_K \end{bmatrix} \downarrow x_r \quad , \tag{B.2}$$

where x_r denotes that the different elements in this vector correspond to the different lateral positions of the receivers. With this notation the prestack data $P(x_r,z_0;x_s,z_0;\omega_i)$ in a 2-D seismic survey may be written as a *matrix*, according to

$$\underset{\sim}{\mathbf{P}}(z_0) = \begin{array}{c} \rightarrow x_s \\ \begin{bmatrix} P_{-K,-M} & \cdots & P_{-K,m} & \cdots & P_{-K,M} \\ \vdots & & \vdots & & \vdots \\ P_{k,-M} & \cdots & P_{k,m} & \cdots & P_{k,M} \\ \vdots & & \vdots & & \vdots \\ P_{K,-M} & \cdots & P_{K,m} & \cdots & P_{K,M} \end{bmatrix} \end{array} \downarrow x_r \quad , \tag{B.3}$$

where x_s denotes the lateral position of the different sources. Each element $P_{k,m}$ corresponds to a fixed lateral receiver coordinate $x_{r,k}$ and a fixed lateral source coordinate $x_{s,m}$. Each column (fixed x_s) in this data matrix represents one (monochromatic) common shot record. Each row (fixed x_r) represents one common receiver record; The diagonal ($x_s=x_r$) represents zero offset data and the anti-diagonal ($x_s=-x_r$) represents common midpoint data (see also Figure 2.3).

In a 3-D seismic survey the (monochromatic) prestack data $P(x_r,y_r,z_0;x_s,y_s,z_0;\omega_i)$ can also be represented by a matrix (Kinneging et al., 1989) according to

$$\underset{\sim}{\mathbf{P}}(z_0) = \begin{bmatrix} \underset{\sim}{P}_{-L,-N} & \cdots & \underset{\sim}{P}_{-L,n} & \cdots & \underset{\sim}{P}_{-L,N} \\ \vdots & & \vdots & & \vdots \\ \underset{\sim}{P}_{1,-N} & \cdots & \underset{\sim}{P}_{1,n} & \cdots & \underset{\sim}{P}_{1,N} \\ \vdots & & \vdots & & \vdots \\ \underset{\sim}{P}_{L,-N} & \cdots & \underset{\sim}{P}_{L,n} & \cdots & \underset{\sim}{P}_{L,N} \end{bmatrix} \begin{matrix} \rightarrow y_s \\ \\ \\ \\ \downarrow y_r \end{matrix}, \tag{B.4}$$

where y_r denotes the different cross-line positions of the receivers and y_s denotes the different cross-line positions of the sources. Each sub-matrix $\underset{\sim}{P}_{l,n}$ corresponds to a fixed cross-line receiver coordinate $y_{r,l}$ and a fixed cross-line source coordinate $y_{s,n}$. The elements in the sub-matrix itself are defined as in (B.3) (see Figure B.1). Note that each column (fixed x_s,y_s) of the total matrix $\underset{\sim}{\mathbf{P}}(z_0)$ represents one (monochromatic) common shot record and each row (fixed x_r,y_r) represents one common receiver record. In this thesis a data matrix $\underset{\sim}{\mathbf{P}}(z_0)$ may represent either a 2-D survey, as in (B.2) ore a 3-D areal survey, as in (B.3). Hence, a data vector $\mathbf{P}(z_0)$ (one column of $\underset{\sim}{\mathbf{P}}(z_0)$) may represent either a 2-D or a 3-D seismic shot record.

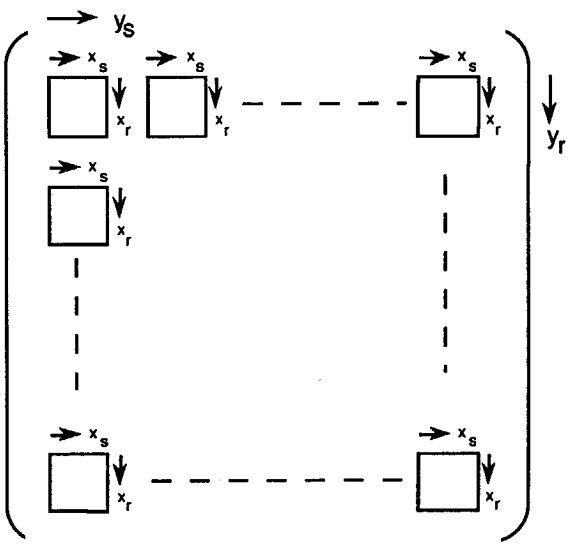

Figure B.1
Organization of the data matrix for a 3-D seismic survey.

B.3 MATRIX NOTATION FOR OPERATORS

Wave field extrapolation can be written as a generalized spatial convolution according to

$$P(x,y,z_m;\omega) = \int_{-\infty}^{\infty}\int W(x,y,z_m;x',y',z_0;\omega)\ P(x',y',z_0;\omega)\ dx'dy' \quad . \tag{B.5}$$

$P(x',y',z_0;\omega)$ represents a quantity related to a wave field at depth level z_0 (e.g. the acoustic pressure or one component of the particle velocity), W represents an operator (here for downward wave field extrapolation) and $P(x,y,z_m;\omega)$ represents a quantity related to a wave field at depth level z_m (here the downward extrapolated wave field). When $P(x,y,z_m;\omega)$ and $P(x',y',z_0;\omega)$ represent pressure wave fields and W represents a forward extrapolation operator, then (B.5) represents the Rayleigh II integral.

If we replace the wave fields P as well as the operator W by their discretized versions, then the integrals are replaced by summations, according to

$$P(k\Delta x,l\Delta y,z_m;\omega) = \tag{B.6}$$
$$\sum_{m=-M}^{M}\sum_{n=-N}^{N} W(k\Delta x,l\Delta y,z_m;m\Delta x',n\Delta y',z_0;\omega)\ P(m\Delta x',n\Delta y',z_0;\omega)\ \Delta x'\Delta y' \quad ,$$

for k=-K, ... , K and l=-L, ..., L.

Here it is assumed that M and N are "sufficiently large" and that Δx and Δy are "sufficiently small". The latter condition can always be satisfied as we deal with *band-limited* seismic data. For an extensive discussion on various aspects of discretization the reader is referred to Berkhout (1985).

In analogy with the previous section, we define data vectors $\mathbf{P}(z_m)$ and $\mathbf{P}(z_0)$ which contain the discretized wave fields $P(x,y,z_m;\omega)$ and $P(x',y',z_0;\omega)$, respectively. Next we replace equation (B.6) by the matrix equation

$$\mathbf{P}(z_m) = \underset{\sim}{\mathbf{W}}(z_m,z_0)\,\mathbf{P}(z_0) \quad . \tag{B.7}$$

This implies that we define the operator matrix $\underset{\sim}{\mathbf{W}}(z_m,z_0)$ according to

$$\underset{\sim}{W}(z_m,z_0) = \begin{bmatrix} \underset{\sim}{W}_{-L,-N} & \cdots & \underset{\sim}{W}_{-L,n} & \cdots & \underset{\sim}{W}_{-L,N} \\ \vdots & & \vdots & & \vdots \\ \underset{\sim}{W}_{l,-N} & \cdots & \underset{\sim}{W}_{l,n} & \cdots & \underset{\sim}{W}_{l,N} \\ \vdots & & \vdots & & \vdots \\ \underset{\sim}{W}_{L,-N} & \cdots & \underset{\sim}{W}_{L,n} & \cdots & \underset{\sim}{W}_{L,N} \end{bmatrix} , \tag{B.8}$$

where the elements of the sub-matrices $\underset{\sim}{W}_{l,n}$ read

$$(\underset{\sim}{W}_{l,n})_{k,m} = \Delta x \Delta y \; W(k\Delta x, l\Delta y, z_m; m\Delta x, n\Delta y, z_0; \omega_i) \; . \tag{B.9}$$

Note the high degree of similarity of this operator matrix $\underset{\sim}{W}(z_m,z_0)$ with the data matrix $\underset{\sim}{P}(z_0)$ defined in (B.4). One column in the data matrix $\underset{\sim}{P}(z_0)$ represents one Fourier component of the data as a function of (x_r,y_r) for a source at $(x_s=m\Delta x, y_s=n\Delta y, z_0)$. Similarly, one column in the operator matrix $\underset{\sim}{W}(z_m,z_0)$ represents one Fourier component of the "spatial impulse response" of the operator as a function of (x,y) for an "impulse" at $(x'=m\Delta x, y'=n\Delta y, z_0)$.

REFERENCES

Alterman, Z. and Karal jr., F.C., 1968, Propagation of elastic waves in layered media by finite difference methods: Bull. of the Seism. Soc. of Am., vol 58, p.367-398.

Al-Yahya, K.M., 1989, Velocity analysis by iterative profile migration: Geophysics, vol. 54, p.718-729.

Berkhout, A.J., 1982, Seismic Migration, Volume A, Theoretical aspects: Elsevier, Amsterdam–New York.

Berkhout, A.J., 1984, Seismic Resolution: Resolving power of acoustical echo techniques, Geophysical Press, London–New York.

Berkhout, A.J., 1984, Seismic Migration; Imaging of acoustic energy by wave field extrapolation: B. Practical Aspects: Developments in solid earth geophysics vol. 14B, Elsevier, Amsterdam.

Berkhout, A.J., 1985, Seismic Migration: Imaging of acoustic energy by wave field extrapolation, Volume A: Theoretical aspects: Elsevier, Amsterdam–Oxford–New York–Tokyo.

Berryhill, J.R., 1984, Wave equation datuming: Geophysics, vol.44, p.1329-1344.

Blacquière, G., 1989, 3D wave field extrapolation in seismic depth migration: PhD. thesis, Delft University of Technology, The Netherlands.

Cox, H.L.H., Ooms, F.P.J., Wapenaar, C.P.A., and Berkhout, A.J., 1988, Macro model estimation using shot record redatuming: 58th SEG meeting, Anaheim, Expanded Abstracts p.904-908.

Denelle, E., Dezard, Y., and Raoult, J.J., 1985, Implementation of a 2-D prestack depth migration scheme on a CRAY 1-S: 55th SEG meeting, Washington D.C., Expanded Abstracts p.318-320.

Deregowski, S.M., 1986, What is DMO?: First Break, vol. 4, p.7-24.

Diebold, J.B., and Stoffa, P.L., 1981, The traveltime equation, tau-p mapping, and inversion of common midpoint data: Geophysics, vol. 46, p.238-254.

Dix, C.H., 1955, Seismic velocities from surface measurements: Geophysics, vol. 20, p.68-86.

Durbaum, H., 1954, Zur Bestimmung von Wellengeschwindigkeiten aus reflexion seismischen Messungen: Geophysical Prospecting, vol. 3, p.151-167.

Geerlings, A.C.G., 1990, Adaptive tracking in seismic exploration: PhD. thesis, Delft University of Technology, The Netherlands.

Gibson, B.S., Odegard, M.E., and Sutton, G.H.,1979, Nonlinear least-squares inversion of traveltime data for a linear velocity-depth relationship: Geophysics, vol. 44, p.185-194.

Gjøystdal, H., and Ursin, B., 1981, Inversion of reflection times in three dimensions: Geophysics, vol. 46, p.972-983.

Grant, F.S., and West, G.F., 1965, Interpretation theory in applied geophysics: McGraw-Hill Book Co.

Haas, J.C. de, and Berkhout, A.J., 1989, Practical approach to nonlinear inversion of amplitude versus offset information: 59th SEG meeting, Dallas, Expanded Abstracts p.839-842.

Hadley, D., Thorson, J., and Maher, S., 1988, Increasing interpretation accuracy: A new approach to interval velocity estimation: The Leading Edge, vol. 9, p.13-16.

Hubral, P., 1976, Interval velocities from surface measurements in the three-dimensional plane layer case: Geophysics, vol. 41, p.223-242.

Jeannot, J.P., Faye, J.P., and Denelle, E.,1986, Prestack migration velocities from depth focusing analysis: 56th SEG meeting, Houston, Expanded Abstracts p.438-440.

Kelly, K.R., Ward, R.W., Treitel, S., and Alford, R.M.,1976, Synthetic seismograms: a finite difference approach: Geophysics, vol 41, p.2-27.

Kinneging, N.A., 1989, Three-dimensional redatuming of shot records: PhD. thesis, Delft University of Technology, The Netherlands.

Kinneging, N.A., Budijecky, V., Wapenaar, C.P.A., and Berkhout, A.J. 1985, Efficient 2D and 3D Shot Record Redatuming: Geophysical Prospecting, vol. 37, p.493-530.

Landa, E., Kosloff, D., Keydar, S., Koren, Z. and Reshef, M., 1988, A method for determination of velocity and depth from seismic reflection data, Geophysical Prospecting, vol. 38, p.223-243.

Lörtzer, G.J.M, 1990, An integrated approach to lithologic inversion: PhD. thesis, Delft University of Technology, The Netherlands.

MacBain, J., 1989, Interval Velocity Analysis for Prestack Depth Migration: 59th SEG meeting, Dallas, Expanded Abstracts p.1233-1237.

Made, P.M. van der, 1988, Determination of Macro Subsurface Models by Generalized inversion: PhD. thesis, Delft University of Technology, The Netherlands.

May, B.T., and Covey, J.D., 1981, An inverse ray method for computing geologic structures from seismic reflections – Zero-offset case: Geophysics, vol. 46, p.268-287.

Mora, P., 1989, Inversion = Migration + Tomography: Geophysics, vol. 54, p.1575-1586.

Parasnis, D.S., 1986, Principles of applied geophysics: Chapman and Hall.

Peels, G.L., 1988, True amplitude wave field extrapolation with applications in seismic shot record redatuming: PhD. thesis, Delft University of Technology, The Netherlands.

R.W. Postma, Marathon Oil Co. and J.P. Jeannot, Dataid Technologies, 1988, Prestack Depth Imaging Beneath A Complex Overburden, Presented at the 58th Annual SEG-meeting, Los Angeles, Poster 9.5

Schoot, A. van der, 1989, Common reflection point stacking: PhD. thesis, Delft University of Technology, The Netherlands.

Shah, P.M., 1973, Use of wavefront curvature to relate seismic data with subsurface parameters: Geophysics, vol. 38, p.812-825.

Shultz, P.S., and Sherwood, J.W.C., 1980, Depth migration before stack: Geophysics, vol. 45, p.376-393.

Taner, M.T., and Koehler, F., 1969, Velocity spectra – digital computer derivation and application of velocity functions: Geophysics, vol. 34, p.859-881.

Tarantola, A., 1987, Inverse Problem theory: Methods for data fitting and model parameter estimation, Elsevier, Amsterdam–Oxford–New York–Tokyo.

Trier, J. van, 1988, Migration velocity analysis using geological constraints: 58th SEG meeting, Anaheim, Expanded Abstracts p.897-900.

Tuchel, G., 1943, Seismische Messungen: Taschenbuch für Angewandte Geophysik, Leipzig.

Wapenaar, C.P.A., 1986, Prestack migration in two and three dimensions: PhD. thesis, Delft University of Technology, The Netherlands.

Wapenaar, C.P.A., and Berkhout, A.J. 1985, Velocity determination in layered systems with arbitrarily curved interfaces by means of wave field extrapolation of CMP data: Geophysics, vol. 50, p.63-76.

Wapenaar, C.P.A., and Berkhout, A.J. 1989, Elastic wave field extrapolation, Elsevier, Amsterdam–Oxford–New York–Tokyo.

Wapenaar, C.P.A., Herrman, P., Verschuur, D.J., and Berkhout, A.J., 1990, Decomposition of multicomponent seismic data into primary P- and S-wave responses: Geophysical Prospecting, vol. 38, p.633-661.

Yilmaz, O., 1987, Seismic data processing, Series: Investigations in Geophysics, vol. 2, SEG, Tulsa.

Yilmaz, O., and Chambers, R., 1984, Migration velocity analysis by wave field extrapolation: Geophysiscs, vol. 49, p.1664-1674.

SUMMARY

To obtain an image of the earth's subsurface, the traveltimes of reflection events in seismic data have to be converted to geologic depths. For one-dimensional subsurfaces this means a re-scaling of the time coordinate. In case of simple subsurface structures re-scaling of the time coordinate should be preceded by time migration. However, for complex subsurfaces depth migration is required and time-to-depth conversion is part of the migration process. In any of the conversion schemes a macro velocity model is needed that predicts the traveltimes of the seismic waves in the subsurface.

A macro velocity model can be parameterized by *macro boundaries*, which represent the major reflectors in the subsurface, and *macro interval velocities*, which are the propagation velocities (and gradients) between the macro boundaries. It is important to realize that one macro boundary in the macro model may actually represent a sequence of thin layers (transition zone).

In the past a lot of research has been done to obtain a description of the macro velocity model. Conventionally, velocity analysis is done directly on the surface measurements (CMP-gathers). Dix (1955) has developed a simple estimation method assuming hyperbolic moveout and plane horizontal interfaces. Taner and Koeler (1969) use velocity spectra obtained from coherency analysis on CMP data to estimate interval velocities for horizontally layered media. In the extensions made by Hubral (1976), the plane interfaces are allowed to have arbitrary dip, but the assumption of hyperbolic moveout is not released. Presently, CMP techniques exist that avoid the hyperbolic assumption (Hadley et al., 1988;

Landa et al., 1988), but still the analysis is performed on the surface measurements.

In current seismic processing a trend exists towards an increasing use of prestack depth migration of seismic data. Opposed to more conventional data processing techniques, prestack depth migration requires a more accurate description of the macro velocity model.

In this thesis a new method is developed to estimate accurate macro velocity models. The philosophy behind the method is to use the sensitivity of prestack migration to estimate the macro velocity model. Since model errors are expressed in the quality of the migration result, the migration process itself can be used to determine these errors.

Using an initial macro velocity model, shot records are downward extrapolated to grid points (depth points) in the subsurface (Chapter 2). The extrapolated data can be reordered into so-called common depth-point (CDP-)gathers, image gathers and focus panels (Chapter 3). If the macro velocity model is correct, horizontal alignment should occur in CDP-gathers at t=0, image gathers should contain horizontally aligned events at all depths, and focus panels should contain foci at t=0 only. If these requirements are not met, the macro velocity model is in error and needs to be updated. The procedure is repeated until convergence has occurred.

In the macro model estimation method presented in this thesis, the deviation from horizontal alignment is used to quantify the errors in the model and to apply update corrections accordingly (Chapter 4). The analysis can be done before or after stacking over all shot records (CDP-stacking). By CDP-stacking the previously mentioned focus panels are generated. The alignment analysis reduces then to a simple focusing analysis.

There are several advantages of extrapolation per individual shot record (as opposed to so-called S-G extrapolation schemes). Above all, it allows to investigate the extrapolated data per shot record, i.e. with shot record extrapolation it is possible to analyse alignment in CDP-gathers and image gathers. Normally, the alignment is quantified by CDP-stacking. However, other coherence measures can be used as well. Furthermore, from a data handling point of view it is convenient to process the data per physical experiment (shot record). Note that in S-G based schemes

CDP-stacking is done implicitly. Hence, in those schemes the extrapolated data can only be inspected after CDP-stacking (focusing analysis).

In conclusion, horizontal alignment of macro reflections in CDP-gathers is an excellent criterion for *verification* and *updating* of macro velocities. After each update the data should be depth migrated with the new macro velocities to evaluate the macro boundaries. The examples discussed in Chapter 5 show that with this approach it is possible to obtain accurate macro velocity models for prestack depth migration.

In complicated situations focus panels can be difficult to interpret. Hence, in these cases it is impossible to converge to the correct solution with focus panels only. The process should be guided by macro geologic models of the area.

Finally, in complicated situations a layer-stripping strategy is preferred.

SAMENVATTING

Om een beeld te maken van de ondergrond moeten de looptijden van reflecties in seismische metingen geconverteerd worden naar geologische diepten. Voor een één-dimensionale ondergrond betekent dit een herschaling van de tijdcoördinaat. In het geval van een eenvoudige ondergrond moet deze herschaling voorafgegaan worden door tijdmigratie. Daarentegen is dieptemigratie vereist in het geval van een complexe ondergrond, waarbij de tijd-diepte-conversie één geheel vormt met het migratie-algoritme. In elk van bovengenoemde diepte conversie schema's is een macro snelheidsmodel nodig, dat de looptijden van de seismische golven in de ondergrond voorspelt.

Een macro snelheidsmodel kan worden beschreven door een aantal macro oppervlakken, gegeven door de belangrijke snelheidsovergangen in de ondergrond, en macro interval snelheden (en gradiënten), gegeven door de voortplantingsnelheden in elke macro laag. Het is belangrijk te realiseren dat een macro oppervlak in het macro model ook een reeks dunne lagen kan representeren (een zogenaamde transitiezone).

In het verleden is veel onderzoek gedaan om een beschrijving te krijgen van snelheidsmodellen. Snelheidsanalyse wordt in het algemeen direct op de oppervlaktemetingen toegepast. Dix (1955) bijvoorbeeld, ontwikkelde een eenvoudige snelheidschattings methode, waarbij hyperbolische "moveout" wordt aangenomen evenals vlakke horizontale reflectoren. Taner en Koehler (1969) maken gebruik van snelheidsspectra, die verkregen zijn uit coherentie analyse op zgn. CMP (common midpoint) datasets. Hierbij wordt wederom de hyperbolische aanname gebruikt. In de uitbreidingen van Dix' methode, voorgesteld door Hubral (1976), mogen de vlakke

reflectoren een willekeurige helling hebben, maar ook in deze methode wordt hyperbolische moveout aangenomen. Tegenwoordig bestaan er CMP technieken waarbij de aanname van hyperbolische moveout wordt vermeden (Hadley et al., 1988; Landa et al., 1988).

In de huidige seismische processing is een trend waarneembaar die duidt op toenemend gebruik van prestack dieptemigratie van seismische data, waarbij de CMP stack wordt vermeden. In tegenstelling tot meer conventionele processing technieken is voor prestack dieptemigratie een accurate beschrijving van het macro snelheidsmodel vereist.

In dit proefschrift is een nieuwe methode ontwikkeld om accurate macro snelheidsmodellen te schatten. Deze methode is gebaseerd op de filosofie om de gevoeligheid van prestack migratie te gebruiken voor het schatten van het macro snelheidsmodel. Omdat modelfouten tot uitdrukking komen in de kwaliteit van het migratie resultaat kan het migratieproces zelf worden gebruikt om deze fouten te bepalen.

Gebruikmakend van een initieel macro snelheidsmodel, worden shot records geëxtrapoleerd naar "grid-punten" in de ondergrond (zogenaamde diepte-punten, hoofdstuk 2). De geëxtrapoleerde data kunnen dan worden geordend in zogenaamde common depth-point (CDP-)gathers, image gathers en focus panels (hoofdstuk 3). Als het macro snelheidsmodel correct is dan moet in CDP-gathers horizontale oplijning plaatsvinden op t=0, image gathers moeten horizontaal opgelijnde reflecties bevatten voor alle diepte-punten en in focus panels mogen slechts foci optreden op t=0. Als aan deze voorwaarden niet is voldaan dan is het macro snelheidsmodel fout en moet het worden aangepast. De procedure wordt herhaald totdat convergentie is opgetreden.

In de macromodel-schattingsmethode die in dit proefschrift wordt behandeld, wordt de afwijking van de horizontale oplijning gebruikt om de fouten in het model te kwantificeren en overeenkomstige correcties toe te passen (hoofdstuk 4). De analyse kan worden gedaan voor of na het optellen van de resultaten voor de verschillende bronposities op het oppervlak (CDP-stacking). Door CDP-stacking kunnen de hiervoor genoemde focus panels worden gegenereerd. De oplijnings-analyse wordt in dat geval gereduceerd tot een eenvoudige focus analyse.

Er zijn verschillende voordelen verbonden aan het afzonderlijk extrapoleren van shot records (in tegenstelling tot zogenaamde S-G extrapolatie schema's). Bovenal staat deze methode de analyse van de geëxtrapoleerde data per shot record toe, m.a.w. door middel van shot record extrapolatie is het mogelijk om de oplijning in CDP-gathers en image gathers te analyseren. Deze oplijning kan worden gekwantificeerd door CDP-stacking, maar andere coherentie criteria kunnen ook worden gebruikt. Ook vanuit het oogpunt van data verwerking is het handig om de data te bewerken per fysisch experiment (shot record). Daarentegen wordt in S-G schemas de CDP-stacking impliciet toegepast. Daarom kunnen de geëxtrapoleerde data slechts na CDP-stacking worden geïnspecteerd (focus analyse).

Concluderend kan gesteld worden dat horizontale oplijning van macro reflecties in CDP-gathers een uitstekend criterium is voor de *verificatie* en *aanpassing* van macro snelheden. Na elke aanpassing moet op de data dieptemigratie worden toegepast om de macro grenzen te bepalen. De voorbeelden in hoofdstuk 5 laten zien dat het met deze methode mogelijk is om accurate macro snelheidsmodellen te verkrijgen die gebruikt kunnen worden in prestack dieptemigratie.

In ingewikkelde gevallen kunnen focus panels moeilijk te interpreteren zijn. In deze gevallen is het moeilijk om naar de correcte oplossing te convergeren met focus panels alleen. Daarom moet het proces gestuurd worden met behulp van macro geologische modellen van het gebied.

Tenslotte, in ingewikkelde situaties is een zg. "layer-stripping" techniek te prefereren.

CURRICULUM VITAE

30 september 1961	geboren te Utrecht
1973-1979	Atheneum B aan het St. Maartens College te Voorburg
1979-1986	studie Technische Natuurkunde aan de toenmalige Technishe Hogeschool te Delft. Afstudeer-onderzoek bij de vakgroep Seismiek and Akoestiek met als titel: "Comparison of three wavenumber mapping techniques and the implementation on a CRAY XMP14 super computer"
1986-1990	promotie-onderzoek achtereenvolgens bij het TRITON en het DELPHI project aan de Technische Universiteit te Delft met als onderwerp: "Estimation of macro velocity models by wave field extrapolation"
1980-1981	lid van de Jeugd Commissie van de Nootdorpse Tennis Club
1985-1986	lid van de Open Toernooi Commissie van de Nootdorpse Tennis Club
1989-heden	lid van de Technische Commissie van de Nootdorpse Tennis Club
Hobbies	tennis, schaken